

THIANTHRENE ORGANIC MATERIALS: SYNTHESIS, PROPERTIES AND
APPLICATIONS

by

Wen Jie Ong

M.Chem., Chemistry, First Class Honors
University of Oxford, 2012

Submitted to the Department of Chemistry
in Partial Fulfillment of the Requirements for the Degree of

DOCTOR OF PHILOSOPHY IN CHEMISTRY
at the
MASSACHUSETTS INSTITUTE OF TECHNOLOGY

February 2019

©2019 Massachusetts Institute of Technology. All rights reserved.

Signature redacted

Signature of Author:

Department of Chemistry

Signature redacted November 12, 2018

Certified by:

)

U

Timothy M. Swager

John D. MacArthur Professor of Chemistry

Thesis Supervisor

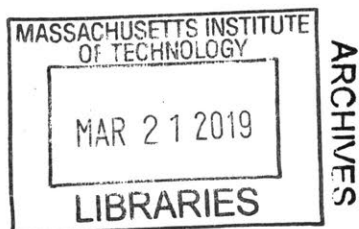
Signature redacted

Accepted by:

Robert W. Field

Haslam and Dewey Professor of Chemistry

Chair, Departmental Committee on Graduate Students



This doctoral thesis has been examined by a Committee of the Department of Chemistry as follows:

Signature redacted

Professor Jeremiah A. Johnson
Chairman

Signature redacted

Professor Timothy M. Swager
Thesis Advisor

Signature redacted

Professor Stephen L. Buchwald
Department of Chemistry

To Jiajing and My Family

THIANTHRENE ORGANIC MATERIALS: SYNTHESIS, PROPERTIES AND APPLICATIONS

by

Wen Jie Ong

Submitted to the Department of Chemistry on November 12, 2018
in Partial Fulfillment of the Requirements for the Degree of
Doctor of Philosophy in Chemistry

ABSTRACT

Thianthrene is a heterocyclic molecule with intriguing electrochemical properties. In this thesis, the synthesis, properties and applications of novel thianthrene-containing organic materials will be discussed. In Chapter 1, key concepts essential for understanding this thesis will be reviewed, including structure, electrochemistry and synthesis of thianthrene, nucleophilic aromatic substitution (S_NAr), and redox flow battery. In Chapter 2, we exploit the dynamic, self-correcting nature of the S_NAr reaction between *ortho*-aryldithiols and *ortho*-aryldifluorides to afford molecules with two, three, and four thianthrene moieties respectively, in excellent yields. The same chemistry is also applied to the synthesis of ladder macrocycles and porous polymer networks. In Chapter 3, we further extend the dynamic S_NAr reaction to the synthesis of ladder thianthrene polymers, comparing their electrochemical, photophysical and thermal properties to the properties of their dibenzo-1,4-dioxin analog. The last two chapters focus on the applications of novel organic materials containing thianthrene and its derivatives. Chapter 4 shows how incorporating thianthrenes into resorcinarene-based cavitand enables electrochemically-induced vase-kite conformation changes. In Chapter 5, we propose a new approach toward designing novel dual anolyte-catholyte molecules by deconstruction of relevant electroactive species. Using thianthrene and anthraquinone as examples, we design and synthesize three new molecular scaffolds exhibiting excellent electrochemical stability over a wide potential range and good solubility for symmetric redox flow battery application.

Thesis Supervisor: Timothy M. Swager

Title: John D. MacArthur Professor of Chemistry

Table of Contents

Title Page	1
Signature Page	3
Dedication	5
Abstract	7
Table of Contents	9
List of Figures.....	12
List of Schemes	15
Chapter 1: Introduction and Backgrounds	16
1.1 Thianthrene	17
1.1.1 Structure	17
1.1.2 Electrochemistry	18
1.1.3 Synthesis	19
1.2 Nucleophilic Aromatic Substitution	20
1.2.1 General	20
1.2.2 Sulfur Nucleophiles	21
1.3 Redox Flow Battery	22
1.4 Objectives	25
1.5 References	25
Chapter 2: Dynamic Self-Correcting Nucleophilic Aromatic Substitution	29
2.1 Introduction	30
2.2 Results and Discussion	32
2.2.1 Two-Point Junction	32
2.2.2 Three-Point Junction	40

2.2.3	Four-Point Junction	43
2.3	Conclusions	46
2.4	Experimental Details	46
2.4.1	General	46
2.4.2	Synthetic Procedures	49
2.5	References	60
2.6	Appendix for Chapter 2	64
 Chapter 3: Thianthrene Ladder Polymers		89
3.1	Introduction	90
3.2	Results and Discussion	91
3.2.1	Synthesis	91
3.2.2	Electrochemical Properties	93
3.2.3	Photophysical Properties and Thermal Stability	94
3.3	Conclusions	96
3.4	Experimental Details	96
3.4.1	General	96
3.4.2	Synthetic Procedures	98
3.5	References	104
3.6	Appendix for Chapter 3	106
 Chapter 4: Redox Switchable Thianthrene Cavitands		114
4.1	Introduction	115
4.2	Results and Discussion	117
4.3	Conclusions	125
4.4	Experimental Details	125
4.4.1	General	125
4.4.2	Synthetic Procedures	126

4.5	References	131
4.6	Appendix for Chapter 4	134
Chapter 5: Dual Anolyte-Catholyte Molecules		145
5.1	Introduction	146
5.2	Results and Discussion	150
	5.2.1 Synthesis and Electrochemical Studies of Model Molecule	150
	5.2.2 Further Synthesis and Electrochemical Studies	152
5.3	Conclusions	157
5.4	Experimental Details	157
	5.4.1 General	157
	5.4.2 Synthetic Procedures	158
5.5	References.....	162
5.6	Appendix for Chapter 5	164
Acknowledgements		171

List of Figures

- Figure 1.1.** Structures of bent thianthrene and its planar analogs.....17
- Figure 1.2.** Different redox states of thianthrene and their corresponding fold angle.....18
- Figure 1.3.** Cyclic voltammetry diagram of thianthrene in liquid SO₂ with tetrabutylammonium hexafluorophosphate as electrolyte (Fc/Fc⁺ marked with *). Reproduced from Ref. 12.....18
- Figure 1.4.** Illustrative S_NAr reactions for preparation of aryl thioethers.....22
- Figure 1.5.** Schematic diagram showing the a) charging, and b) discharging modes of a RFB...23
-
- Figure 2.1.** Reaction between a dithiol or tetrathiol nucleophile and three different model electrophiles. a) Formation of two-point, three-point, and four-point junctions by S_NAr using 3,4,5,6-tetrafluorophthalonitrile **1**, hexafluorobenzene **2**, and octafluoronaphthalene **3**, respectively. The orange arrows show possible sites for connection to 1,2-benzenedithiol **4** and 1,2,4,5-benzenetetrathiol **8**. Those are thermodynamically favored and lead to ladder macrocycles and networks, respectively, as shown in Figures 2.2 (**5**), 2.5a (**6**) and 2.6a (**7**). b) Under kinetic control, **1**, **2**, and **3** form other connections.....32
- Figure 2.2.** Dynamic, self-correcting S_NAr reaction. a) Model reaction illustrating dynamic, self-correcting nature of S_NAr reaction. Conditions: **1** or **9** (1 equiv), **4** (1 or 2 equiv), K₂CO₃ (3 or 6 equiv), DMF, r.t. or 80 °C. b) Proposed mechanism for reaction of **9** with **4**.....34
- Figure 2.3.** Facile exchange of dithiol nucleophiles. a) Substitution of 1,2-benzenedithiol units on **5** with toluene-3,4-dithiol **11**. b) ¹H NMR spectra taken in TCE-*d*₂ at 85 °C showing facile exchange of benzenedithiols (Spectrum 1: **5**, Spectrum 2: crude product of **5** (1 equiv) and **11** (1 equiv), Spectrum 3: **12a–b**, Spectrum 4: crude product of **5** (1 equiv) and **11** (10 equiv), Spectrum 5: **13a–c**).....36
- Figure 2.4.** Model reaction, synthesis and characterization of porous ladder polymer network **19**. a) Reactions of **2** (1 equiv) with **4** (2 or 3 equiv) under various conditions to afford only **16**, a mixture of **16** and **6**, or only **6**. b) Synthesis of porous ladder polymer network **19** using **2** and **8** as monomers. c) N₂ adsorption (filled squares) and desorption (hollow squares) isotherms of **19**. *S*_{BET} is the Brunauer–Emmett–Teller surface area, and P and P₀ are the equilibrium and saturation pressures of N₂ at 77 K respectively. d) SEM image (×30,000 magnification) of **19** drop-casted using a dispersion of **19** in DMF onto silicon wafer.....41
- Figure 2.5.** Model reaction, synthesis and characterization of porous ladder polymer network **20**. a) Synthesis of tetra-substituted product **7** using **3** and **4**. b) Cyclic voltammetry of **7** showing four distinct redox signals. c) Synthesis of porous ladder polymer network **20** using **3** and **8** as monomers. d) N₂ adsorption (filled squares) and desorption (hollow squares) isotherms of **20**. *S*_{BET} is Brunauer–Emmett–Teller surface area, and P and P₀ are the equilibrium and saturation pressures

of N₂ at 77 K respectively. e) SEM image (×30,000 magnification) of **20** drop-casted using a dispersion of **20** in DMF onto silicon wafer.....44

Figure 3.1. Structures of thianthrene ladder polymers **P1** and **P2**.....91

Figure 3.2. Synthesis of polymers a) **P1**, **P2**, and b) **P3** by S_NAr reactions.....93

Figure 3.3. Cyclic voltammetry of a) **P1** and b) **P2** drop casted on a Pt button working electrode. The grey plots show cyclic voltammetry using the same electrode before the polymers were drop casted.....94

Figure 3.4. Photophysical properties of a) **P1**, b) **P2** and c) **P3**, and d) thermal stability of **P1**, **P2** and **P3**. The emission spectra of **P1**, **P2** and **P3** were excited at 300 nm, 410 nm and 420 nm respectively. The excitation spectra of **P1** and **P2** were both monitored at 550 nm.....95

Figure 4.1. Structure of thianthrene-containing cavitand **1**.....116

Figure 4.2. Different redox states of thianthrene and their corresponding fold angles.....117

Figure 4.3. Vase-kite conformation change of thianthrene-containing cavitand **1** upon electrochemical stimuli.....117

Figure 4.4. ¹H NMR spectra of **1** before (blue) and after (maroon) addition of TFA.....119

Figure 4.5. UV-Vis spectrum of **1** in CH₂Cl₂ at different TFA concentrations.....120

Figure 4.6. Cyclic voltammetry diagram of **1** in CH₂Cl₂ at 100 mV s⁻¹ scan rate with TBAPF₆ as supporting electrolyte and Fc/Fc⁺ as external reference.....121

Figure 4.7. Spectroelectrochemistry of **1** in CH₂Cl₂.....121

Figure 4.8. ¹H NMR spectra of **7** before (blue) and after (maroon) oxidation.....124

Figure 4.9. ¹H NMR spectra of **1** before (blue) and after (maroon) oxidation.....124

Figure 5.1. Schematic diagram of a RFB.....146

Figure 5.2. Two approaches for designing dual anolyte-catholyte molecules, namely by using a) molecules that inherently possess dual oxidative and reductive properties, and b) tethered molecules with both anolyte and catholyte moieties.....148

Figure 5.3. New approach toward designing novel dual anolyte-catholyte molecules by deconstruction of relevant electroactive species. The green lines represent linker molecules....149

Figure 5.4. Cyclic voltammetry of model molecule **6** at a) 50 mV s⁻¹ (10 scans), b) 200 mV s⁻¹ (20 scans), and c) 500 mV s⁻¹ (50 scans).....151

Figure 5.5. Cyclic voltammetry of **7** at a) 50 mV s^{-1} (10 scans), and b) 500 mV s^{-1} (100 scans)..153

Figure 5.6. Cyclic voltammetry of **12** at a) 50 mV s^{-1} (10 scans) and b) 500 mV s^{-1} (100 scans), and **13** at c) 50 mV s^{-1} (10 scans) and d) 500 mV s^{-1} (100 scans).....156

List of Schemes

Scheme 1.1. Two approaches for synthesizing substituted thianthrenes, namely (1) direct functionalization of thianthrene, and (2) heterocyclization of precursor with desired functional groups.....	20
Scheme 1.2. Mechanism for nucleophilic aromatic substitution.....	20
Scheme 2.1. Synthesis of ladder macrocycle 15 . Monomers 8 and 14 at 0.005 M and 0.1 M concentration give the same mixture of ladder macrocycles in excellent yields. Faster equilibration and reaction time can be achieved by heating or using higher concentration.....	39
Scheme 3.1. Synthesis of nucleophilic monomers 3 and 5	92
Scheme 4.1. Synthesis of thianthrene-containing cavitand 1	118
Scheme 4.2. Synthesis of quinoxaline wall 7 . ^a A highly polar crude mixture (soluble in MeOH) was obtained.....	122
Scheme 5.1. Synthesis of model molecule 6	150
Scheme 5.2. Synthesis of 1,2-quinone 7	152
Scheme 5.3. Synthesis of dithiol nucleophile 11	154
Scheme 5.4. Synthesis of highly soluble dual anolyte-catholyte molecules 12 and 13	154

Chapter 1

Introduction and Backgrounds

Abstract

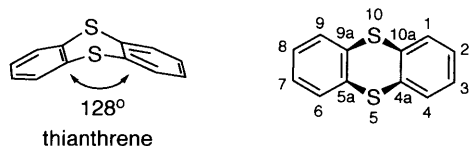
This chapter gives an overview of key concepts explored in the thesis. The structure, electrochemistry and synthesis of thianthrene is discussed. We then revisit the mechanism and general trends in the nucleophilic aromatic substitution (S_NAr) reaction, placing special emphasis on sulfur nucleophiles. These two topics represent the two underlying themes of our discussion. In this thesis, we will demonstrate how a diverse range of thianthrene-containing organic materials, ranging from small molecules to porous polymer networks, can be synthesized by the simple yet versatile S_NAr reaction. Given the rich electrochemistry of thianthrene, we will also introduce key concepts of redox flow battery, as a potential application of thianthrene derivatives.

1.1 Thianthrene

1.1.1 Structure

Thianthrene is a heterocyclic compound comprised of two benzene rings connected by two vicinal sulfur atoms.¹ In its neutral state, thianthrene is a bent molecule with a fold angle of 128° between the two planes of benzene rings. The bent structure of thianthrene sets it apart from its planar analogs, such as anthracene,² phenazine,³ and dibenzo-1,4-dioxin,⁴ in which both sulfur atoms are replaced by carbon, nitrogen and oxygen respectively (Fig. 1.1). This folded structure appears to be favored in the neutral state due to less effective $3p_z-\pi^*_{cc}$ orbital overlap and electron delocalization,⁵ and is in line with the observed dipole moment of 1.5 D.⁶ As a semi-flexible ring system, thianthrene undergoes facile inversion with an energy barrier of 6-7 kcal mol⁻¹.⁷

Bent structure:



Planar structures:

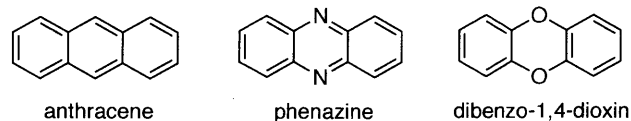


Figure 1.1. Structures of bent thianthrene and its planar analogs.

By comparing thianthrene's C–S bond length of 1.77 Å with the typical C–S single bond value of 1.82 Å, the C–S bond of thianthrene is estimated to possess ~25% double bond character,⁸⁻⁹ presumably through the participation of sulfur *d* and *p* orbitals in the bonding. The measured C–S

bond length of thianthrene agrees well with C–S values in other sulfur-containing aromatic compounds such as phenyl sulfide.

1.1.2 Electrochemistry

Thianthrene has been studied extensively for its redox activity,¹⁰⁻¹² and an interesting aspect of its redox chemistry is the geometric changes that accompany oxidation (Fig. 1.2). Upon oxidation, both the radical cation and the dication attain planarity with a fold angle of $\sim 180^\circ$.¹³ A representative cyclic voltammery is reproduced below illustrating the reversible oxidation of thianthrene and its radical cation (Fig. 1.3).

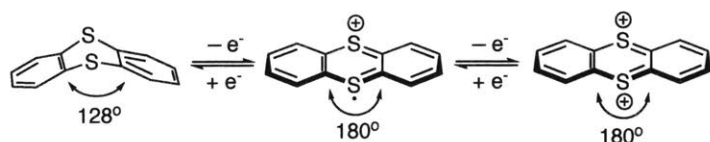


Figure 1.2. Different redox states of thianthrene and their corresponding fold angle.

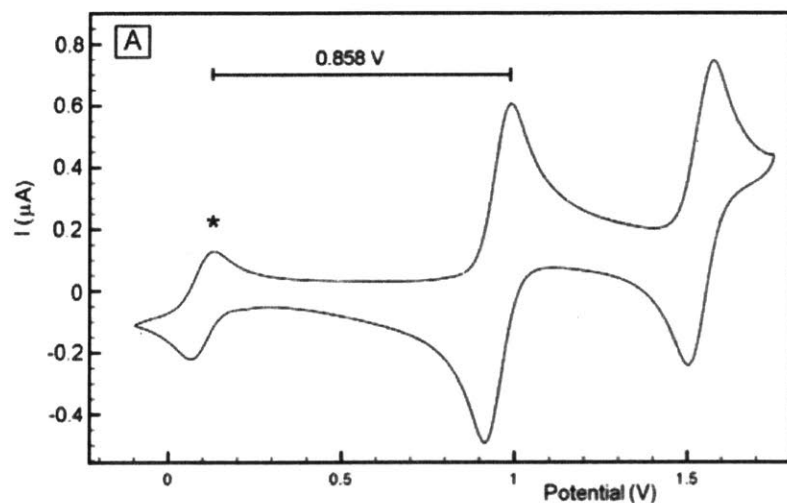


Figure 1.3. Cyclic voltammery diagram of thianthrene in liquid SO_2 with tetrabutylammonium hexafluorophosphate as electrolyte (Fc/Fc^+ marked with *). Reproduced from Ref. 12.

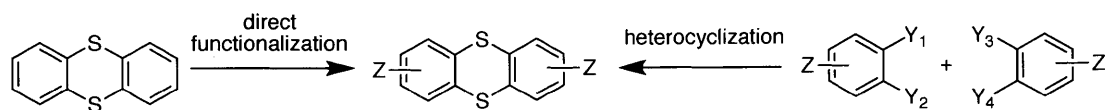
1.1.3 Synthesis

Early work on thianthrene synthesis focuses on the direct reaction of benzene with sulfur, S_2Cl_2 or SCl_2 in the presence of aluminum chloride.¹⁴ Alternatively, thianthrene can be prepared from the reaction between *o*-dichlorobenzene and hydrogen sulfide at 550 °C.¹⁵ Pyrolysis of diphenyl disulfide can also afford thianthrene.¹⁶

In order for thianthrene to be incorporated into more complex organic materials, functional groups need to be appended to the phenyl rings of thianthrene. Functionalized thianthrene molecules can be synthesized via two general approaches: (1) direct functionalization of thianthrene, and (2) heterocyclization of precursors with the desired functional groups installed (Scheme 1.1).

The former usually involves electrophilic aromatic substitution reactions such as bromination and Friedel-Crafts acylation.¹⁷⁻¹⁹ A disadvantage however is the lack of regioselectivity – a mixture of 2,7-substituted and 2,8-substituted thianthrene is usually formed, with the 2,7-regioisomer as the major product.

Representative examples of the latter approach include cyclization of 2-chloro-5-nitrobenzenethiol to 2,7-dinitrothianthrene,²⁰ and metal-free reaction between amphiphilic benzodithioloimines and arynes.²¹ This latter approach allows for precise control of substituent position, but is limited by the availability and cost of starting materials.

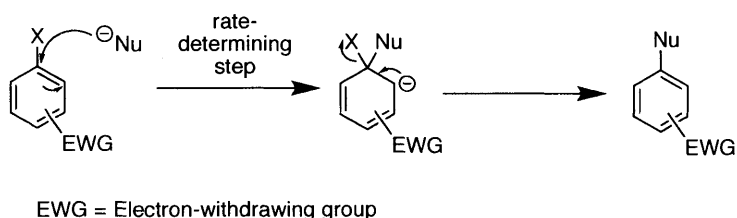


Scheme 1.1. Two approaches for synthesizing substituted thianthrenes, namely (1) direct functionalization of thianthrene, and (2) heterocyclization of precursors with desired functional groups.

1.2 Nucleophilic Aromatic Substitution

1.2.1 General

Nucleophilic aromatic substitution (S_NAr) is a convenient way of functionalizing aromatic rings. There are three key features of the S_NAr reaction to consider, namely (1) electron deficiency at an aromatic carbon, (2) nature of leaving group attached to the electron-deficient aromatic carbon, and (3) the reactivity of the attacking nucleophile.²² The generally accepted mechanism for S_NAr involves attack of a nucleophile Nu^- on the carbon bearing a leaving group X to form a Meisenheimer complex, followed by loss of the leaving group to regain aromaticity (Scheme 1.2). Due to the loss of aromaticity that accompanies the nucleophilic attack, the first step tends to be slow and is hence the rate-determining step.



Scheme 1.2. Mechanism for nucleophilic aromatic substitution.

Since the nucleophilic attack is the rate-determining step, more electron-deficient arenes undergo S_NAr more readily.²³ Since more electronegative halides are better at stabilizing the negatively-charged Meisenheimer complex than less electronegative ones, leaving group reactivity decreases in the order of $F^- \gg Cl^- > Br^- > I^-$. There is a myriad of nucleophiles, such as primary and secondary amines, alkoxides and cyanides, that are commonly used in S_NAr . As a rule of thumb, negatively charged species are stronger nucleophiles than their neutral counterparts, e.g. $NH_2^- > NH_3$, and nucleophilicity decreases across a row and increases down a group in the period table, e.g. amine > alcohol, and thiol > alcohol.

1.2.2 Sulfur Nucleophiles

As noted above, thiols are strong nucleophiles and undergo S_NAr reactions much more readily than the corresponding alcohols. As we will discuss in later chapters, benzene-1,2-dithiols are versatile nucleophiles in synthesizing thianthrene-containing organic materials. Using the illustrative examples below, we will highlight a few salient aspects of sulfur nucleophiles.

Given the lower pK_a and higher nucleophilicity of thiol than alcohol, it is possible to use thiol as a nucleophile using a mild base such as K_2CO_3 at room temperature in an alcohol solvent (Fig. 1.4a).²⁴ In contrast to $tBuOK$ which reacts exclusively as a sterically hindered base, $tBuSNa$ is an effective nucleophile and can be used to afford tetrathiolether (Fig. 1.4b).²⁵

Arylthiols are also excellent nucleophiles and can readily react with electron-deficient arenes under similar reaction conditions to alkylthiols. When 4-aminothiophenol is reacted with 4,5-dichlorophthalonitrile, thiol outcompetes amine and reacts preferentially as the nucleophile

(Fig. 1.4c).²⁶ Benzene-1,2-dithiol undergoes double S_NAr reactions to form two C–S bonds and afford thianthrene-containing naphthalene tetracarboxylic diimides (Fig. 1.4d).²⁷

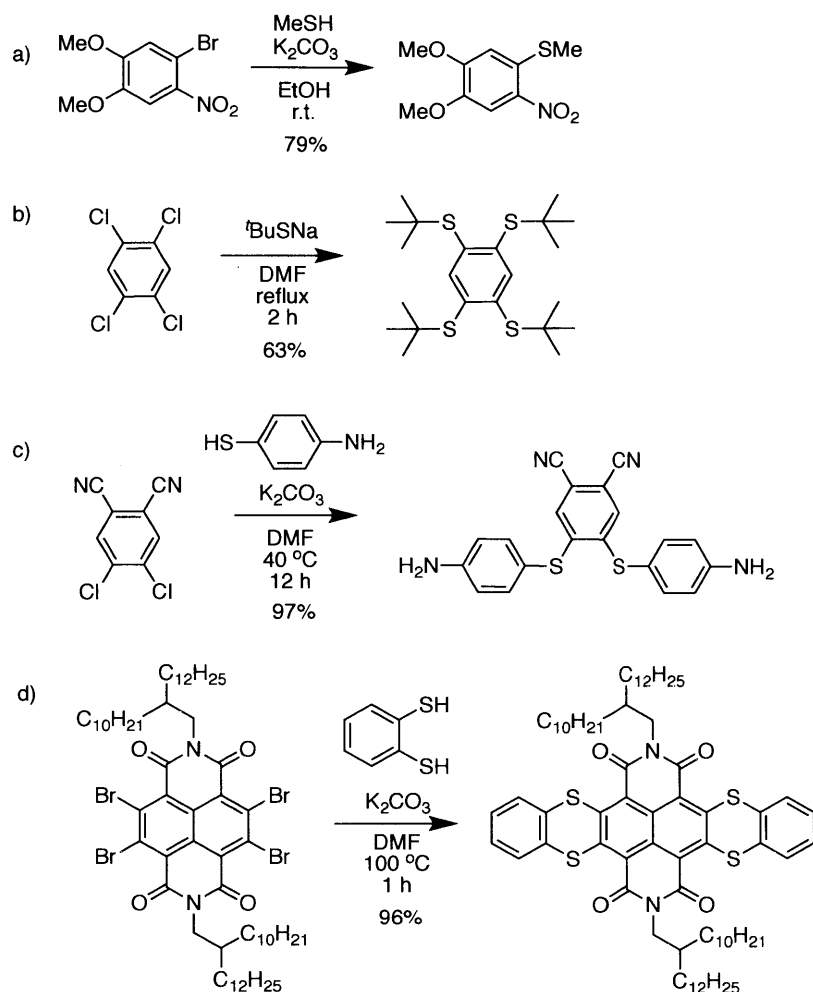


Figure 1.4. Illustrative S_NAr reactions for preparation of aryl thioethers.

1.3 Redox Flow Battery

Redox flow batteries (RFBs) have emerged as an attractive solution for providing inexpensive, large-scale grid energy storage, which is crucial for expediting the adoption of renewable energy and improving grid stability and efficiency.²⁸⁻²⁹ Over the last few years, a

number of novel chemistries have been reported using various organic redox species in both aqueous and non-aqueous systems.³⁰

RFBs operate by using external energy, e.g. solar energy from the sun or wind energy harnessed from wind turbines, to generate oxidized species at the cathode and reduced species at the anode (Fig. 1.5a).³¹ These species are then pumped and stored in external reservoirs until the energy is required, e.g. in the absence of sunlight or wind. To release the stored chemical energy, the charged catholyte and anolyte species are pumped back into the cell to react at their respective electrodes and discharged (Fig. 1.5b).

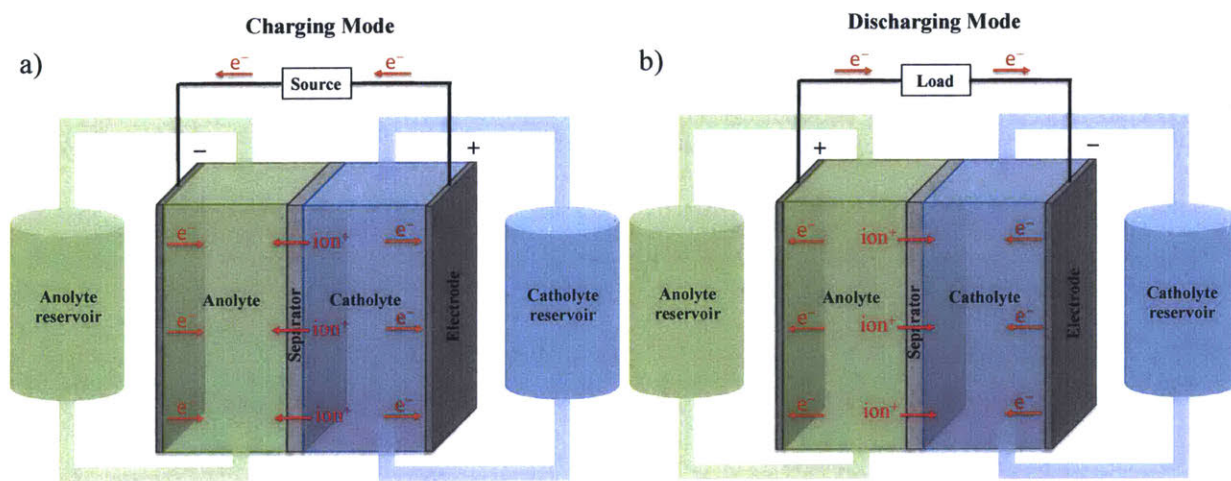


Figure 1.5. Schematic diagram showing the a) charging, and b) discharging modes of a RFB.

Several parameters are used to evaluate the electrochemical performance of a RFB. The most important parameter to consider is energy density which is given by the equation:

$$\text{Energy density} = \frac{nCFV}{\mu_v}$$

where n is the number of electrons transferred in the reaction, C is the lower concentration of the two electrolytes, F is Faraday's constant, V is the voltage of the battery, and μ_v is the volume factor ($\mu_v = 1 + \text{lower electrolyte concentration} / \text{higher electrolyte concentration}$).³⁰

Hence, in order to achieve high energy density, we need to simultaneously maximize the number of electrons involved in the redox reactions (n), the solubility of the redox species (C), and the potential difference between the anolyte and catholyte (V). It is important to realize that these factors can influence one another, and consequently a compromise is often required. For example, increasing the number of charges on a species tends to reduce its solubility in common organic solvents. Molecular weight of the redox species also needs to be considered since small molecules tend to have better solubility, and are more likely to attain high gravimetric energy density.

The choice of solvent is a key consideration as well. Besides influencing the solubility of the redox species involved, the electrochemical stability window of solvent dictates the maximum potential difference permissible between the anolyte and catholyte. Potential reaction between the solvent and charged states of the anolyte and catholyte should also be considered. For example, we found that radical cations of thianthrene are unstable in the presence of solvents such as DMF, NMP and propylene carbonate. Through astute molecular design of electroactive species and choice of solvent, it is possible to achieve highly soluble anolyte and catholyte with a wide redox potential range spanning the potential window of the solvent.

1.4 Objectives

This thesis is entitled “Thianthrene Organic Materials: Synthesis, Properties and Applications”. In this thesis, we will explore the synthesis and applications of various novel organic materials containing thianthrene and its derivatives, ranging from small molecules to porous polymer networks. In addition to thianthrene, the other underlying theme is the S_NAr reaction which is our method of choice for accessing thianthrene and its derivatives.

We commence our study by investigating the dynamic, self-correcting nature of the S_NAr reaction between *ortho*-aryldithiols and *ortho*-aryldifluorides in Chapter 2. We then apply this insight to the synthesis of thianthrene ladder polymers in Chapter 3, where we compare their electrochemical, photophysical and thermal properties to the properties of their dibenzo-1,4-dioxin analog.

As we will return to throughout this thesis, thianthrene possesses intriguing redox properties which can be exploited for molecular switching and energy storage applications. In Chapter 4, we incorporate thianthrene into resorcinarene-based cavitand and demonstrate redox activated vase-to-kite conformation change upon oxidation. In Chapter 5, we propose a new approach for designing novel dual anolyte-catholyte molecules through deconstruction of thianthrene and anthraquinone. These molecules exhibit good solubility and excellent electrochemically stability over a wide potential range.

1.5 References

- 1 For a general review on thianthrene, see Joule, J. A. Thianthrenes in Advances in Heterocyclic Chemistry Vol. 48; Academic Press: New York, 1990.

- 2 McL Mathieson, A.; Robertson, J. M.; Sinclair, V. C. *Acta Crystallogr.* **1950**, 3 (4), 245.
- 3 Herbstein, F. H.; Schmidt, G. M. J. *Acta Crystallogr.* **1955**, 8 (7), 399.
- 4 Cullinane, N. M.; Rees, W. T. *J. Chem. Soc., Faraday Trans.* **1940**, 35 (0), 507.
- 5 Kim, S.; Kwon, Y.; Lee, J.-P.; Choi, S.-Y.; Choo, J. *J. Mol. Struct.* **2003**, 655 (3), 451.
- 6 Le Fevre, R. J. W. *Dipole Moment*; Methuen: London, 1953.
- 7 Chandra, A. K. *Tetrahedron* **1963**, 19 (3), 471.
- 8 Rowe, I.; Post, B. *Acta Crystallogr.* **1956**, 9 (10), 827.
- 9 Rowe, I.; Post, B. *Acta Crystallogr.* **1958**, 11 (5), 372.
- 10 Shine, H. J.; Piette, L. *J. Am. Chem. Soc.* **1962**, 84 (24), 4798.
- 11 Rapta, P.; Kress, L.; Hapiot, P.; Dunsch, L. *Phys. Chem. Chem. Phys.* **2002**, 4 (17), 4181.
- 12 Becka, J.; Bredowb, T.; Tjahjantoa, R. T. *Z. Naturforsch.* **2009**, 64b, 145.
- 13 Bock, H.; Rauschenbach, A.; Näther, C.; Kleine, M.; Havlas, Z. *Chem. Ber.* **1994**, 127 (10), 2043.
14. Breslow, D. S.; Skolnik, H. *The Chemistry of Heterocyclic Compounds Vol. 21*; John Wiley & Sons, 1966.
- 15 Deryagina, É. N.; Shagun, L. G.; Ivanova, G. M.; Vakul'skaya, T. I.; Modonov, V. B.; Vitkovskii, V. Y.; Voronkov, M. G. *Zh. Org. Khim.* **1978**, 14, 2401.

- 16 Schönberg, A.; Mustafa, A. *J. Chem. Soc.* **1949**, (0), 889.
- 17 Gilman, H.; Swayampati, D. R. *J. Am. Chem. Soc.* **1955**, 77 (22), 5944.
- 18 Gilman, H.; Swayampati, D. *J. Org. Chem.* **1958**, 23 (2), 313.
- 19 Prema, S.; Srinivasan, M. *Eur. Polym. J.* **1987**, 23 (11), 897.
- 20 Still, I. W. J.; Sayeed, V. A. *Synth. Commun.* **1983**, 13 (14), 1181.
- 21 Pawliczek, M.; Garve, L. K. B.; Werz, D. B. *Chem. Commun.* **2015**, 51 (44), 9165.
- 22 Caron, S.; Ghosh, A. Nucleophilic Aromatic Substitution in Practical Synthetic Organic Chemistry; John Wiley & Sons: Hoboken, New Jersey, 2011.
- 23 Bunnett, J. F.; Zahler, R. E. *Chem. Rev.* **1951**, 49 (2), 273.
- 24 Dillard, R. D.; Yen, T. T.; Stark, P.; Pavey, D. E. *J. Med. Chem.* **1980**, 23 (7), 717.
- 25 Reddy, T. J.; Iwama, T.; Halpern, H. J.; Rawal, V. H. *J. Org. Chem.* **2002**, 67 (14), 4635.
- 26 Riebe, S.; Vallet, C.; van der Vight, F.; Gonzalez-Abradelo, D.; Wölper, C.; Strassert, C. A.; Jansen, G.; Knauer, S.; Voskuhl, J. *Chem. Eur. J.* **2017**, 23 (55), 13660.
- 27 Li, C.; Xiao, C.; Li, Y.; Wang, Z. *Org. Lett.* **2013**, 15 (3), 682.
- 28 Dunn, B.; Kamath, H.; Tarascon, J.-M. *Science* **2011**, 334 (6058), 928.
- 29 Wang, W.; Luo, Q.; Li, B.; Wei, X.; Li, L.; Yang, Z. *Adv. Funct. Mater.* **2013**, 23 (8), 970.

- 30 Ding, Y.; Zhang, C.; Zhang, L.; Zhou, Y.; Yu, G. *Chem. Soc. Rev.* **2018**, *47* (1), 69.
- 31 Noack, J.; Roznyatovskaya, N.; Herr, T.; Fischer, P. *Angew. Chem. Int. Ed.* **2015**, *54* (34), 9776.

Chapter 2

Dynamic Self-Correcting Nucleophilic Aromatic Substitution

Abstract

Dynamic covalent chemistry, with its ability to correct synthetic dead-ends, allows for the synthesis of elaborate extended network materials in high yields. However, the limited number of reactions amenable to dynamic covalent chemistry necessarily confines the scope and functionality of materials synthesized. Herein, we explore the dynamic and self-correcting nature of nucleophilic aromatic substitution (S_NAr), using *ortho*-aryldithiols and *ortho*-aryldifluorides that condense to produce redox-active thianthrene units. We demonstrate the facile construction of two-point, three-point and four-point junctions by reaction between a dithiol nucleophile and three different model electrophiles that produces molecules with two, three, and four thianthrene moieties respectively, in excellent yields. The regioselectivity observed is driven by thermodynamics; other connections form under kinetic control. We also show that the same chemistry can be extended to the synthesis of novel ladder macrocycles and porous polymer networks with BET surface area up to $813 \text{ m}^2 \text{ g}^{-1}$.

Parts of this chapter were adapted and reprinted with permission from Ong, W. J.; Swager, T. M. "Dynamic self-correcting nucleophilic aromatic substitution" *Nat. Chem.* **2018**, *10*, 1023.

2.1 Introduction

Dynamic covalent chemistry wherein the facile exchange of molecular components under the conditions of thermodynamic control offers the ability to make extended network materials that are not accessible under statistical kinetic conditions.^{1,2} Specifically, the ability for bonds to form, break, and reform under dynamic equilibrium corrects synthetic dead-ends and enables “error-checking”. This useful feature has been exploited for the synthesis of two-dimensional (2-D) and three dimensional (3-D) structures in high yields, which would otherwise be difficult to achieve under kinetic control.³⁻⁵ Despite a growing interest in the field of dynamic covalent chemistry, the application of dynamic covalent reactions to the synthesis of organic materials has largely been confined to imine condensation,⁶ boronic ester condensation,^{7,8} disulfide exchange,⁹ olefin metathesis,¹⁰ and alkyne metathesis,¹¹ thereby limiting the scope and functionality of materials synthesized.¹² It is therefore desirable to expand the repertoire of dynamic covalent chemistry with other well-established reactions.

Nucleophilic aromatic substitution (S_NAr) is a versatile reaction that has been used in the synthesis of macrocycles,¹³⁻¹⁵ polymers,^{16,17} molecular cages,¹⁸ and cross-linked networks.^{19,20} Interestingly, although S_NAr is known to be reversible, its dynamic nature has rarely been exploited for design and synthesis of novel organic materials.^{21,22} There are abundant opportunities with S_NAr to create high aromatic content materials with electronic properties and complex analogs of highly durable poly(arylethers) and poly(arylsulfides). As a result, we have targeted the dynamic, self-correcting property of S_NAr reactions for the construction of multi-point junctions, to access organic materials with novel architectures and properties.⁵

Our approach to developing useful dynamic S_NAr methods has been to focus on systems that will find thermodynamic minima by producing ring structures. Specifically, we have targeted *ortho*-aryldithiols and *ortho*-aryldifluorides, which condense to produce thianthrenes. The thianthrene structure is interesting as it is non-planar in its neutral state and with reversible oxidation it transforms to a planar state.²³ Using 3,4,5,6-tetrafluorophthalonitrile **1**, hexafluorobenzene **2**, and octafluoronaphthalene **3** as model electrophiles, we can predictably produce two-point, three-point, and four-point junctions by reaction with dithiol nucleophile **4** (Fig. 2.1a). The observed regioselectivity is driven by thermodynamics as other connections form under kinetic conditions (Fig. 2.1b). Accordingly, in one step we produce molecules **5**, **6** and **7** with multiple redox-active thianthrene units. These molecules possess multiple stable oxidation states at high potentials and are hence promising scaffolds for achieving high energy density in redox flow batteries.²⁴ We also report herein that similar dynamic S_NAr condensations with 1,2,4,5-benzenetetrathiol **8** give facile access to ladder macrocycles and polymer networks. We anticipated that the rigidity of the ladder structure, coupled with the non-planar thianthrene units, will be highly beneficial in conferring intrinsic porosity and high surface area to the resulting polymer networks.

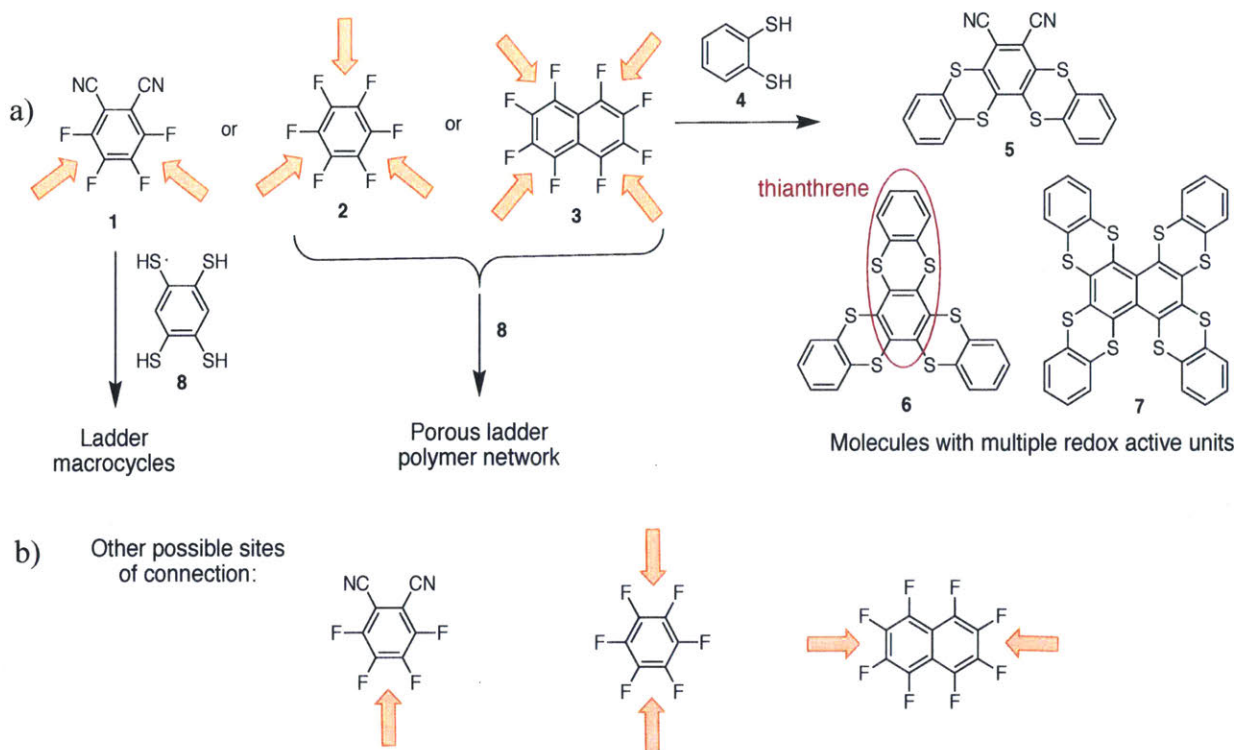


Figure 2.1. Reaction between a dithiol or tetrathiol nucleophile and three different model electrophiles. a) Formation of two-point, three-point, and four-point junctions by S_NAr using 3,4,5,6-tetrafluorophthalonitrile **1**, hexafluorobenzene **2**, and octafluoronaphthalene **3**, respectively. The orange arrows show possible sites for connection to 1,2-benzenedithiol **4** and 1,2,4,5-benzenetetrathiol **8**. Those are thermodynamically favored and lead to ladder macrocycles and networks, respectively, as shown in Figures 2.2 (**5**), 2.5a (**6**) and 2.6a (**7**). b) Under kinetic control, **1**, **2**, and **3** form other connections.

2.2 Results and Discussion

2.2.1 Two-Point Junction

We commenced our dynamic covalent chemical studies by evaluating a model system using **1** as the electrophile and **4** as the nucleophile. All reactions are carried out at both room

temperature and 80 °C, with no observable difference in product distribution or yield. When **1** was subjected to two equivalents of **4**, di-thianthrene **5** is formed in 94% yield (Fig. 2.2a). When one equivalent of **4** was used instead, the symmetrical thianthrene **9** was obtained in 50% yield as the major product, which was accompanied by minor di-thianthrene **5** in 5% yield. The remaining mass balance is a complex mixture of compounds, presumably involving intermediates from the conversion of **9** to **5**. Interestingly, unsymmetrical thianthrene **10** was not observed. Compounds **9** and **10** could be easily differentiated by the number and coupling of ¹⁹F NMR signals observed – **9** being symmetrical has only one singlet while **10** should have two doublets.

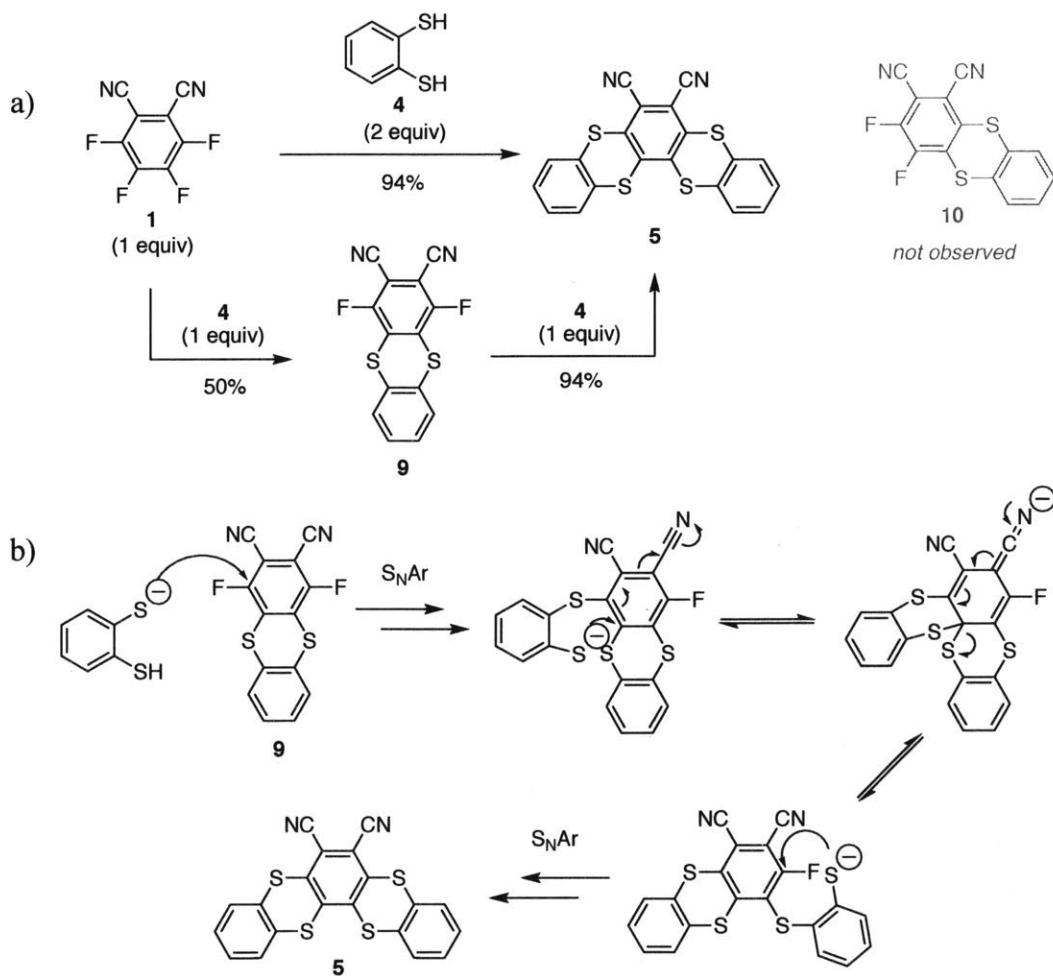


Figure 2.2. Dynamic, self-correcting S_NAr reaction. a) Model reaction illustrating dynamic, self-correcting nature of S_NAr reaction. Conditions: **1** or **9** (1 equiv), **4** (1 or 2 equiv), K_2CO_3 (3 or 6 equiv), DMF, r.t. or 80 °C. b) Proposed mechanism for reaction of **9** with **4**.

The formation of **9**, instead of **10** is interesting because nominally one would expect **10** to be an intermediate en route to **5**. Additionally, when we subject **9** to a further equivalent of **4**, compound **5** was obtained in 94% yield as the sole product. This is important as we obtain the desired product **5** even when we started from the “incorrect” kinetic intermediate **9**, which would have been a synthetic dead-end in the absence of “error-checking”.

Based on these results, we propose that after initial kinetic formation of **9**, the second thiolate displaces one of the remaining fluorides and then reacts with the vicinal carbon to form a transient thioacetal anion, which can reversibly fragment and allow for the error correction (Fig. 2.2b). The liberated thiolate then engages in S_NAr reaction with the remaining fluoride to afford the thermodynamic product **5**.

The fact that **9** reacts with **4** to afford **5** in excellent yield confirms that the C–S bonds can be readily formed, broken, and reformed. To further probe the dynamic nature of the C–S bond, we reacted **5** with 1 and 10 equivalents of toluene-3,4-dithiol **11** at 80 °C (Fig. 2.3a). The reason for selecting methyl substituted **11** as the attacking nucleophile is three-fold: (1) the methyl provides a NMR handle, (2) it has similar nucleophilicity to **4**, and (3) the substitution will not sterically hinder the S_NAr reactions.²⁵

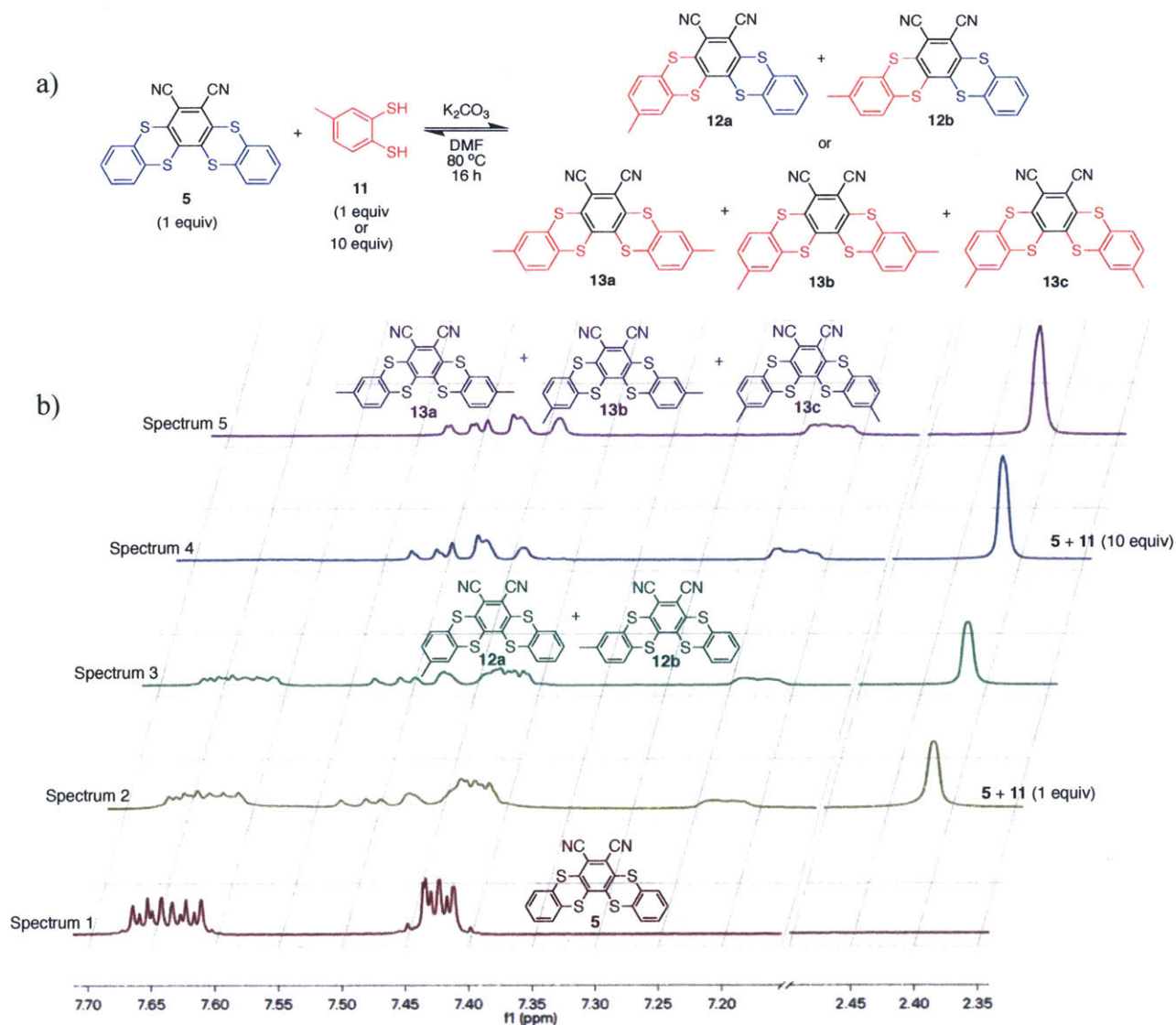


Figure 2.3. Facile exchange of dithiol nucleophiles. a) Substitution of 1,2-benzenedithiol units on **5** with toluene-3,4-dithiol **11**. b) ^1H NMR spectra taken in $\text{TCE-}d_2$ at 85°C showing facile exchange of benzenedithiols (Spectrum 1: **5**, Spectrum 2: crude product of **5** (1 equiv) and **11** (1 equiv), Spectrum 3: **12a–b**, Spectrum 4: crude product of **5** (1 equiv) and **11** (10 equiv), Spectrum 5: **13a–c**).

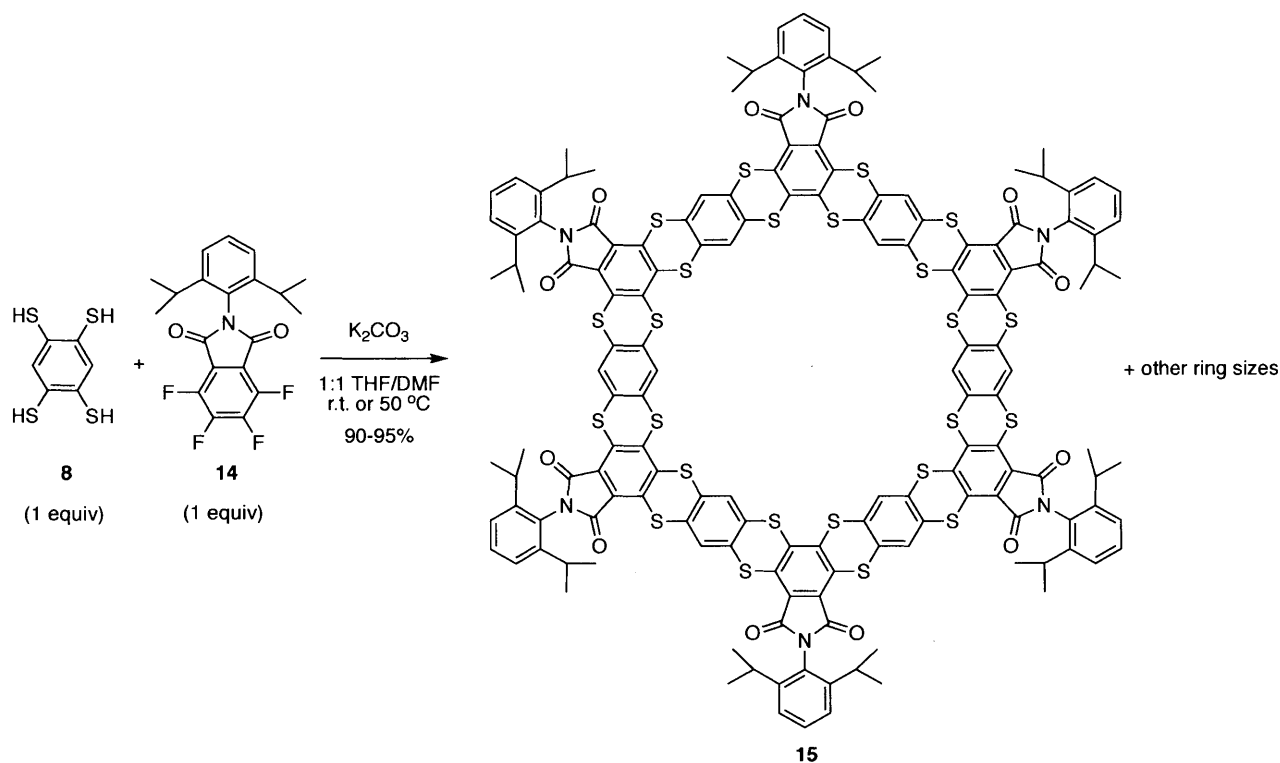
The equilibrium shown in Fig. 2.3 is analyzed by ^1H NMR wherein depending on the progression and equivalents of **11** we expect to see new signals for two single-substituted isomers **12a–b** and three double-substituted isomers **13a–c**. In this analysis, we perform a rough reaction workup with a MeOH washing to remove excess starting materials. For reference, the single-substituted isomers **12a–b** were prepared separately by reacting **9** with one equivalent of **11**, while double-substituted isomers **13a–c** were prepared by reacting **1** directly with two equivalents of **11**. When **5** (spectrum 1) was subjected to one equivalent of **11**, the NMR spectrum of the product (spectrum 2) displays signals for **12a–b** (spectrum 3), suggesting that **11** is incorporated into **5** to give **12a–b** (Fig. 2.3b). The formation of **12** in the reaction was further confirmed by the observation of the $[\text{12}+\text{NH}_4]^+$ molecular ion peak in HRMS. When **5** is subjected to 10 equivalents of **11**, the NMR spectrum of the product (spectrum 4) is that of **13a–c** (spectrum 5). The formation of compound **13** was again confirmed by the observation of the molecular ion $[\text{13}+\text{NH}_4]^+$ using HRMS. Given the huge excess of **11** used, virtually all the original aryl thiol ethers in **5** have been displaced by **11** to afford **13**. Taken together, the results in Fig. 2.2 and 2.3 demonstrate the dynamic nature of $\text{S}_{\text{N}}\text{Ar}$ under relatively mild conditions, and more importantly, the possibility of correcting synthetic dead-ends.

Encouraged by reversible formation of two-point junctions, we have investigated $\text{S}_{\text{N}}\text{Ar}$ synthesis of ladder macrocycles. Attempts to synthesize the ladder macrocycle directly from **1** and 1,2,4,5-benzenetetrathiol **8** resulted in an insoluble orange solid that was difficult to characterize. Thus, we replaced the activating nitrile groups of **1** with the imide in 2-(2,6-diisopropylphenyl)-4,5,6,7-tetrafluoroisindoline-1,3-dione **14**.²⁶ The imide group allows for the attachment of solubilizing side-chains, in addition to having comparable electron-withdrawing activation of the substrate and chemical stability under basic conditions.²⁶⁻²⁸

To demonstrate that imide **14** behaves as a similar electrophile to **1** in dynamic S_NAr reactions, we performed a model reaction analogous to Fig. 2.2 using **14** and **4** (Supplementary Fig. 2.1). The symmetrical thianthrene was obtained in 90% yield when one equivalent of **4** was used, and the di-thianthrene was obtained in either 93% yield directly from **14** using two equivalents of **4** or in 87% yield after further addition of one equivalent of **4** to the symmetrical thianthrene. The higher yield obtained for this symmetrical thianthrene as compared to **9** is likely the result of a lower propensity to react with a second dithiol **4**. In addition to the imide functional group as the electron-withdrawing group in the electrophile, we also tested other ester and amide functional groups, and found them to be unsuitable in model reactions. Specifically, esters are too labile under basic conditions and amides are insufficient electron-withdrawing groups for the S_NAr reaction (Supplementary Fig. 2.1).

Using **8** as the nucleophile and **14** as the electrophile, we were able to synthesize a mixture of ladder macrocycles **15** in 90-95% yield at both 0.005 M and 0.1 M concentration of each monomer (Scheme 2.1). At 0.005 M monomer concentration, the reaction requires 5 days to complete at room temperature or 2 days at 50 °C. At 0.1 M monomer concentration, we were able to achieve faster equilibration and the reactions were found to be complete by 2 days at room temperature or 1 day at 50 °C. We also tested different imides and find that the diisopropylphenyl imide yields a macrocycle with excellent solubility (>30 mg/mL) while a *n*-tetradecyl side chain affords an insoluble macrocycle. MALDI Mass Spectrometric analysis of **15** shows a mixture of ladder macrocycles with different ring sizes (Supplementary Fig. 2.2). The highest intensity peak corresponds to the macrocycle shown (6 repeating units). The observed isotopic MALDI-MS distribution corresponds well to the isotopic distribution calculated for the macrocycles of different ring sizes, confirming that macrocycles are formed instead of linear oligomers. Moreover, the high

yield (90-95%) obtained provides further evidence for efficient thermodynamic conversion to the two-point junctions. Attempts to separate the macrocycles by recycling preparative gel permeation chromatography and flash column chromatography on silica gel proved ineffective in the isolation of pure individual macrocycles with different ring sizes. Photophysical measurements of **15** reveal a large Stokes shift of 162 nm in the absorption and emission spectra (Supplementary Fig. 2.3). Additionally, cyclic voltammetry shows that **15** is redox active with $E_{1/2} = 1.02$ V vs. Fc/Fc⁺, which is as expected higher than thianthrene ($E_{1/2} = 0.82$ V vs. Fc/Fc⁺) as a result of the electron-withdrawing effect of the imide group.



Scheme 2.1. Synthesis of ladder macrocycle **15**. Monomers **8** and **14** at 0.005 M and 0.1 M concentration give the same mixture of ladder macrocycles in excellent yields. Faster equilibration and reaction time can be achieved by heating or using higher concentration.

2.2.2 Three-Point Junction

After successful demonstration of the two-point junction systems, we directed our efforts to more complex structures. Higher connectivity is afforded by perfluoroarene electrophiles **2** and **3** that provide for three- and four-point junctions, respectively. Although the lower S_NAr reactivity of **2** and **3** as compared to **1** dictates harsher reactions conditions to correct synthetic dead-ends, we hypothesized that the initial lower reactivity is compensated with the formation of activating thioethers as the reaction progresses.^{29,30} The activating nature of the thioether residue is supported by the observation that when **9** is subjected to one equivalent of thiophenol, the di-substituted product is formed exclusively in 80% yield with respect to thiophenol, and the expected mono-substituted product is not observed (Supplementary Fig. 2.4). Hence, a *para*-thioether is better at stabilizing the negatively charged S_NAr intermediate than a corresponding fluorine. Similar *para*-thioether directing/activating effects have been previously reported.³¹

Hexafluorobenzene **2** has proved to be a viable electrophile and when subjected to two equivalents of **4** at room temperature in DMF, di-thianthrene **16** is obtained in 91% yield (Fig 2.4a, Supplementary Fig. 2.5). Similarly, with three equivalents of **4** at 80 °C for 16 h, a mixture of **16** (major) and tri-thianthrene **6** (minor) was obtained. Optimized conditions of 120°C in DMF/THF for 2 days produced the tri-thianthrene **6** in 84% yield. The identities of **16** and **6** were confirmed by using HRMS and ¹⁹F and ¹H NMR spectroscopy. Neither the mono-thianthrene **17** nor *ortho*-di-thianthrene product **18** were observed in the reactions between **2** and **4**. Cyclic voltammetry of **16** shows two redox peaks at $E_{1/2} = 0.96$ V and 1.19 V vs. Fc/Fc⁺, while that of **6** shows three redox peaks at $E_{1/2} = 0.82$ V, 1.23 V, and 1.56 V vs. Fc/Fc⁺ (Supplementary Fig. 2.10 and 2.11).

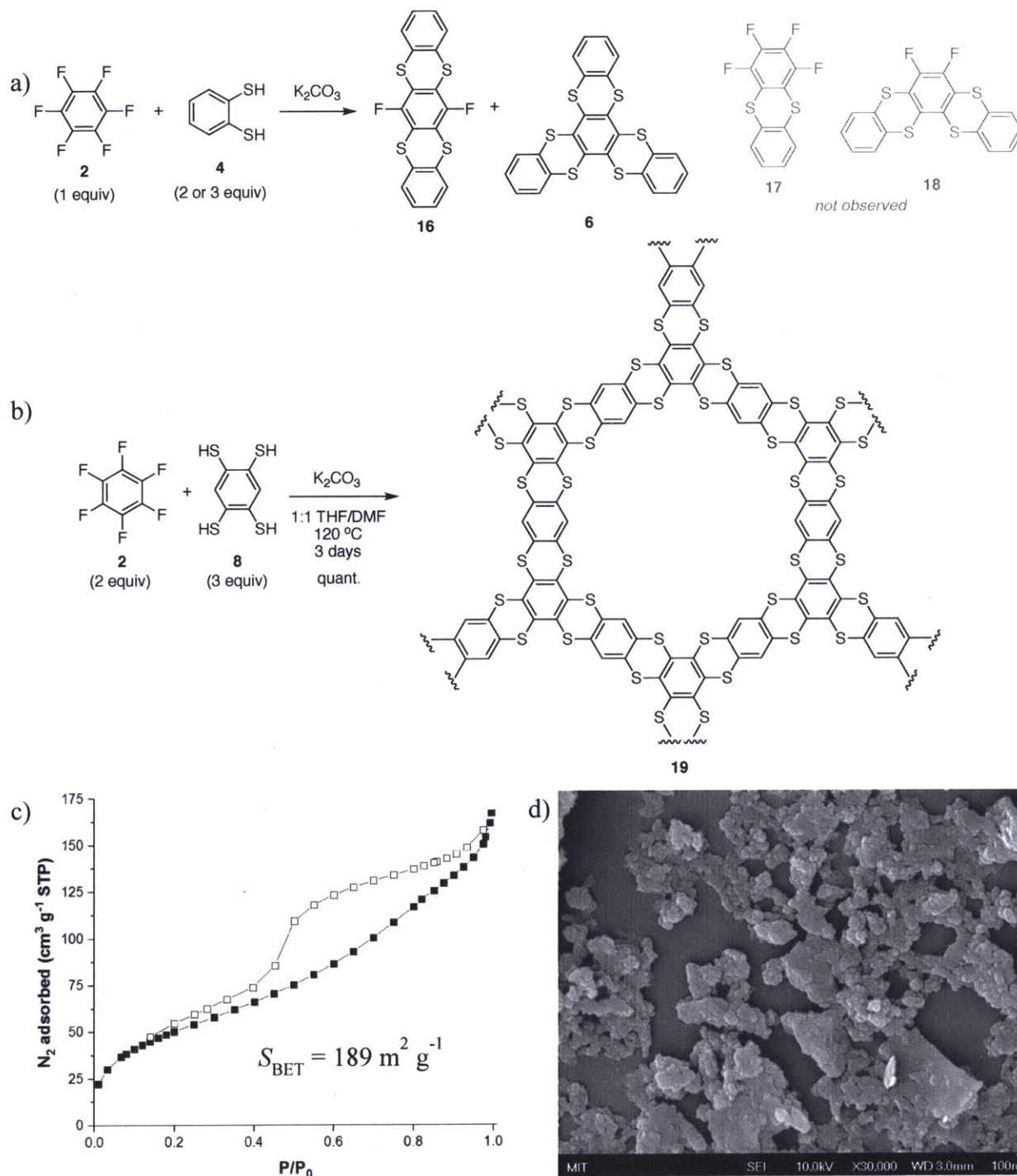


Figure 2.4. Model reaction, synthesis and characterization of porous ladder polymer network **19**.
 a) Reactions of **2** (1 equiv) with **4** (2 or 3 equiv) under various conditions to afford only **16**, a mixture of **16** and **6**, or only **6**. b) Synthesis of porous ladder polymer network **19** using **2** and **8** as

monomers. c) N₂ adsorption (filled squares) and desorption (hollow squares) isotherms of **19**. S_{BET} is the Brunauer–Emmett–Teller surface area, and P and P_0 are the equilibrium and saturation pressures of N₂ at 77 K respectively. d) SEM image ($\times 30,000$ magnification) of **19** drop-casted using a dispersion of **19** in DMF onto silicon wafer.

Having established that **2** displays dynamic covalent processes, we targeted extended systems by pairing it with **8** at 120 °C for 3 days to afford a yellow solid in quantitative yield (Fig. 2.4b). A plausible structure of **19** is included to illustrate the three-point junction, though other ring sizes are likely also present as evidenced by different rings obtained in the synthesis of macrocycle **15**. The resultant ladder polymer network **19** exhibits intrinsic porosity and a Type II adsorption isotherm indicative of a macroporous structure,³² and a Brunauer–Emmett–Teller (BET) surface area of 189 m² g⁻¹ (Fig. 2.4c). The desorption displays Type H2 hysteresis, which suggests differences in that adsorption and desorption mechanisms.³² Scanning electron microscope (SEM) image of **19** revealed agglomeration of small ≈ 10 nm particles into flakes and larger sheets (Fig. 2.4d). Comparison of the infrared spectrum of **19** and the absence of SH bands at 2536 and 2517 cm⁻¹ indicates that monomers **2** and **8** are consumed and converted to the porous polymer network (Supplementary Fig. 2.13). X-ray photoelectron spectroscopy (XPS) of **19** indicates the presence of carbon, sulfur and fluorine (Supplementary Fig. 2.14). With each successive S_NAr reaction, one fluorine atom is replaced by one sulfur atom. Hence, the stoichiometric ratio of sulfur to fluorine as determined by XPS provides a measure for the extent of polymerization, and is calculated to be only 3.5 for **19**, presumably as a result of poor solubility and precipitation before the reaction goes to completion. It is plausible that the bulk of **19** has a higher stoichiometric ratio of sulfur to fluorine than 3.5. Thermogravimetric analysis (TGA) of **19**

reveals a 10% weight loss at 305 °C, with a gradual increase in the rate of weight loss with increasing temperature (Supplementary Fig. 2.15).

2.2.3 Four-Point Junction

The three-point junction of **19** necessarily results in sizable pores and rings larger than 6 repeating units are likely present as noted above. These effects can produce a partial interpenetrating network that prevents a regular structure for **19**. We hypothesized that a reduction in the pore size of a ladder polymer network could be accomplished by moving to a four-point junction. In restricting the pore size, we eliminate the possibility of forming interpenetrating polymer networks. To demonstrate a four-point junction we reacted octafluoronaphthalene **3** with **4** to provide tetra-thianthrene product **7** in 88% yield (Fig. 2.5a). Cyclic voltammetry of **7** reveals four distinct redox peaks at $E_{1/2} = 0.77$ V, 0.98 V, 1.39 V, and 1.54 V vs. Fc/Fc⁺ (Fig. 2.5b).

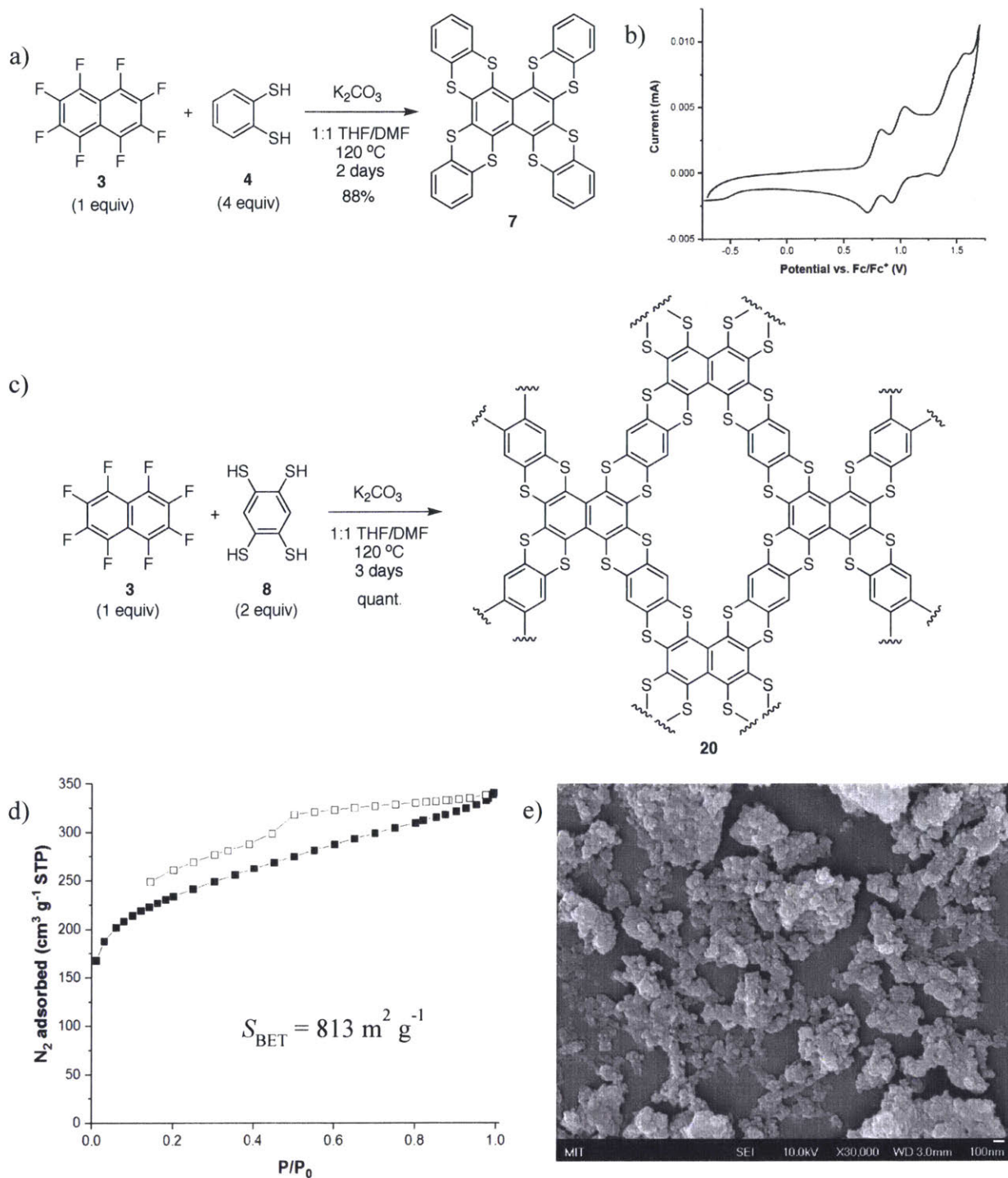


Figure 2.5. Model reaction, synthesis and characterization of porous ladder polymer network **20**.

a) Synthesis of tetra-substituted product **7** using **3** and **4**. b) Cyclic voltammetry of **7** showing four distinct redox signals. c) Synthesis of porous ladder polymer network **20** using **3** and **8** as

monomers. d) N₂ adsorption (filled squares) and desorption (hollow squares) isotherms of **20**. S_{BET} is Brunauer–Emmett–Teller surface area, and P and P₀ are the equilibrium and saturation pressures of N₂ at 77 K respectively. e) SEM image (×30,000 magnification) of **20** drop-casted using a dispersion of **20** in DMF onto silicon wafer.

Ladder polymer **20** with four-point junctions is produced by reacted **3** with **8** at 120 °C for 3 days (Fig. 2.5c). The idealized structure of **20** is included to illustrate the four-point junction. The brick-red solid is produced in quantitative yield and has different porosity than **19**. Specifically a Type I isotherm and a large absorption volume at low relative pressure suggests a microporous structure.³² The upward slope of the adsorption branch at higher relative pressures further suggests that larger pores are also present (Fig. 2.5d).³³ The hysteric step observed in the desorption branch indicates that the pores are not all slit-like.³⁴ The BET surface area calculated from N₂ adsorption isotherm of **20** is 813 m² g⁻¹, which is significantly higher than that of **19** and is comparable to other microporous polymers.²⁸ The SEM image of **20** also shows agglomeration of small particles of the order of tens of nanometer in length into flakes and larger sheets (Fig. 2.5e). This structure, like that of **19**, is likely responsible for the larger pores. However, when compared to **19**, the agglomeration in **20** is less extensive and can account for its higher BET surface area. The incorporation of monomers **3** and **8** into the porous polymer network and the complete consumption of thiols was again confirmed by infrared spectroscopy (Supplementary Fig. 2.18). XPS of **20** also indicates the presence of carbon, sulfur and fluorine (Supplementary Fig. 2.19), similar to **19**. The stoichiometric ratio of sulfur to fluorine is calculated to be 7.2 for **20**, suggesting a higher degree of polymerization of **3** as compared to **2**. In contrast to **19**, the TGA of **20** reveals a more linear weight loss with temperature (Supplementary Fig. 2.20).

2.3 Conclusions

By exploiting the dynamic and self-correcting feature of the S_NAr reaction, we were able to achieve facile construction of two-point, three-point and four-point junctions to afford molecules with two, three and four thianthrene units in excellent yields. These molecules exhibiting multiple redox peaks at high potentials are promising electroactive species for organic redox flow batteries, and efforts to determine their performance are underway. The same chemistry has also been applied to the synthesis of ladder macrocycles and porous polymer networks, with BET surface area up to $813 \text{ m}^2 \text{ g}^{-1}$. Efforts to further exploit the S_NAr reaction, and other well-established dynamic covalent reactions,^{35,36} are underway.

2.4 Experimental Details

2.4.1 General

Anhydrous DMF was purchased from Aldrich as Sure-Seal Bottles and used as received. CH_2Cl_2 and THF were purified by passage through two alumina columns of an Inert solvent purification system. All other chemicals were of reagent grade and used as received. All air and water sensitive synthetic manipulations were performed in flame-dried glassware under an argon atmosphere using standard Schlenk techniques.

NMR spectra were recorded on a 400 MHz or 500 MHz spectrometer. High temperature NMR spectra were recorded at $85 \text{ }^\circ\text{C}$ using TCE- d_2 , DMSO- d_6 , or *o*-DCB- d_4 as solvent. Chemical shifts δ are reported in ppm downfield from tetramethylsilane using the residual solvent signals (CDCl_3 : δ_{H} 7.26 ppm, δ_{C} 77.16 ppm / CD_2Cl_2 : δ_{H} 5.32 ppm, δ_{C} 53.84 ppm / TCE- d_2 : δ_{H} 6.00 ppm, δ_{C} 73.78 ppm / DMSO- d_6 : δ_{H} 2.50 ppm, δ_{C} 39.52 ppm / *o*-DCB- d_4 : δ_{H} 7.19 ppm, δ_{H} 6.93 ppm), or

α,α,α -trifluorotoluene (δ_F -63.72 ppm) as an internal reference. For ^1H NMR, coupling constants J are given in Hz and the resonance multiplicity is described as s (singlet), d (doublet), t (triplet), sept (septet), dd (doublet of doublets), m (multiplet), and br (broad).

High-resolution mass spectrometry (HRMS) was performed using an Ion Cyclotron Resonance Mass Spectrometer with either Electrospray Ionization (ESI) or Direct Analysis in Real Time (DART) as the ionization technique. Where noted, additional mass spectra were obtained using Matrix-Assisted Laser Desorption/Ionization-Time-of-Flight (MALDI-TOF). MALDI samples were prepared by dissolving 0.5 mg of sample in 300 μL of THF, followed by mixing 20 μL of the sample solution with 20 μL of *trans*-2-[3-(4-*tert*-butylphenyl)-2-methyl-2-propenylidene]malononitrile matrix (50 mg in 1 mL of THF) and 1 μL of sodium trifluoroacetate dopant (1 mg in 1 mL of THF), and finally spotting 1 μL of the resultant mixture.

UV-vis spectroscopy was recorded on a UV-vis spectrophotometer, and corrected for background signal with a solvent-filled cuvette. Fluorescence spectra were measured using right-angle detection. Samples were excited with a 450 W xenon short arc lamp, and fluorescence was detected with a detector. All photophysical measurements were performed with spectral grade CH_2Cl_2 .

Electrochemical measurements were carried at a scan rate of 50 mV s^{-1} in anhydrous 4:1 *o*-DCB/MeCN electrolyte, using a three-electrode cell configuration consisting of a quasi-internal Ag wire reference electrode submerged in 0.01 M AgNO_3 /0.1 M tetrabutylammonium hexafluorophosphate (TBAPF₆) anhydrous MeCN solution, a Pt button (1.6 mm in diameter) working electrode, and a Pt coil counter electrode. All potentials were referenced to the ferrocene/ferrocenium (Fc/Fc^+) redox couple.

Surface area measurements were conducted on a Micromeritics ASAP 2020 Accelerated Surface Area and Porosimetry Analyzer. Each sample (30–50 mg) was degassed at 80 °C for 12 h and then backfilled with N₂. N₂ isotherms were generated by incremental exposure to ultrahigh-purity nitrogen up to 1 atm in a liquid nitrogen (77 K) bath, and surface parameters were determined using BET adsorption models included in the instrument software (Micromeritics ASAP 2020 V3.03).

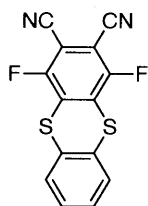
The surface morphology was investigated using a scanning electron microscope (SEM) (JEOL JSM-6700F FESEM) with an accelerating voltage of 10 kV. Prior to characterization, the samples were Au/Pd sputter-coated with a thickness of 4 nm in a sputter coater (Denton Vacuum Desk V). X-ray diffraction (XRD) analysis was carried out using a diffractometer (PANalytical X'Pert Pro MPD) with Cu K α radiation, 0.15418 nm. Thermogravimetric analysis (TGA) was carried out with TA Instruments Q50 at 10 °C min⁻¹ under N₂ atmosphere. Infrared (IR) spectra were measured on Thermo Scientific Nicolet 6700 Fourier Transform Infrared Spectrometer using the Attenuated Total Reflectance (ATR) mode on a germanium crystal.

X-ray photoelectron spectroscopy (XPS) measurements were performed on a Physical Electronics Versaprobe II X-ray photoelectron spectrometer with a hemispherical energy analyzer and a monochromated X-ray source (Al K α , 1486.6 eV). Survey scans were collected with a X-ray setting of 200 μ m, 50 W, and 15 kV and a pass energy of 187.85 eV at a base pressure of 10⁻⁹ Torr. XPS spectra were processed with the MultiPak software.

¹H–¹³C cross-polarization (CP) magic-angle spinning (MAS) experiments were performed on a home-built 500 MHz spectrometer (courtesy of Dr. D. Ruben, FBML-MIT) equipped with a 3.2 mm Bruker (Billerica, MA) triple-resonance MAS probe. Experiments were performed at room

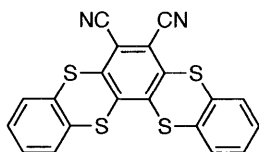
temperature and a MAS frequency of 20 kHz. The pulse width of the ^1H $\pi/2$ pulse was 3 μs , followed by a CP contact time of 2 ms and an acquisition period of 7.6 ms with TPPM proton decoupling. Spectra were referenced to adamantane (40.49 ppm) relative to DSS (0 ppm). The number of scans for the ^{13}C NMR spectra of **19** and **20** were 8192 and 4096 scans, respectively, with a recycle delay of 3 s between scans.

2.4.2 Synthetic Procedures



1,4-Difluorothianthrene-2,3-dicarbonitrile (**9**)

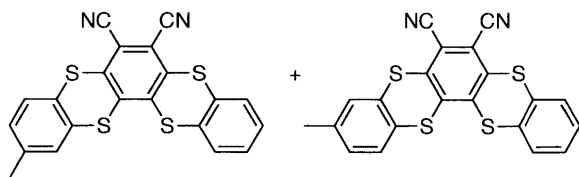
To a Schlenk flask with a stirrer containing 3,4,5,6-tetrafluorophthalonitrile (100 mg, 0.5 mmol) and K_2CO_3 (207 mg, 1.5 mmol) under argon was added DMF (5 mL) and 1,2-benzenedithiol (57.5 μL , 0.5 mmol). The reaction was stirred at room temperature or 80 $^\circ\text{C}$ for 16 h. The mixture was cooled and precipitated into an aqueous 1 M HCl solution. The precipitate was dissolved in CH_2Cl_2 and filtered. The filtrate was concentrated and purified by gel column chromatography using 1:1 toluene/hexane to toluene to obtain **9** as a yellow powder (76.1 mg, 50%). R_f (toluene) = 0.6. ^1H NMR (500 MHz, CDCl_3): δ 7.52 (dd, J = 5.9, 3.4 Hz, 2H), 7.40 (dd, J = 5.9, 3.4 Hz, 2H). ^{19}F NMR (471 MHz, CDCl_3): -104.6 (s). ^{13}C NMR (126 MHz, CDCl_3) δ 155.7 (d, J = 259.3 Hz), 134.4 (dd, J = 15.0, 7.7 Hz), 130.9, 129.9, 129.8, 109.8, 102.3 (dd, J = 16.7, 6.7 Hz). HRMS (DART) m/z calculated for $\text{C}_{14}\text{H}_8\text{F}_2\text{N}_3\text{S}_2$ $[\text{M}+\text{NH}_4]^+$: 320.0122, found 320.0138.



Benzo[5,6][1,4]dithiino[2,3-*a*]thianthrene-6,7-dicarbonitrile (5)

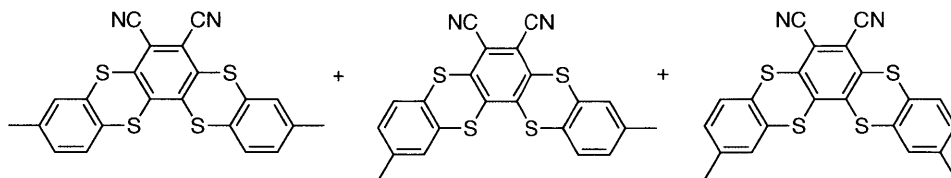
To a Schlenk flask with a stirrer bar containing 3,4,5,6-tetrafluorophthalonitrile (100 mg, 0.5 mmol) and K_2CO_3 (415 mg, 3.0 mmol) under argon was added DMF (5 mL) and 1,2-benzenedithiol (115 μ L, 1.0 mmol). The reaction was stirred at room temperature or 80 °C for 16 h. The mixture was precipitated into an aqueous 1 M HCl solution, filtered and washed with water and methanol to obtain **5** as a yellow powder (190.8 mg, 94%). 1H NMR (400 MHz, $DMSO-d_6$, 85 °C): 7.76–7.69 (4H, m), 7.51–7.46 (4H, m). A ^{13}C NMR could not be obtained due to insufficient solubility. HRMS (DART) m/z calculated for $C_{20}H_{12}N_3S_4$ $[M+NH_4]^+$: 421.9909, found 421.9911.

Alternatively, to a Schlenk flask with a stirrer bar containing **9** (30 mg, 0.1 mmol) and K_2CO_3 (41.5 mg, 0.3 mmol) under argon was added DMF (2 mL) and 1,2-benzenedithiol (11.5 μ L, 0.1 mmol). The reaction was stirred at 80 °C or room temperature for 16 h. The mixture precipitated into an aqueous 1 M HCl solution and filtered. The precipitate was washed with water, methanol and then a 1:3 CH_2Cl_2 /ethanol mixture to obtain a yellow powder (37.9 mg, 94%).



Methylbenzo[5,6][1,4]dithiino[2,3-*a*]thianthrene-6,7-dicarbonitrile (12)

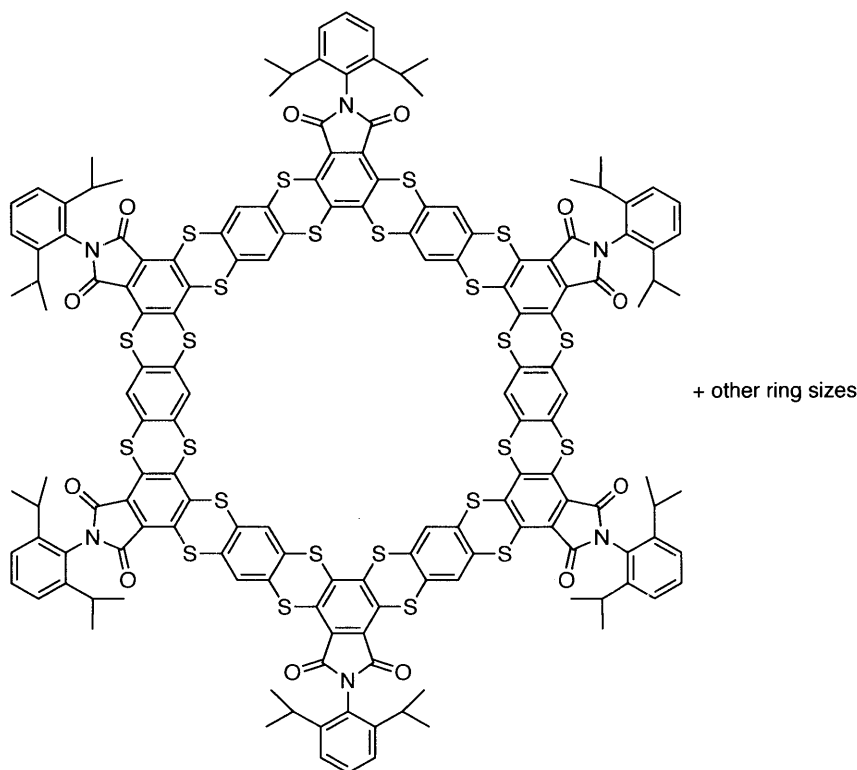
To a Schlenk flask with a stirrer bar containing **9** (30 mg, 0.1 mmol) and K_2CO_3 (41.5 mg, 0.3 mmol) under argon was added DMF (2 mL) and toluene-3,4-dithiol (13.3 μ L, 0.1 mmol). The reaction was stirred at room temperature for 16 h. The mixture was precipitated into an aqueous 1 M HCl solution and filtered. The precipitate was washed with water, methanol and then a 1:3 CH_2Cl_2 /EtOH mixture to obtain a yellow powder as a mixture of two isomers (33.2 mg, 79%). 1H NMR (400 MHz, TCE- d_2 , 85 $^\circ$ C) δ 7.66–7.61 (m, 2H), 7.53–7.41 (m, 4H), 7.24–7.22 (m, 1H), 2.41 (s, 3H). HRMS (DART) m/z calculated for $C_{21}H_{14}N_3S_4$ $[M+NH_4]^+$: 436.0065, found 436.0067.



Dimethylbenzo[5,6][1,4]dithiino[2,3-*a*]thianthrene-6,7-dicarbonitrile (13)

To a Schlenk flask with a stirrer bar containing 3,4,5,6-tetrafluorophthalonitrile (100 mg, 0.5 mmol) and K_2CO_3 (415 mg, 3.0 mmol) under argon was added DMF (5 mL) and toluene-3,4-dithiol (132 μ L, 1.0 mmol). The reaction was stirred at room temperature for 16 h. The mixture was precipitated into an aqueous 1 M HCl solution, filtered and washed with water and methanol to obtain a yellow powder as a mixture of three isomers (200.5 mg, 93%). 1H NMR (400 MHz,

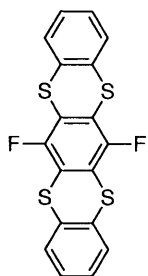
TCE-*d*₂, 85 °C) δ 7.51 (dd, *J* = 8.1, 1.5 Hz, 1H), 7.48 (d, *J* = 8.1 Hz, 1H), 7.47–7.44 (m, 2H), 7.24–7.21 (m, 2H), 2.41 (s, 6H). **HRMS** (DART) *m/z* calculated for C₂₂H₁₆N₃S₄ [M+NH₄]⁺: 450.0222, found 450.0227.



Ladder Macrocycle (15)

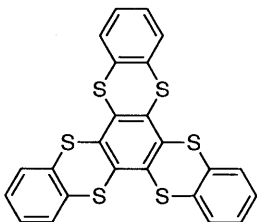
To a sealed tube with a stirrer bar containing K₂CO₃ (83 mg, 0.60 mmol), 2-(2,6-diisopropylphenyl)-4,5,6,7-tetrafluoroisindoline-1,3-dione (37.9 mg, 0.10 mmol) and 1,2,4,5-benzenetetrathiol (20.6 mg, 0.10 mmol) under argon was added THF (0.5 mL) and DMF (0.5 mL). The reaction was stirred at room temperature for 2 days or at 50 °C for 1 day. The mixture was concentrated and precipitated into an aqueous 1 M HCl solution. The precipitate was filtered and washed with water, methanol, hexane, acetone and ethyl acetate to obtain an orange solid as a mixture of macrocycles with different ring sizes (48.0 mg, 95%). Alternatively, the reaction can

also be performed under high dilution conditions using THF (10 mL) and DMF (10 mL) at room temperature for 5 days or at 50 °C for 2 days to obtain the product in comparable yield. **¹H NMR** (500 MHz, TCE-*d*₂) δ 7.79–7.69 (m, 2H), 7.47 (br, 1H), 7.28 (br, 2H), 2.60 (br, 2H), 1.14 (br, 12H) for repeat unit. **¹³C NMR** (126 MHz, TCE-*d*₂) δ 165.2, 146.9, 140.8, 133.9, 133.5, 133.0, 130.3, 128.6 (br), 126.5, 126.1, 123.9, 29.2, 24.0 for repeat unit.



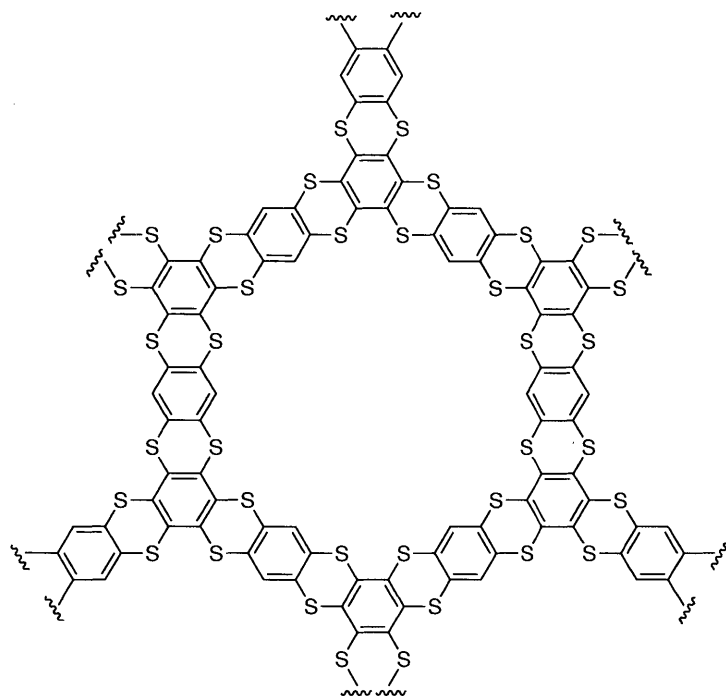
6,13-Difluorobenzo[5,6][1,4]dithiino[2,3-*b*]thianthrene (16)

To a Schlenk flask with a stirrer bar containing K₂CO₃ (0.415 g, 3.0 mmol) under argon was added DMF (5 mL), hexafluorobenzene (57.7 μL, 0.5 mmol) and 1,2-benzenedithiol (115 μL, 1.0 mmol). The reaction was stirred at room temperature for 16 h. The mixture was precipitated into an aqueous 1 M HCl solution, filtered and washed with water and methanol to obtain **16** as a white powder (178.1 mg, 91%). **¹H NMR** (500 MHz, DMSO-*d*₆, 85 °C) δ 7.65 (dd, *J* = 5.8, 3.3 Hz, 4H), 7.41 (dd, *J* = 5.8, 3.3 Hz, 4H). A **¹³C NMR** could not be obtained due to insufficient solubility. **¹⁹F NMR** (471 MHz, DMSO-*d*₆, 85 °C) δ -112.8. **HRMS** (DART) *m/z* calculated for C₁₈H₈F₂S₄ [M]⁺: 389.9477, found 389.9486.



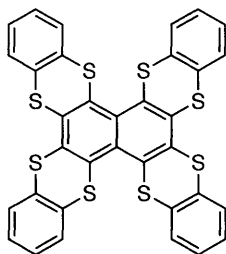
Benzo[5,6][1,4]dithiino[2,3-*a*]benzo[5,6][1,4]dithiino[2,3-*c*]thianthrene (6)

To a sealed tube with a stirrer bar containing K_2CO_3 (0.622 g, 4.5 mmol) under argon was added DMF (10 mL), hexafluorobenzene (57.7 μ L, 0.5 mmol), 1,2-benzenedithiol (173 μ L, 1.5 mmol) and THF (10 mL). The reaction was stirred at 120 °C for 2 days. The mixture was concentrated and precipitated into an aqueous 1 M HCl solution. The precipitate was filtered and washed with water and methanol to afford **6** as a white solid (205.8 mg, 84%). 1H NMR (500 MHz, TCE- d_2 , 85°C) δ 7.63 (dd, $J = 5.8, 3.3$ Hz, 6H), 7.33 (dd, $J = 5.8, 3.3$ Hz, 6H). ^{13}C NMR (126 MHz, TCE- d_2 , 85°C) δ 134.9, 134.5, 128.9, 128.1. HRMS (DART) m/z calculated for $C_{24}H_{16}NS_6$ $[M+NH_4]^+$: 509.9602, found 509.9611.



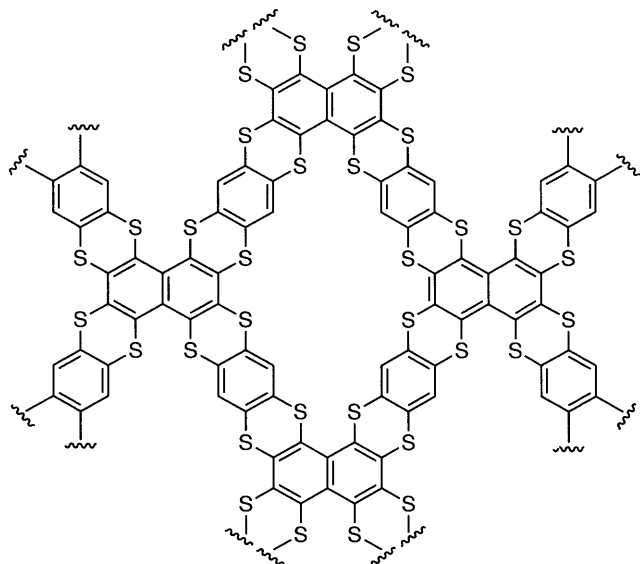
Porous ladder polymer network (19)

To a sealed tube with a stirrer bar containing K_2CO_3 (332 mg, 2.4 mmol) and 1,2,4,5-benzenetetrathiol (82.5 mg, 0.4 mmol) under argon was added THF (20 mL), hexafluorobenzene (30.8 μ L, 0.267 mmol) and DMF (20 mL). On addition of DMF, yellow solution turned orange solution. The reaction was stirred at 120 $^{\circ}C$ for 3 days. The mixture was concentrated and precipitated into an aqueous 1 M HCl solution. The precipitate was filtered and washed with water and THF to obtain **19** as a yellow solid (100 mg, quant.).



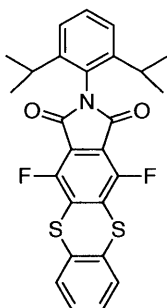
Benzo[5',6']][1,4]dithiino[2',3':3,4]thianthreno[1,2-*a*]benzo[5,6][1,4]dithiino[2,3-*c*]thianthrene (7)

To a sealed tube with a stirrer bar containing K_2CO_3 (0.829 g, 6.0 mmol) and octafluoronaphthalene (136.05 mg, 0.5 mmol) under argon was added THF (10 mL), DMF (10 mL) and 1,2-benzenedithiol (230 μ L, 2.0 mmol). The reaction was stirred at 120 °C for 2 days. The mixture was concentrated and precipitated into an aqueous 1 M HCl solution. The precipitate was filtered and washed with water and methanol to afford **7** as a bright yellow powder (298.4 mg, 88%). 1H NMR (500 MHz, TCE- d_2 , 85 °C) δ 7.71 (dd, $J = 7.5, 1.6$ Hz, 4H), 7.62 (dd, $J = 7.4, 1.7$ Hz, 4H), 7.38–7.31 (m, 8H). ^{13}C NMR (126 MHz, TCE- d_2 , 85 °C) δ 137.5, 137.1, 136.7, 133.5, 133.2, 128.83, 128.79, 128.2, 128.1. HRMS (DART) m/z calculated for $C_{34}H_{16}S_8$ $[M]^-$: 679.9018, found 679.9026.



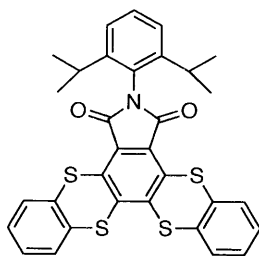
Porous ladder polymer network (20)

To a sealed tube with a stirrer bar containing K_2CO_3 (332 mg, 2.4 mmol), octafluoronaphthalene (54.4 mg, 0.2 mmol) and 1,2,4,5-benzenetetrathiol (82.5 mg, 0.4 mmol) under argon was added THF (20 mL) and DMF (20 mmol). On addition of DMF, yellow solution turned red solution. The reaction was stirred at 120 °C for 3 days. The mixture was concentrated and precipitated into an aqueous 1 M HCl solution. The precipitate was filtered and washed with water and THF to obtain **20** as a brick-red solid (105 mg, quant.).



2-(2,6-Diisopropylphenyl)-4,11-difluoro-1*H*-benzo[5,6][1,4]dithiino[2,3-*f*]isoindole-1,3(2*H*)-dione (S2)

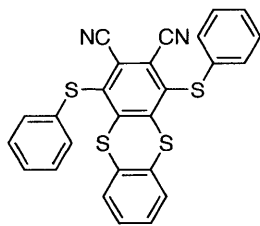
To a Schlenk flask with a stirrer bar containing 2-(2,6-diisopropylphenyl)-4,5,6,7-tetrafluoroisoindoline-1,3-dione (190 mg, 0.5 mmol) and K_2CO_3 (207 mg, 1.5 mol) under argon was added THF (2.5 mL), 1,2-benzenedithiol (58 μ L, 0.5 mmol) and DMF (2.5 mL). The reaction was stirred at room temperature for 16 h. The mixture was concentrated and precipitated into an aqueous 1 M HCl solution. The precipitate was filtered, washed with water and methanol and purified by gel column chromatography using 1:1 toluene/hexane to give **S2** as a yellow powder (216.7 mg, 90%). $R_f = 0.35$ (1:1 toluene/hexane). 1H NMR (400 MHz, $CDCl_3$): δ 7.56 (dd, $J = 5.8, 3.4$ Hz, 2H), 7.46 (t, $J = 7.8$ Hz, 1H), 7.38 (dd, $J = 5.8, 3.4$ Hz, 2H), 7.28 (d, $J = 7.8$ Hz, 2H), 2.65 (sept, $J = 6.8$ Hz, 2H), 1.15 (d, $J = 6.8$ Hz, 12H). ^{19}F NMR (471 MHz, $CDCl_3$): δ -113.8. ^{13}C NMR (101 MHz, $CDCl_3$) δ 163.3, 150.1 (dd, $J = 265.5, 4.3$ Hz), 147.3, 135.3 (dd, $J = 13.0, 8.1$ Hz), 132.2, 130.6, 129.6, 129.4, 126.1, 124.2, 116.3 (dd, $J = 10.3, 5.8$ Hz), 29.5, 24.1. HRMS (DART) m/z calculated for $C_{26}H_{25}F_2N_2O_2S_2$ $[M+NH_4]^+$: 499.1320, found 499.1359.



7-(2,6-Diisopropylphenyl)-6H-benzo[5,6][1,4]dithiino[2,3-e]benzo[5,6][1,4]dithiino[2,3-g]isoindole-6,8(7H)-dione (S1)

To a Schlenk flask with a stirrer bar containing 2-(2,6-diisopropylphenyl)-4,5,6,7-tetrafluoroisoindoline-1,3-dione (94.8 mg, 0.25 mmol) and K_2CO_3 (207 mg, 1.5 mmol) in THF (2.5 mL) under argon was added 1,2-benzenedithiol (58 μ L, 0.5 mmol) and DMF (2.5 mL). The reaction was stirred at room temperature for 16 h. The mixture was concentrated and precipitated into an aqueous 1 M HCl solution. The precipitate was filtered and washed with water and methanol to obtain **S1** as a yellow powder (135.2 mg, 93%). **1H NMR** (500 MHz, TCE- d_2) δ 7.62–7.57 (m, 4H), 7.48 (t, J = 7.8 Hz, 1H), 7.37–7.35 (m, 4H), 7.29 (d, J = 7.8, 2H), 2.65 (sept, J = 6.4 Hz, 2H), 1.15 (d, J = 6.4 Hz, 12H). **^{13}C NMR** (126 MHz, TCE- d_2) δ 165.7, 147.0, 141.8, 133.6, 132.5, 132.4, 130.1, 129.3, 129.0, 128.9, 128.7, 126.3, 126.1, 123.8, 29.1, 24.0. **HRMS** (DART) m/z calculated for $C_{32}H_{29}N_2O_2S_4$ $[M+NH_4]^+$: 601.1106, found 601.1102.

Alternatively, to a Schlenk flask with a stirrer bar containing K_2CO_3 (31.1 mg, 0.225 mmol) and **S2** (36.1 mg, 0.075 mmol) under argon was added THF (1 mL), 1,2-benzenedithiol (8.6 μ L, 0.075 mmol) and DMF (1 mL). The reaction was stirred at room temperature for 16 h. The mixture was concentrated and precipitated into an aqueous 1 M HCl solution. The precipitate was filtered and washed with water and methanol to obtain a yellow powder (38.0 mg, 87%).



1,4-Bis(phenylthio)thianthrene-2,3-dicarbonitrile (**S3**)

To a Schlenk flask with a stirrer bar containing 1,4-difluorothianthrene-2,3-dicarbonitrile (30 mg, 0.1 mmol) and K_2CO_3 (20.7 mg, 0.15 mmol) under argon was added DMF (5 mL) and thiophenol (10.3 μ L, 0.1 mmol). The reaction was stirred at room temperature for 16 h. The mixture precipitated into an aqueous 1 M HCl, filtered, and washed with water and methanol. The precipitate was purified by gel column chromatography using toluene to give **S3** as a yellow solid (20.0 mg, 80% yield). $R_f = 0.4$ (toluene). 1H NMR (400 MHz, CD_2Cl_2) δ 7.35–7.28 (m, 14 H). ^{13}C NMR (126 MHz, CD_2Cl_2) δ 149.7, 138.2, 133.4, 133.2, 130.7, 130.0, 129.6, 129.1, 128.5, 122.0, 114.5. HRMS (DART) m/z calculated for $C_{26}H_{18}N_3S_4$ $[M+NH_4]^+$: 500.0378, found 500.0396.

2.5 References

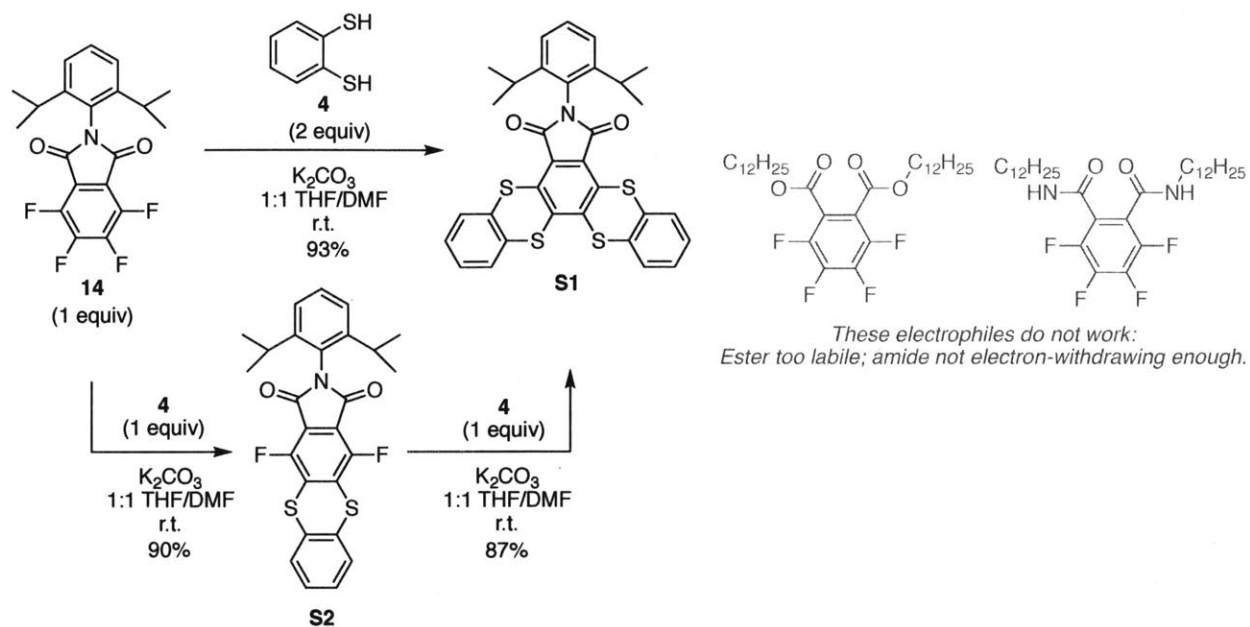
- 1 Rowan, S. J.; Cantrill, S. J.; Cousins, G. R. L.; Sanders, J. K. M.; Stoddart, J. F. *Angew. Chem. Int. Ed.* **2002**, *41*, 898.
- 2 For a comprehensive review of dynamic covalent chemistry, see Yu, C.; Jin, Y.; Zhang, W. *Dynamic Covalent Chemistry: Principles, Reactions, and Applications*; Wiley-VCH: Weinheim, 2017.
- 3 Jin, Y.; Wang, Q.; Taynton, P.; Zhang, W. *Acc. Chem. Res.* **2014**, *47*, 1575.

- 4 Mastalerz, M. *Angew. Chem. Int. Ed.* **2010**, *49*, 5042.
- 5 Zou, W.; Dong, J. Luo, Y. Zhao, Q.; Xie, T. *Adv. Mater.* **2017**, *29*, 1606100.
- 6 Belowich, M. E.; Stoddart, J. F. *Chem. Soc. Rev.* **2012**, *41*, 2003.
- 7 Cromwell, O. R.; Chung, J.; Guan, Z. *J. Am. Chem. Soc.* **2015**, *137*, 6492.
- 8 Bapat, A. P.; Roy, D.; Ray, J. G.; Savin, D. A.; Sumerlin, B. S. *J. Am. Chem. Soc.* **2011**, *133*, 19832.
- 9 Black, S. P.; Sanders, J. K. M.; Stefankiewicz, A. R. *Chem. Soc. Rev.* **2014**, *43*, 1861.
- 10 Lu, Y.-X.; Tournilhac, F.; Leibler, L.; Guan, Z. *J. Am. Chem. Soc.* **2012**, *134*, 8424.
- 11 Wang, Q.; Yu, C.; Zhang, C.; Long, H.; Azarnoush, S.; Jin, Y.; Zhang, W. *Chem. Sci.* **2016**, *7*, 3370.
- 12 Jin, Y.; Yu, C.; Denman, R. J.; Zhang, W. *Chem. Soc. Rev.* **2013**, *42*, 6634.
- 13 Guo, Q.-H.; Fu, Z.-D.; Zhao, L.; Wang, M.-X. *Angew. Chem. Int. Ed.* **2014**, *53*, 13548.
- 14 Fu, Z.-D.; Guo, Q.-H.; Zhao, L.; Wang, D.-X.; Wang, M.-X. *Org. Lett.* **2016**, *18*, 2668.
- 15 Wackerly, J. W.; Zhang, M.; Nodder, S. T.; Carlin, S. M.; Katz, J. L. *Org. Lett.* **2014**, *16*, 2920.
- 16 Jayakannan, M.; Ramakrishnan, S. *Macromol. Rapid Commun.* **2001**, *22*, 1463.
- 17 Long, T. M.; Swager, T. M. *J. Am. Chem. Soc.* **2003**, *125*, 14113.

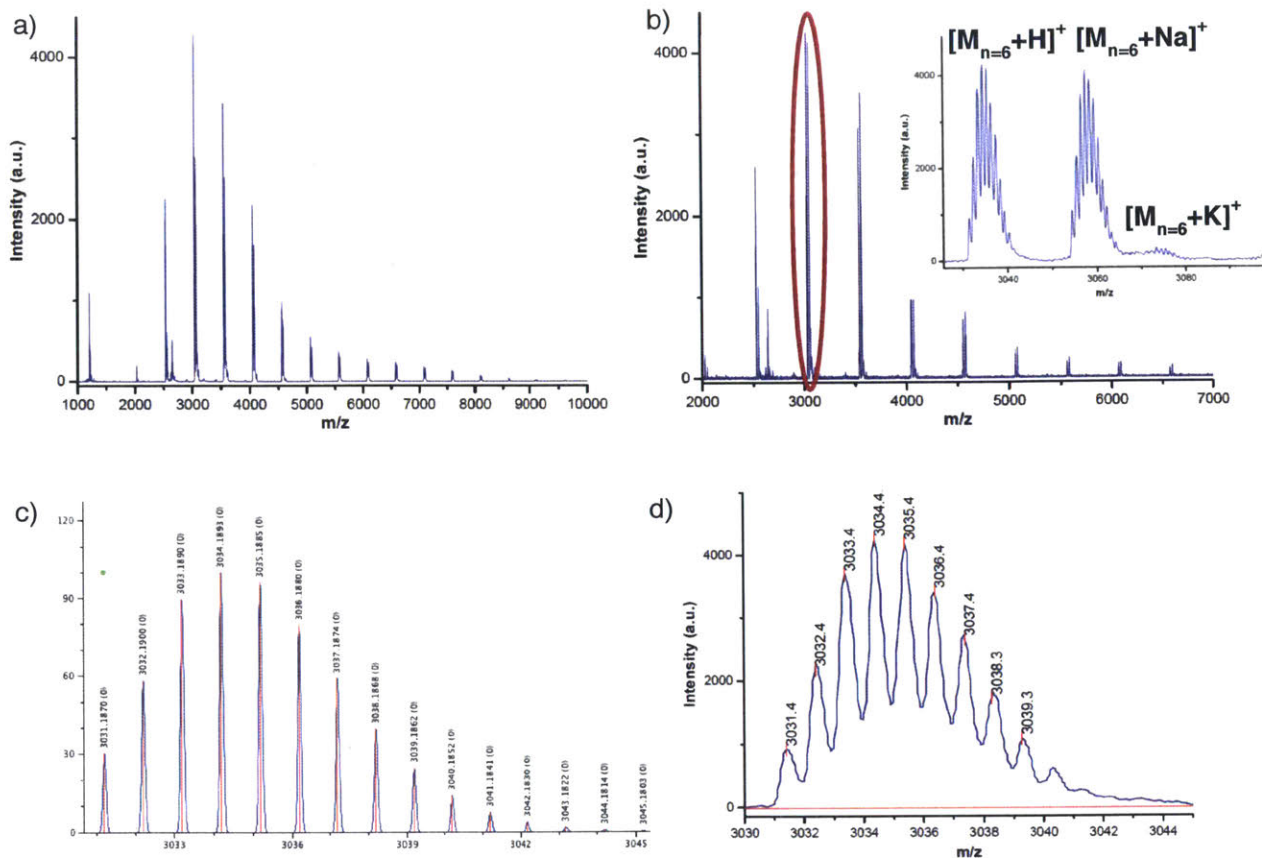
- 18 Katz, J. L.; Selby, K. J.; Conry, R. R. *Org. Lett.* **2005**, *7*, 3505.
- 19 Mueller, A.; Kowalewski, T.; Wooley, K. L. *Macromolecules* **1998**, *31*, 776.
- 20 Alsbaiee, A.; Smith, B. J.; Xiao, L.; Ling, Y.; Helbling, D. E.; Dichtel, W. R. *Nature* **2016**, *529*, 190.
- 21 Wu, Z.-C.; Guo, Q.-H.; Wang, M.-X. *Angew. Chem. Int. Ed.* **2017**, *56*, 7151.
- 22 Ben-Haida, A.; Baxter, I.; Colquhoun, H. M.; Hodge, P.; Kohnke, F. H.; Williams, D. J. *Chem. Commun.* **1997**, 1533.
- 23 For a general review on thianthrene, see Joule, J. A. *Thianthrenes in Advances in Heterocyclic Chemistry Vol. 48*; Academic Press: New York, 1990.
- 24 Ding, Y.; Zhang, C.; Zhang, L.; Zhou, Y.; Yu, G. *Chem. Soc. Rev.* **2018**, *47*, 69.
- 25 Bunnett, J. F.; Zahler, R. E. *Chem. Rev.* **1951**, *49*, 273.
- 26 Makhseed, S.; Ibrahim, F.; Samuel, J. *Polymer* **2012**, *53*, 2964.
- 27 Hargreaves, M. K.; Pritchard, J. G.; Dave, H. R. *Chem. Rev.* **1970**, *70*, 439.
- 28 McKeown, N. B.; Budd, P. M. *Chem. Soc. Rev.* **2006**, *35*, 675.
- 29 Mayor, M.; Lehn, J.-M. *Helv. Chim. Acta* **1997**, *80*, 2277.
- 30 Wu, H.; Zhao, P.; Li, X.; Chen, W.; Ågren, H.; Zhang, Q.; Zhu, L. *ACS Appl. Mater. Interfaces* **2017**, *9*, 3865.

- 31 Spokoyny, A. M; Zou, Y.; Ling, J. J.; Yu, H.; Lin, Y.-S.; Pentelute, B. L. *J. Am. Chem. Soc.* **2013**, *135*, 5946.
- 32 Sing, K. S. W.; Everett, D. H.; Haul, R. A. W.; Moscou, L.; Pierotti, R. A.; Rouquérol, J.; Siemieniowska, T. *Pure Appl. Chem.* **1985**, *57*, 603.
- 33 Pandey, P.; Farha, O. K.; Spokoyny, A. M.; Mirkin, C. A.; Kanatzidis, M. G.; Hupp, J. T.; Nguyen, S. T. *J. Mater. Chem.* **2011**, *21*, 1700.
- 34 Chakraborty, S.; Colon, Y. J.; Snurr, R. Q.; Nguyen, S. T. *Chem. Sci.* **2015**, *6*, 384.
- 35 Wilson, A.; Gasparini, G.; Matile, S. *Chem. Soc. Rev.* **2014**, *43*, 1948.
- 36 Lascano, S.; Zhang, K.-D.; Wehlauch, R.; Gademann, K.; Sakai, N.; Matile, S. *Chem. Sci.* **2016**, *7*, 4720.

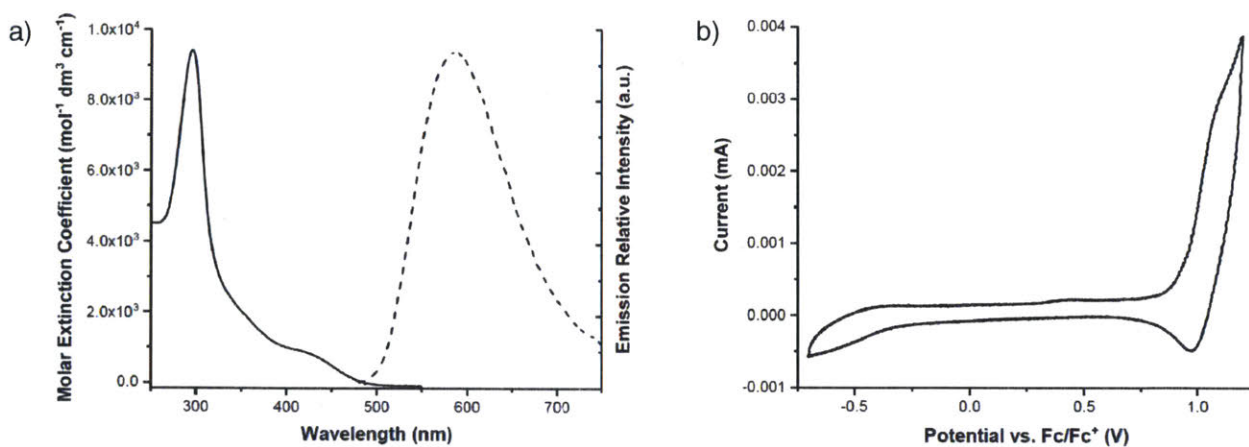
2.6 Appendix for Chapter 2



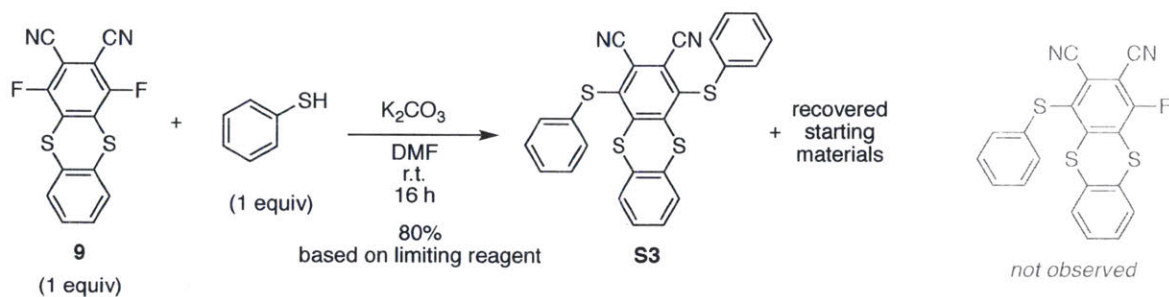
Supplementary Figure 2.1. Model reaction for synthesis of ladder macrocycle **14**.



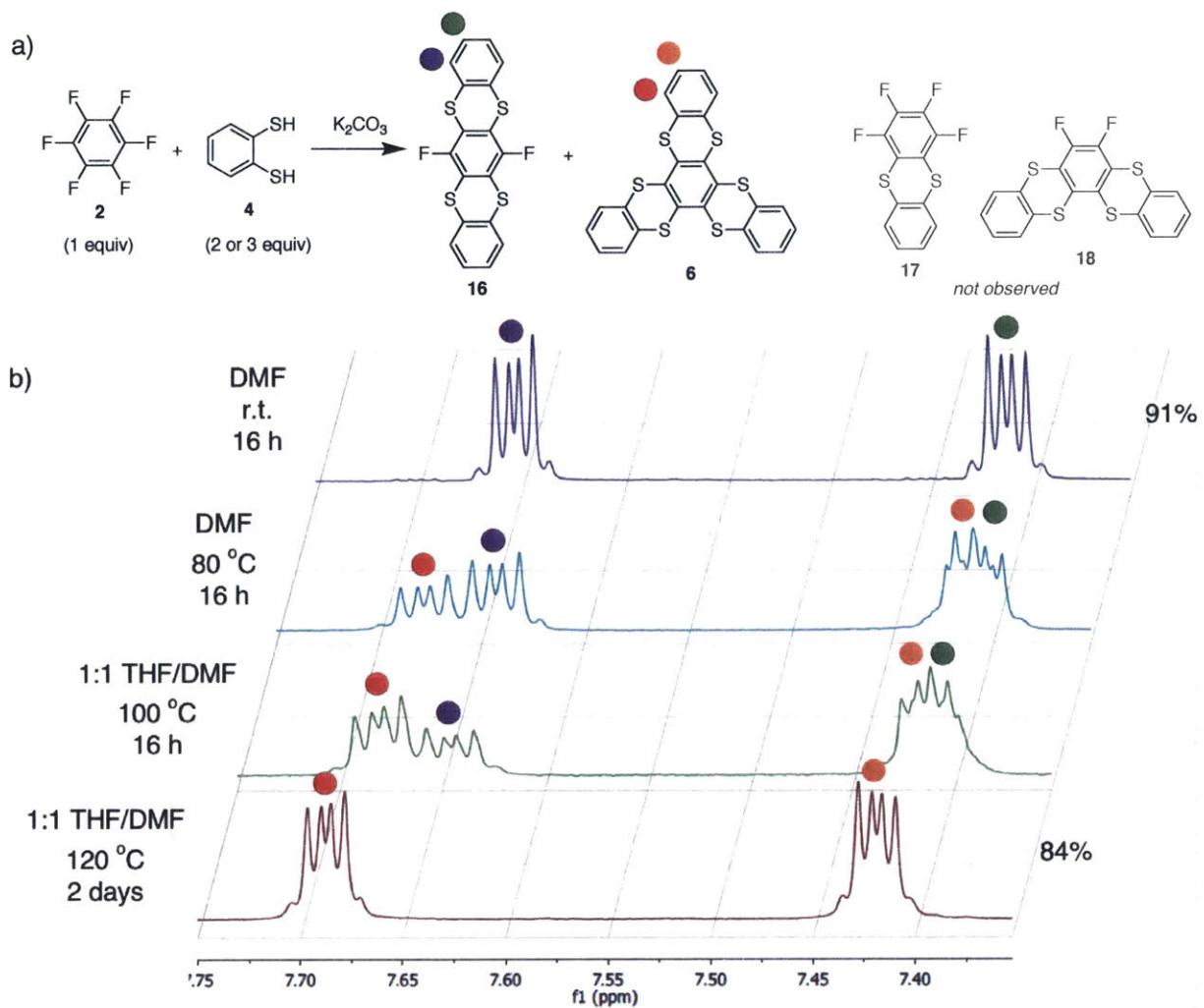
Supplementary Figure 2.2. MALDI analysis of macrocycle **15** under a) linear mode and b) reflector mode. For each ring size, we observe isotopic distributions of various molecular ions. For example, we observe $[15_{n=6}+H]^+$, $[15_{n=6}+Na]^+$, and $[15_{n=6}+K]^+$ for the n=6 macrocycle. c) Calculated isotopic distribution of $[15_{n=6}+H]^+$. d) Observed isotopic distribution of $[15_{n=6}+H]^+$.



Supplementary Figure 2.3. a) Photophysical properties using 8×10^{-5} M of repeating units of **15** in CH_2Cl_2 . Excitation wavelength for emission spectrum is 450 nm. b) Cyclic voltammetry of **15**.

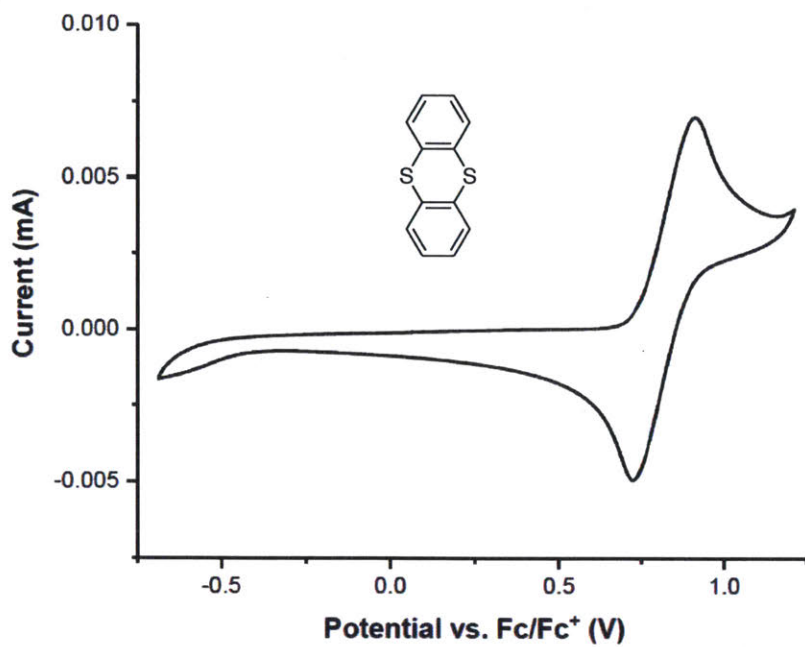


Supplementary Figure 2.4. Model reaction of **9** (1 equiv) reacting with thiophenol (1 equiv).

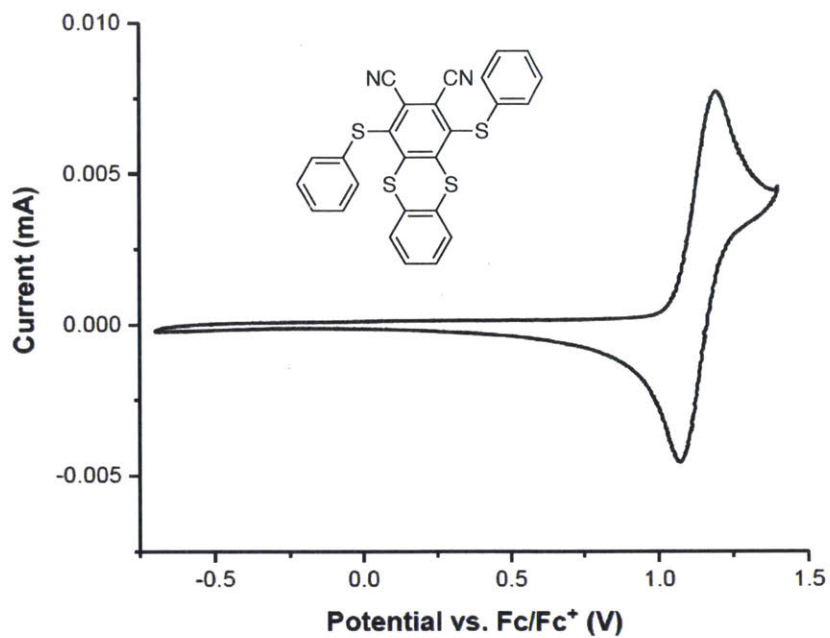


Supplementary Figure 2.5. a) Reactions of **2** (1 equiv) with **4** (2 or 3 equiv) under different conditions. b) ^1H NMR spectra of products in $\text{DMSO-}d_6$ at 85 °C.

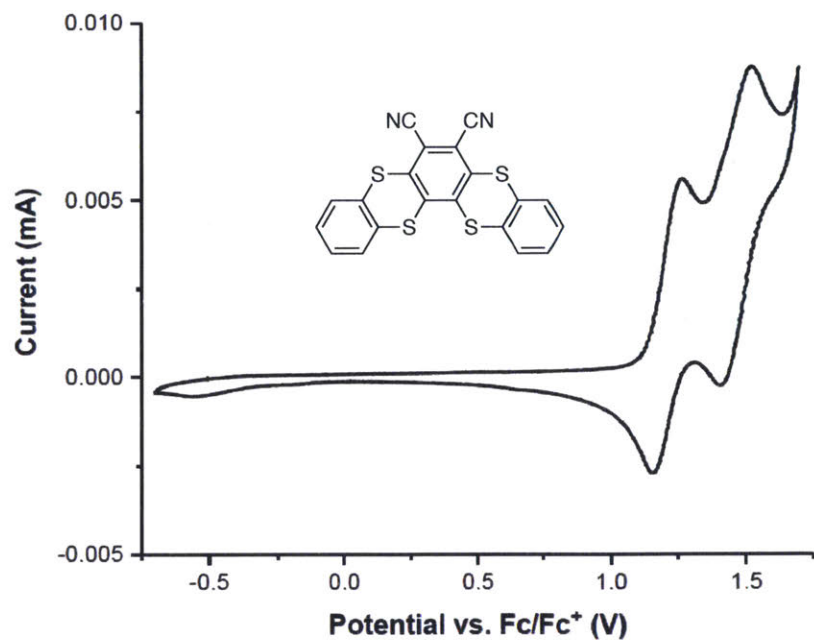
Cyclic Voltammetry (CV) of Compounds



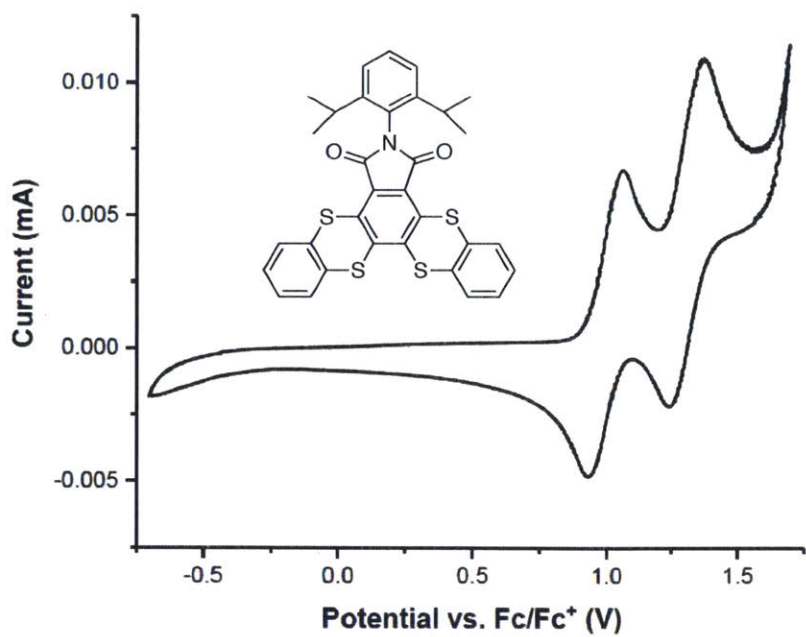
Supplementary Figure 2.6. CV of thianthrene.



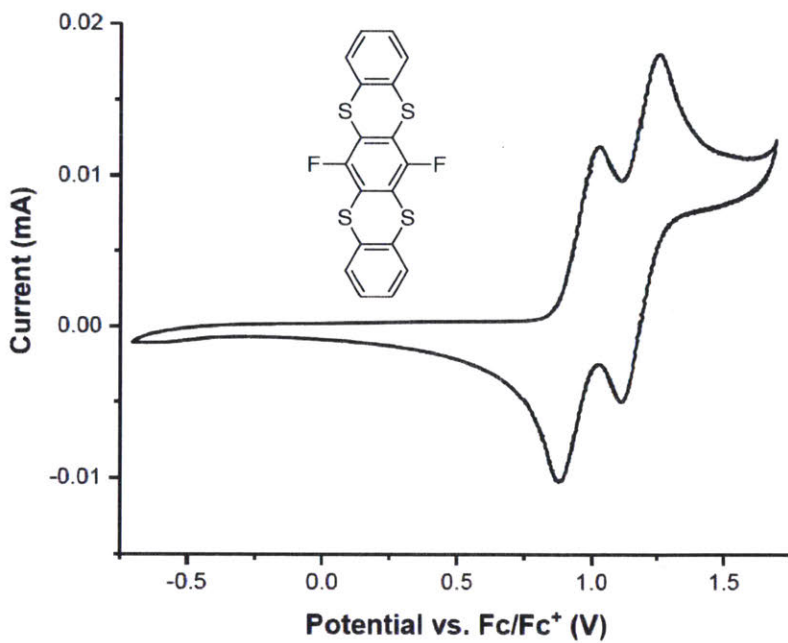
Supplementary Figure 2.7. CV of S3.



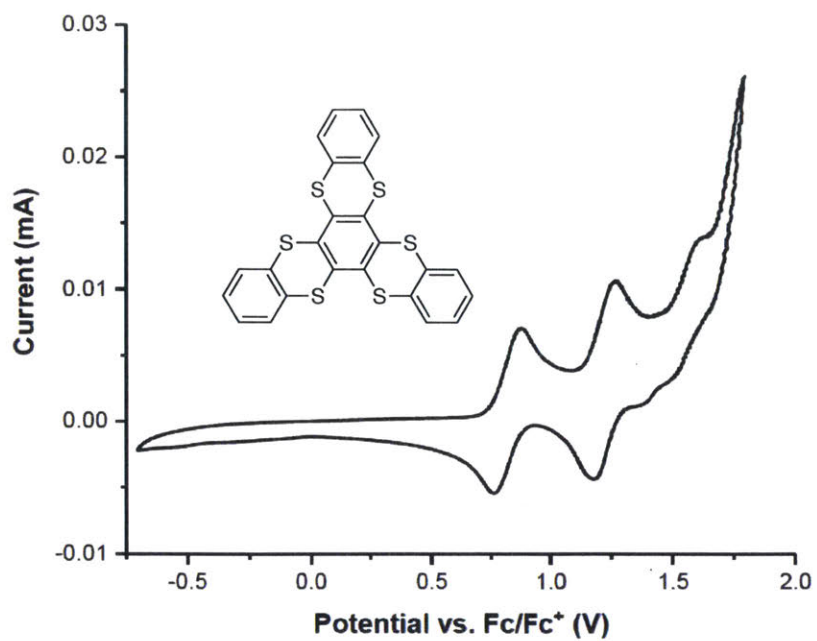
Supplementary Figure 2.8. CV of 5.



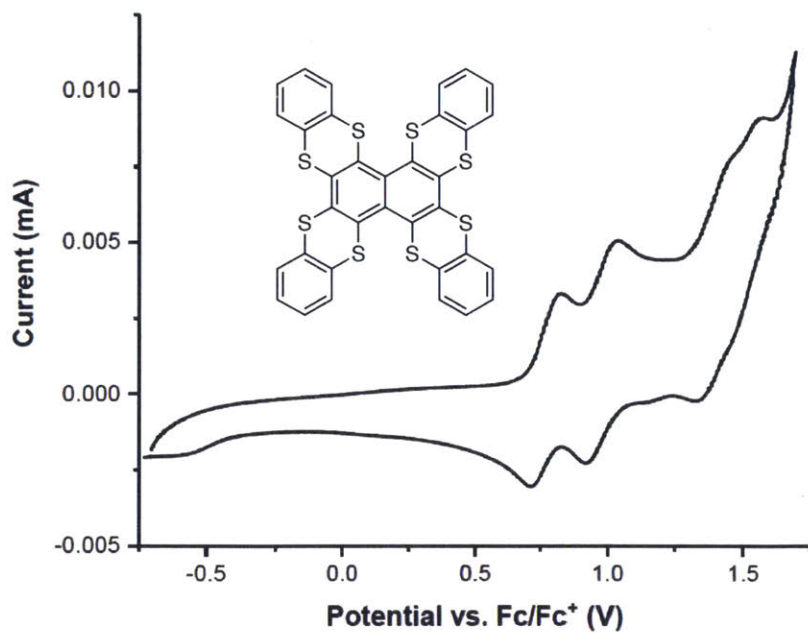
Supplementary Figure 2.9. CV of S1.



Supplementary Figure 2.10. CV of 16.

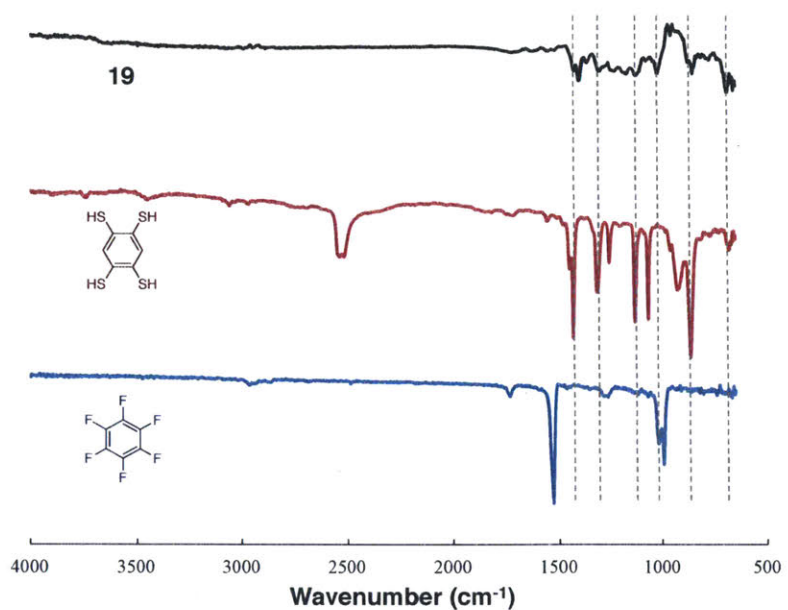


Supplementary Figure 2.11. CV of 6.

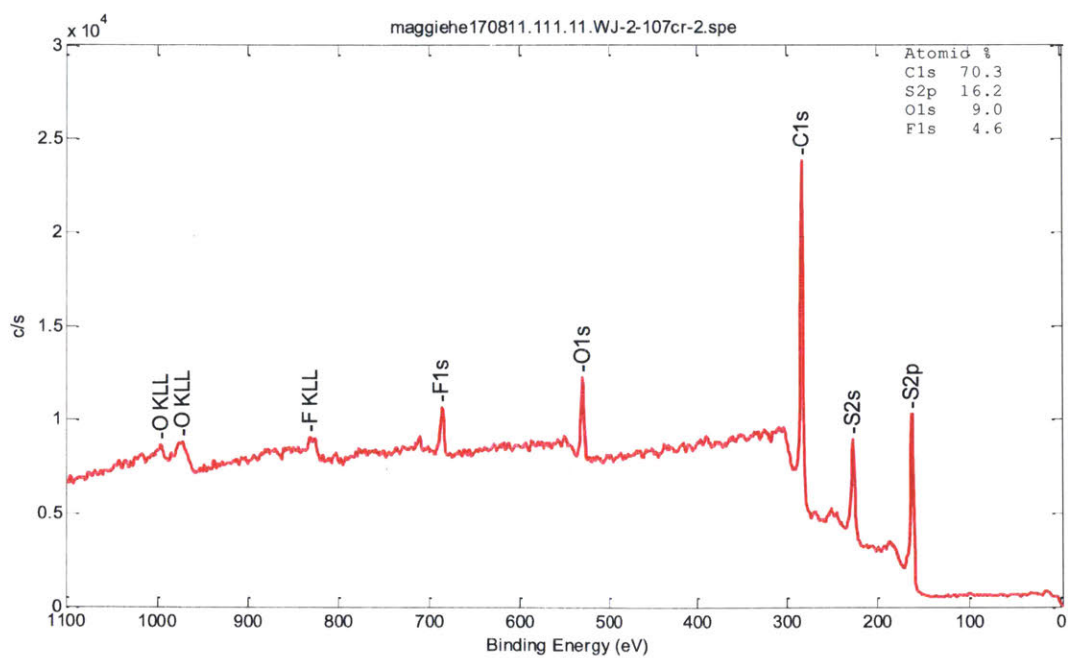


Supplementary Figure 2.12. CV of 7.

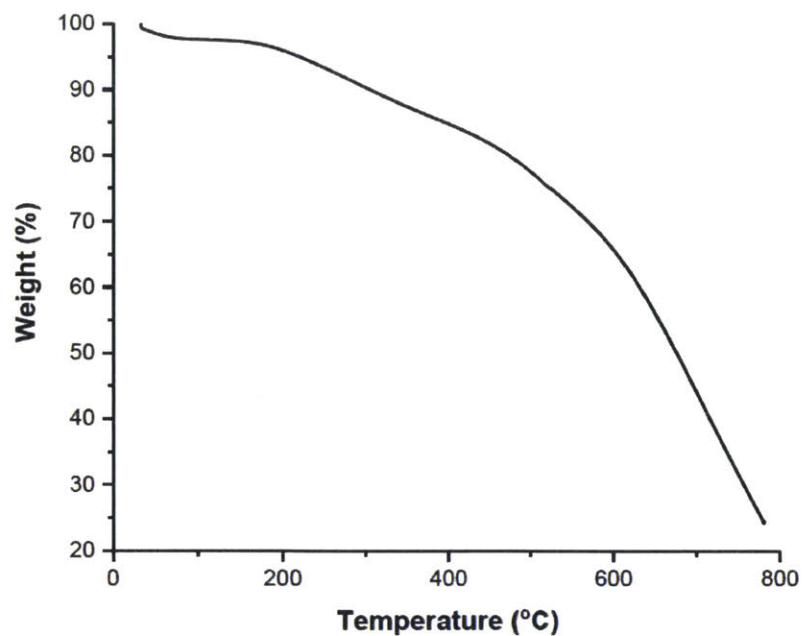
Characterization of porous polymer network 19



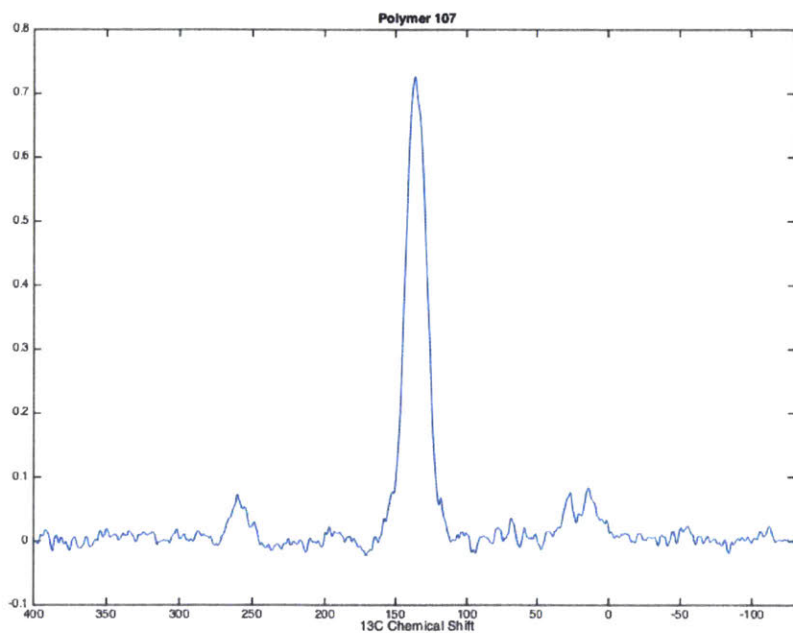
Supplementary Figure 2.13. Infrared spectra of 19 and monomers.



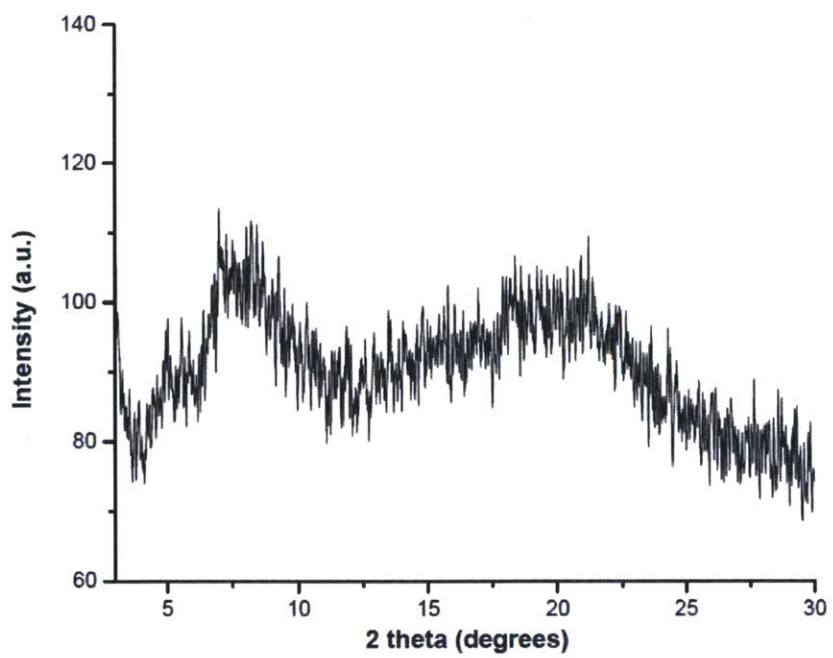
Supplementary Figure 2.14. X-ray photoelectron spectroscopy (XPS) of 19.



Supplementary Figure 2.15. Thermogravimetric analysis (TGA) of 19.

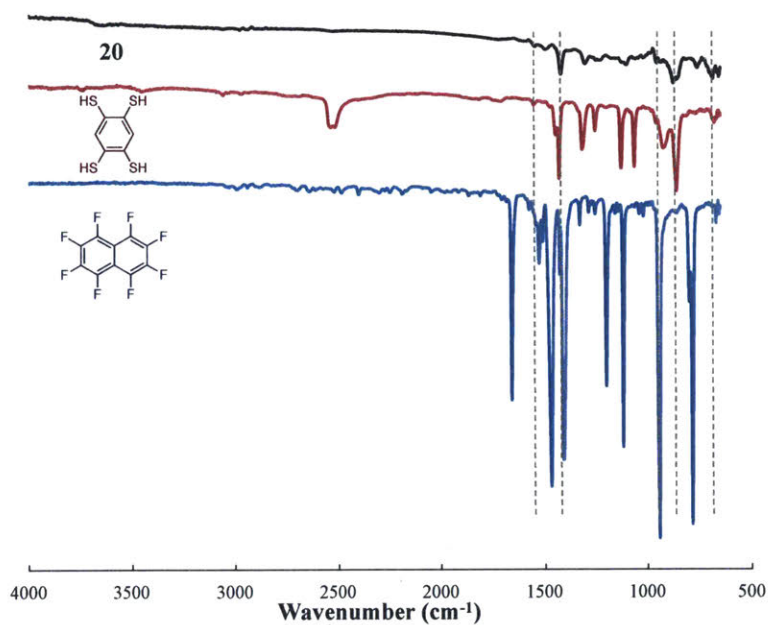


Supplementary Figure 2.16. ¹³C solid state NMR (ssNMR) of 19.

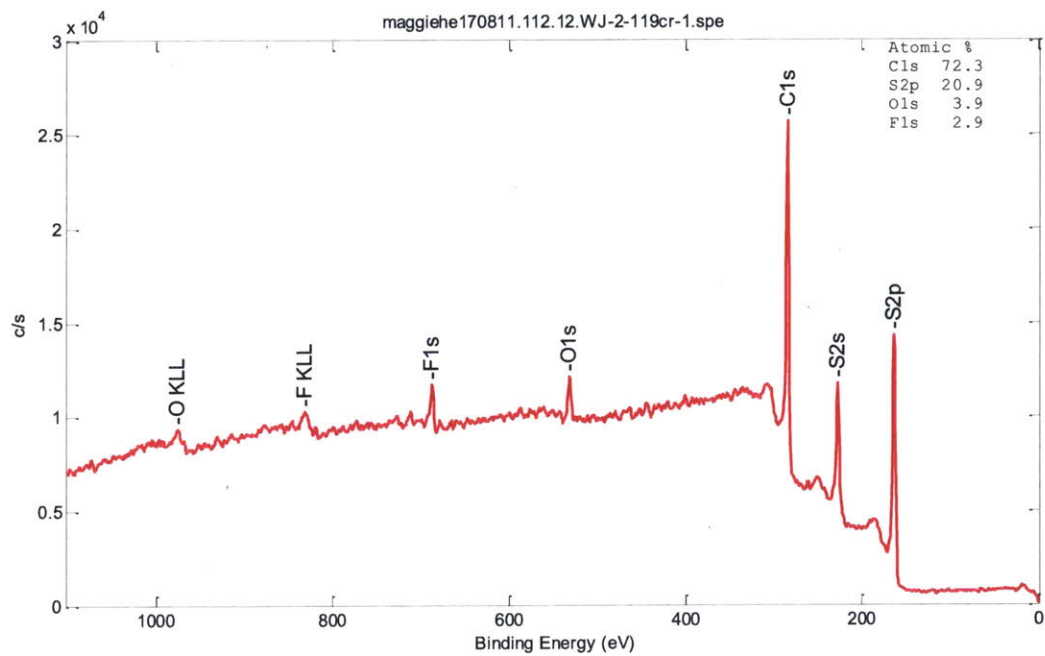


Supplementary Figure 2.17. X-ray diffraction (XRD) of **19** with smoothing.

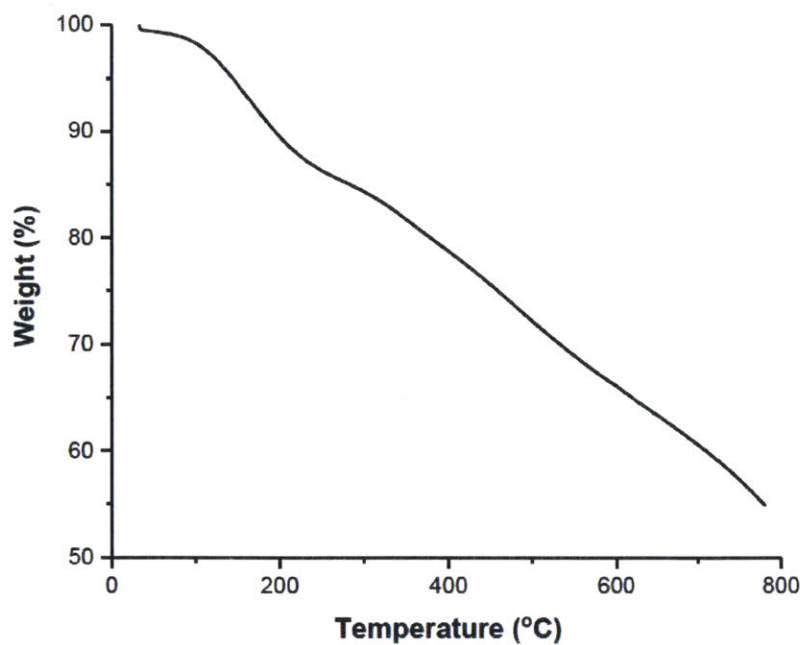
Characterization of Porous Polymer Network 20



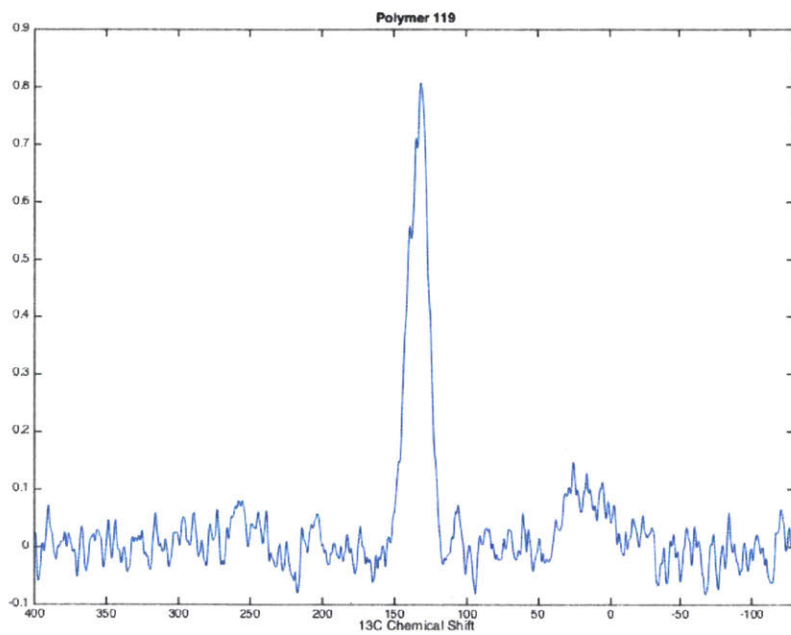
Supplementary Figure 2.18. Infrared spectra of **20** and monomers.



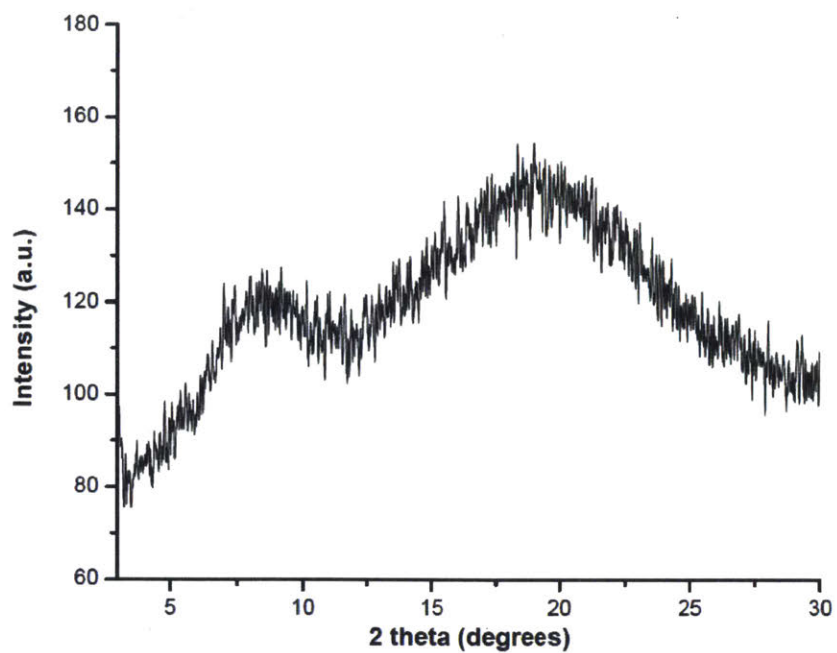
Supplementary Figure 2.19. XPS of **20**.



Supplementary Figure 2.20. TGA of 20.

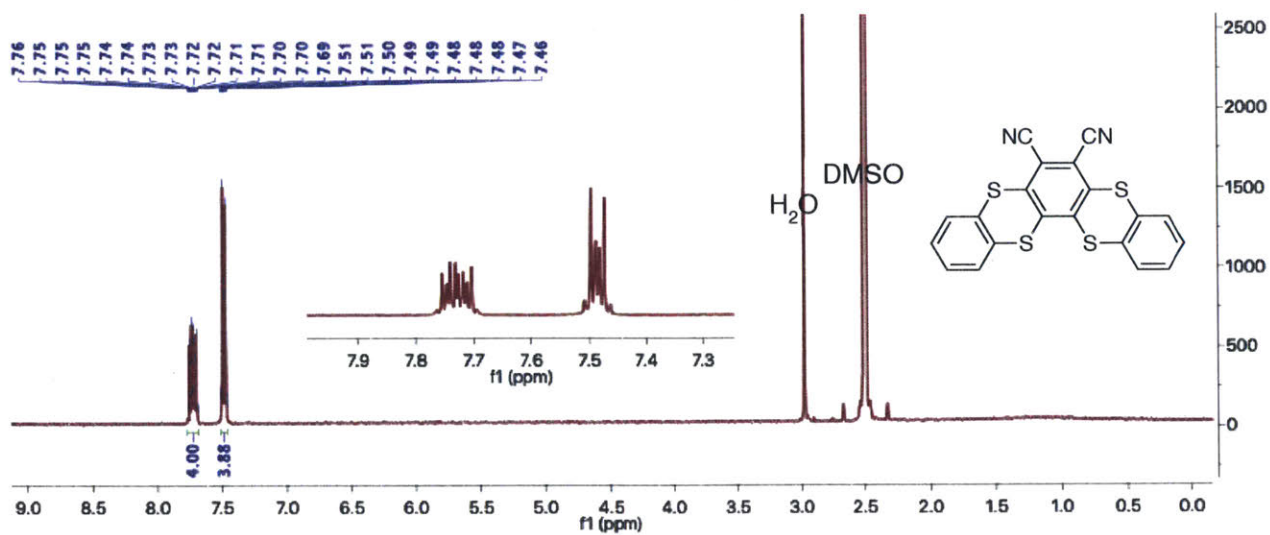


Supplementary Figure 2.21. ¹³C ssNMR of 20

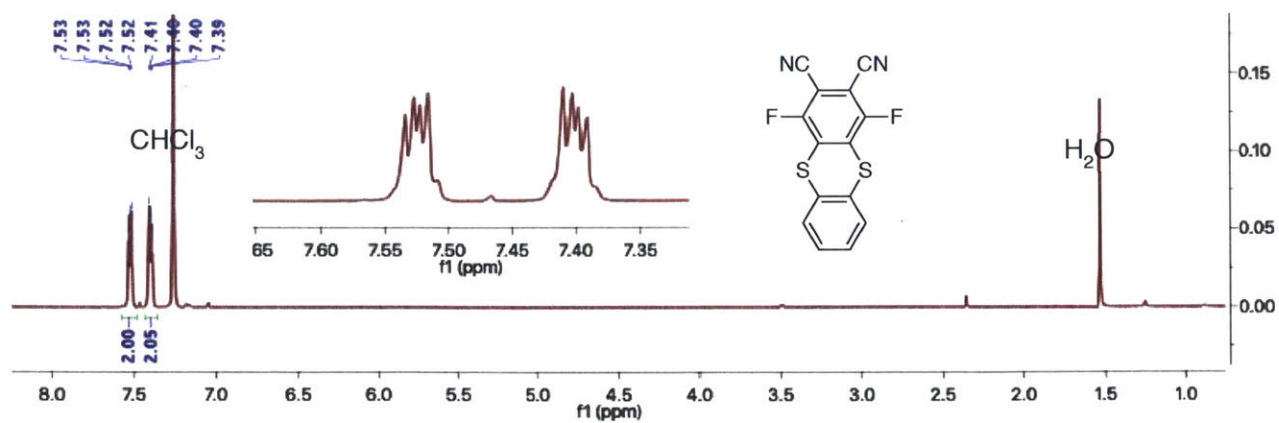


Supplementary Figure 2.22. XRD of 20 with smoothing.

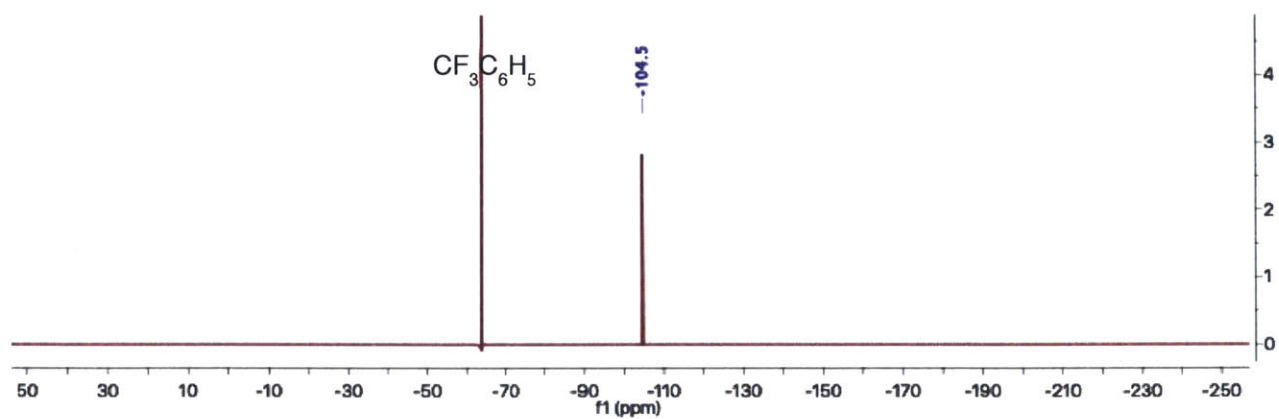
NMR Spectra



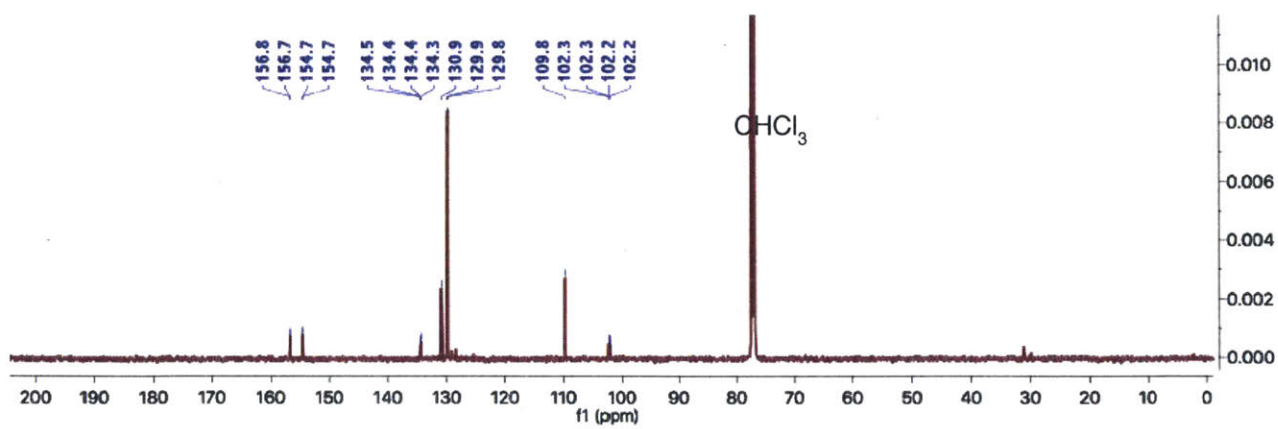
¹H NMR spectrum (400 MHz, DMSO-*d*₆, 85 °C) of **5**.



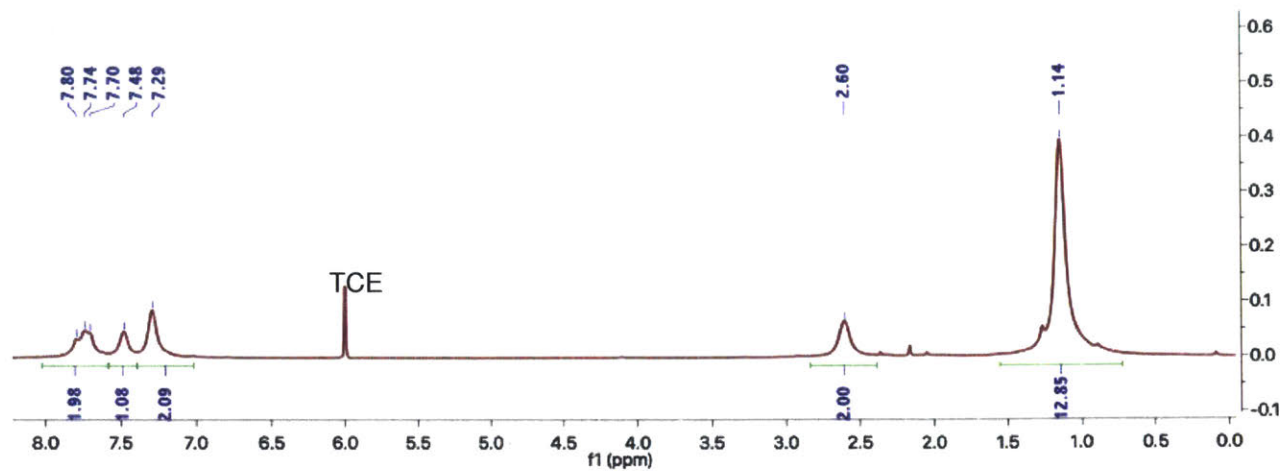
$^1\text{H NMR}$ spectrum (500 MHz, CDCl_3) of **9**.



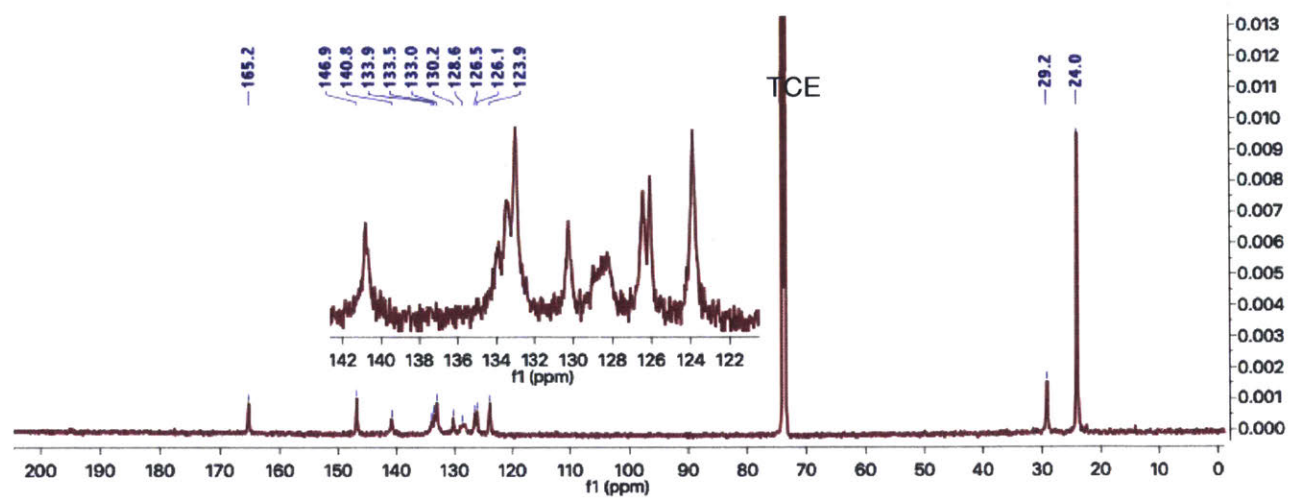
$^{19}\text{F NMR}$ spectrum (471 MHz, CDCl_3) of **9**.



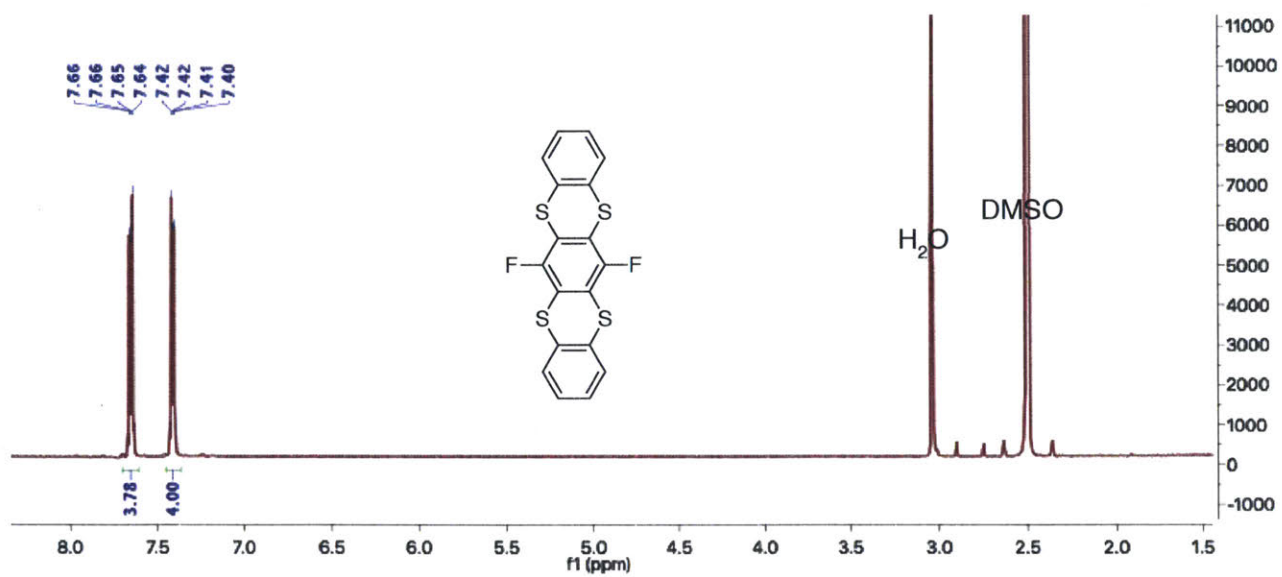
^{13}C NMR spectrum (126 MHz, CDCl_3) of **9**.



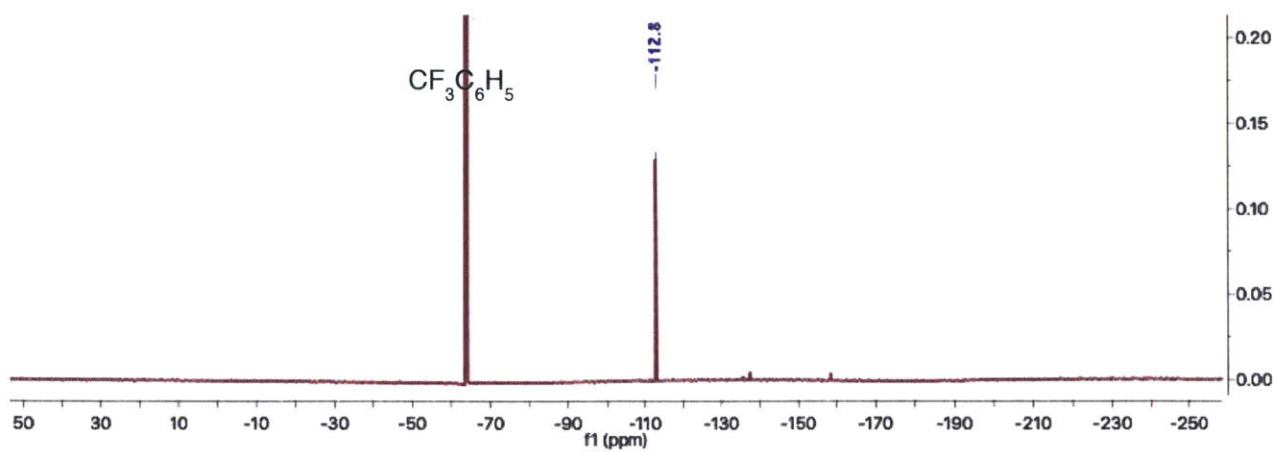
¹H NMR spectrum (500 MHz, TCE-*d*₂) of ladder macrocycle **15**.



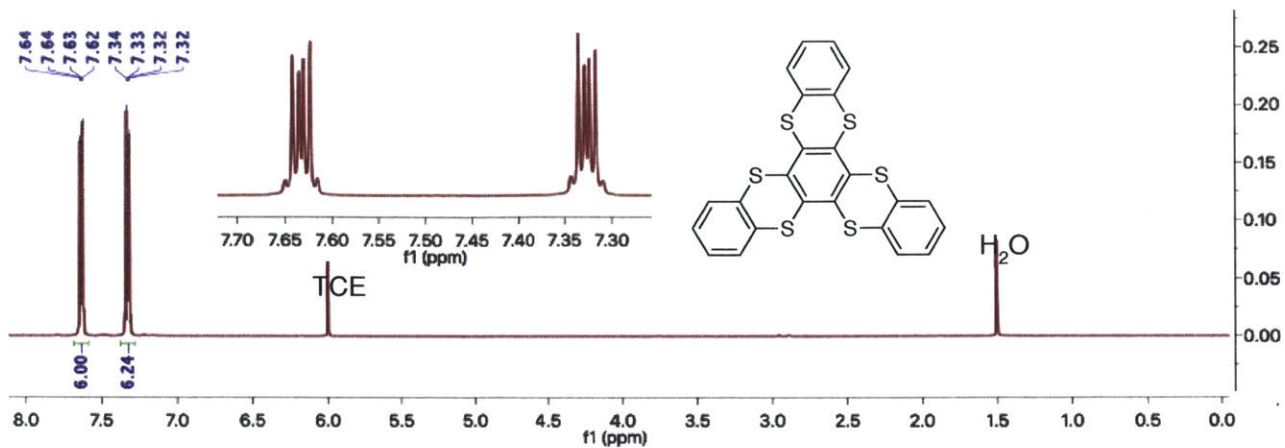
¹³C NMR spectrum (126 MHz, TCE-*d*₂) of ladder macrocycle **15**.



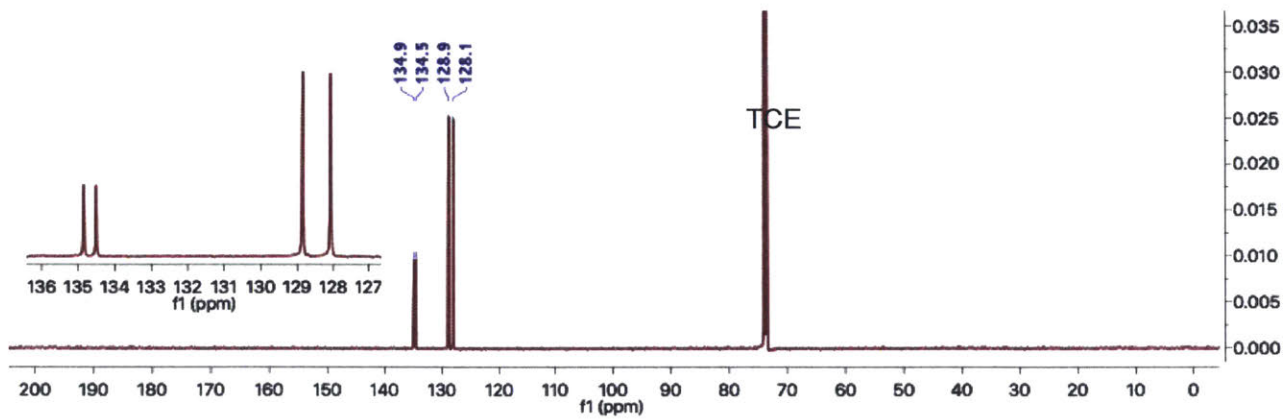
¹H NMR spectrum (500 MHz, DMSO-*d*₆, 85 °C) of **16**.



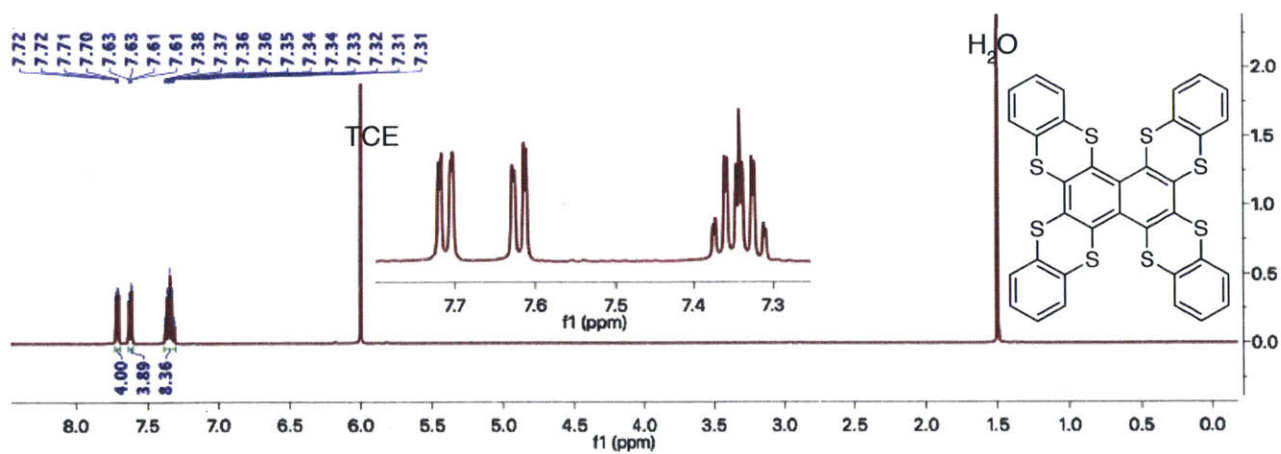
¹⁹F NMR spectrum (471 MHz, DMSO-*d*₆, 85 °C) of **16**.



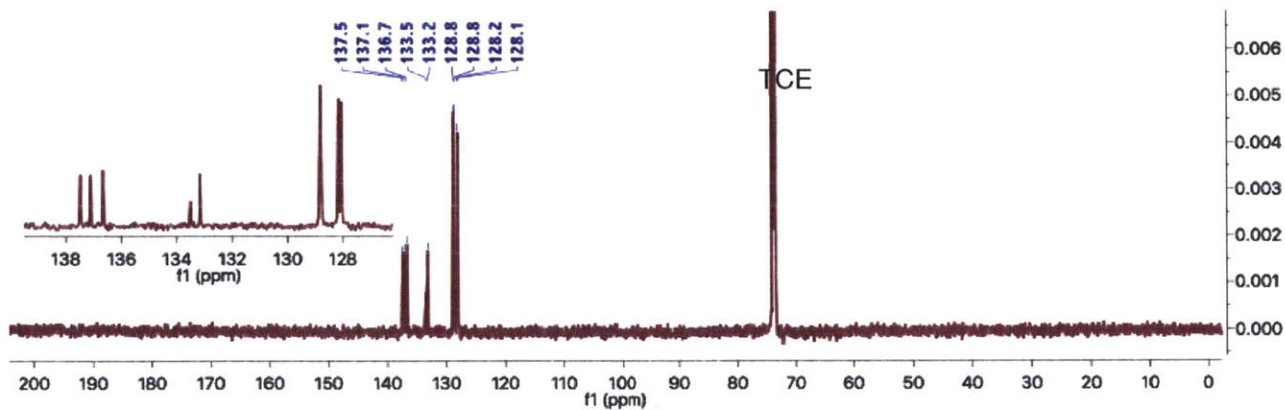
^1H NMR spectrum (500 MHz, TCE-d_2 , 85°C) of **6**.



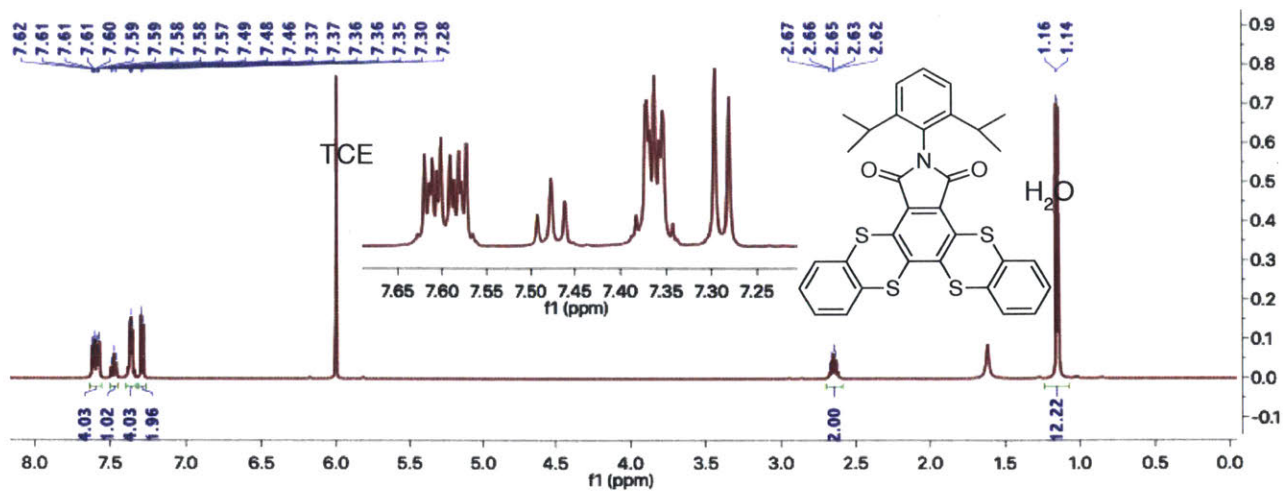
^{13}C NMR spectrum (500 MHz, TCE-d_2 , 85°C) of **6**.



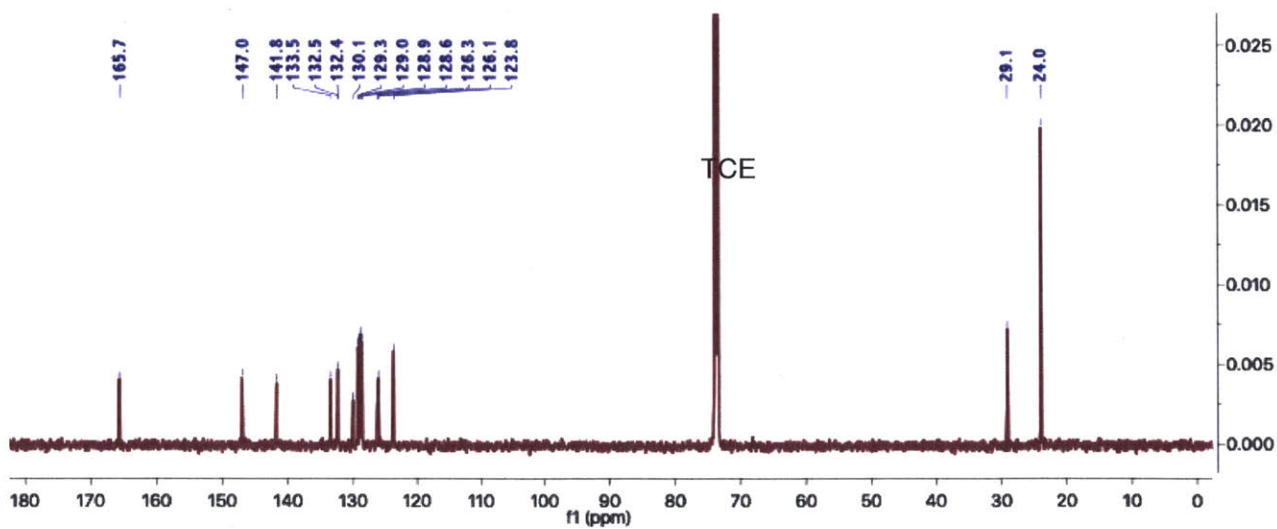
¹H NMR spectrum (500 MHz, TCE-d₂, 85 °C) of 7.



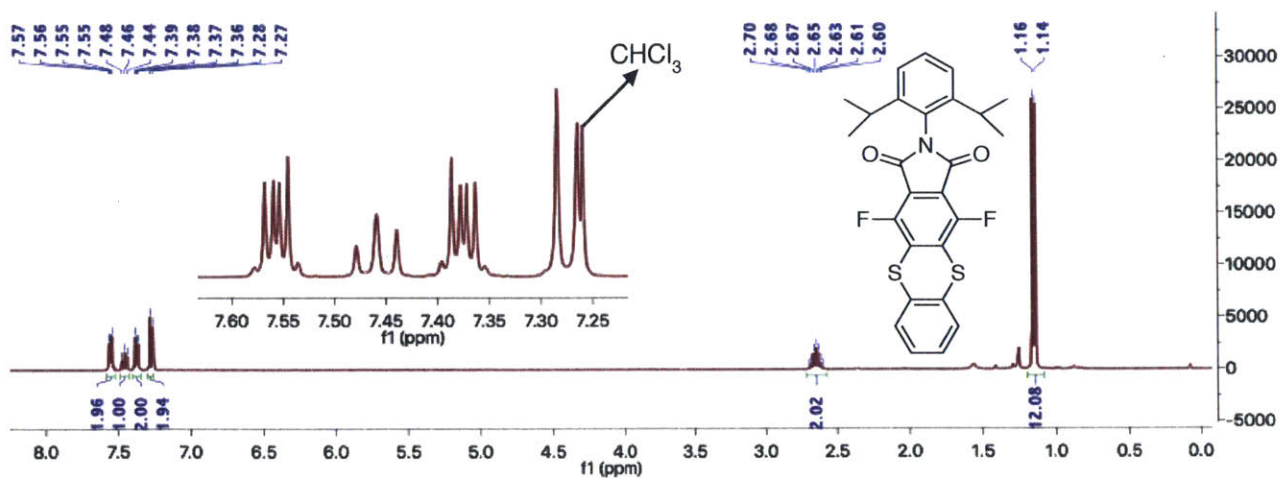
¹³C NMR spectrum (126 MHz, TCE-d₂, 85 °C) of 7.



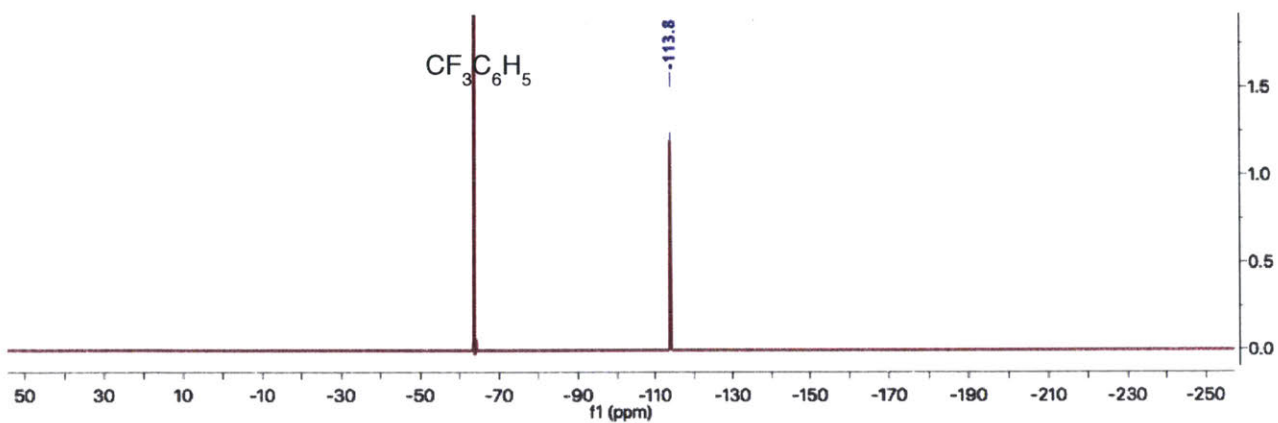
¹H NMR spectrum (500 MHz, TCE-*d*₂) of S1.



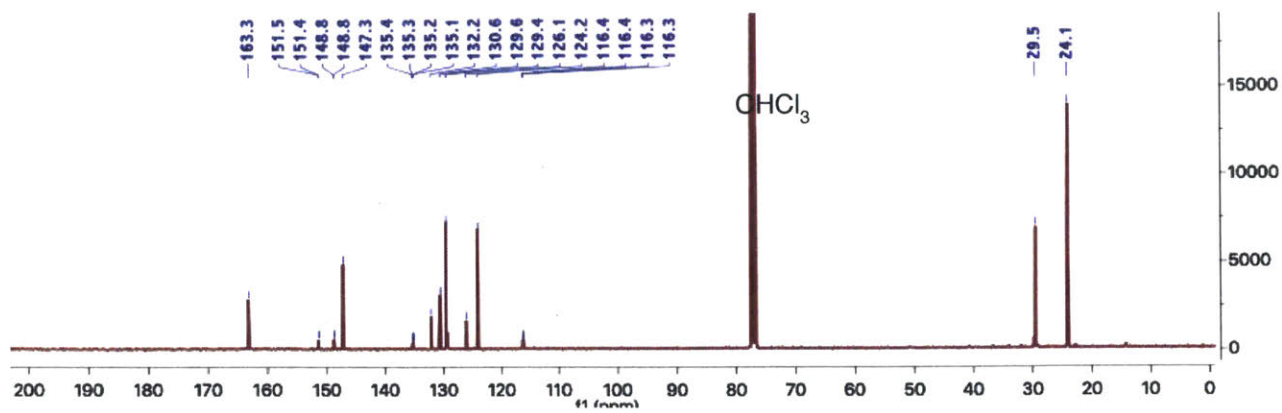
¹³C NMR spectrum (126 MHz, TCE-*d*₂) of S1.



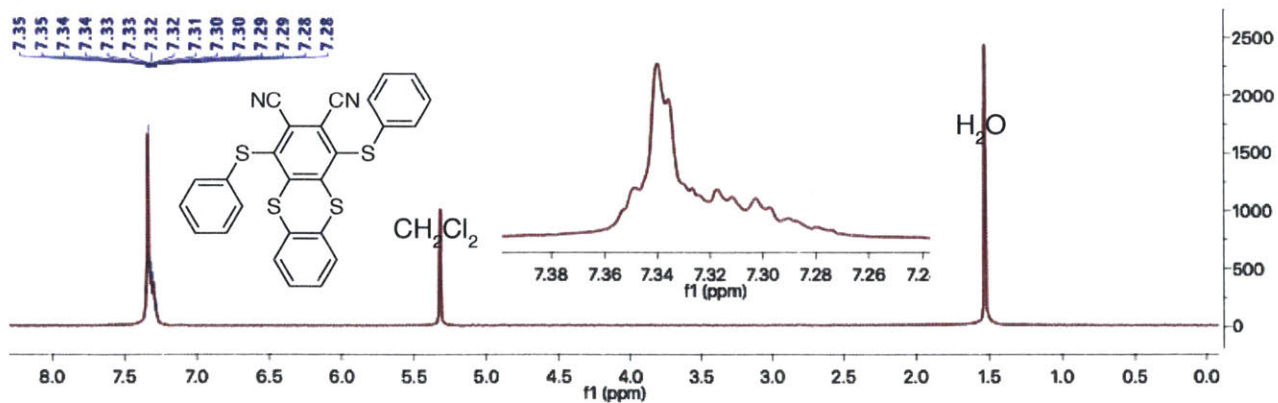
^1H NMR spectrum (400 MHz, CDCl_3) of S2.



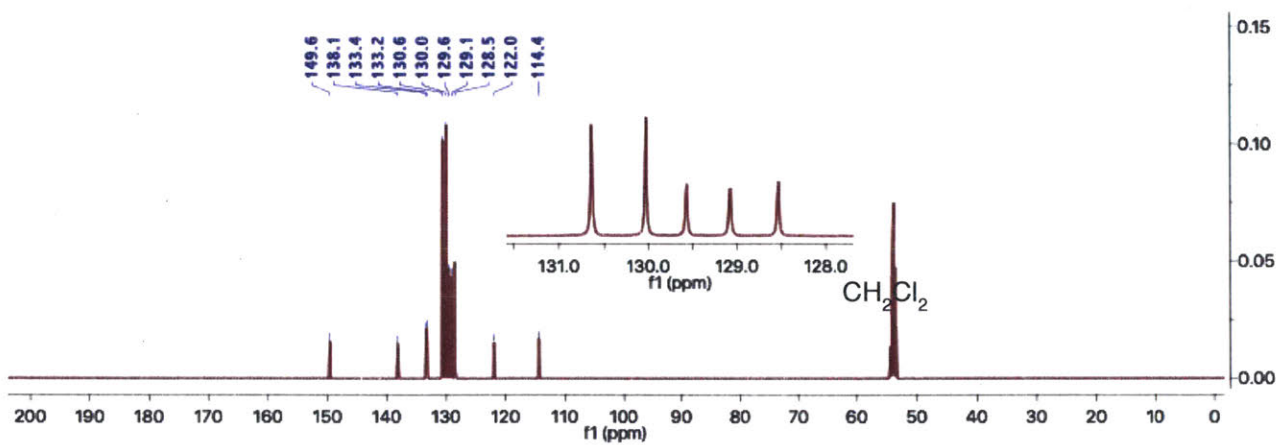
^{19}F NMR spectrum (471 MHz, CDCl_3) of S2.



^{13}C NMR spectrum (101 MHz, CDCl_3) of **S2**.



^1H NMR spectrum (400 MHz, CD_2Cl_2) of S3.



^{13}C NMR spectrum (126 MHz, CD_2Cl_2) of S3.

Chapter 3

Thianthrene Ladder Polymers

Abstract

While ladder polymers have been studied extensively for the past decades, their synthesis, characterization and potential applications have often been stymied by the presence of singly connected defects along their polymer backbones and their limited solubility. By exploiting the dynamic, self-correcting nature of the nucleophilic aromatic substitution reactions between *ortho*-aryldithiols and *ortho*-aryldifluorides, we hope to reduce defect formations and synthesize thianthrene ladder polymers. In addition, we incorporated triptycene and appended alkyl chains to each repeating unit to ensure that the resulting polymers are readily soluble in common organic solvents. Herein, we report the synthesis of two novel thianthrene ladder polymers in good yields. In contrast to dibenzodioxin, thianthrene confers the corresponding ladder polymers with interesting electrochemical and optoelectronic properties. For example, one of the polymers has an oxidation peak at $E_{1/2} = 1.32$ V vs. Ag/AgNO₃ and an unexpectedly large Stokes shift of 152 nm between its absorption and emission spectra.

3.1 Introduction

In contrast to conventional single-stranded polymers, monomers in a ladder polymer are connected to each other by two bonds, giving rise to a structure resembling the rails and rungs of a ladder.¹ Early studies in the 1960-70s focused on thermal, chemical and mechanical stability of the ladder structure, since cleavage of a single bond along the polymer backbone does not result in decrease of molecular weight and hence degradation of the polymer.² More recently, their potential applications in gas separation and organic electronics have been explored in depth.³⁻⁶ The double stranded structure of ladder polymers restricts free torsional rotation of sigma bonds between monomers, thereby conferring rigidity to the overall molecular architecture. This structural rigidity has been exploited in contorted, non-conjugated structures to create highly porous materials with high permeability and selectivity for gas separation,⁷⁻⁸ and in planar, conjugated structures for their excellent optoelectronic properties owing to effective delocalization of π orbitals and favorable intermolecular stacking.⁹⁻¹¹

There are two general approaches for synthesizing ladder polymers: (1) direct ladder polymerization, in which two bonds are formed in one step, and (2) zipping of a linear precursor, in which the second bond is formed between functional side groups on adjacent monomers after the initial polymerization.¹²⁻¹³ Where possible, it is often advantageous to pursue the former as it is more step efficient and avoids intermolecular branching or crosslinking that may occur during the zipping step. However, it can be challenging to avoid singly connected defects in direct ladder polymerization due to the demanding requirement of forming two bonds at the same time for every addition of one monomer. Singly connected defects along the polymer backbone can have adverse effects on the microporosity or optoelectronic properties of the resulting polymer.

In light of our recent work on dynamic self-correcting nucleophilic aromatic substitution (S_NAr),¹⁴ we hypothesized that by harnessing the self-correcting nature of the S_NAr reactions between *ortho*-aryldithiols and *ortho*-aryldifluorides, we can potentially reduce defect formations and afford thianthrene ladder polymers (Fig. 3.1). Thianthrene has been extensively studied for its redox activity.¹⁵⁻¹⁶ In its neutral state, it adopts a bent structure with a fold angle of 128°. Upon oxidation, both thianthrene radical cation and dication are planar with a fold angle of ~180°.¹⁷ Moreover, since ladder polymers tend to have limited solubility due to reduced conformational freedom and entropic driving force of mixing, we incorporate triptycene and flexible alkyl chains into our polymer design to enhance its solubility.

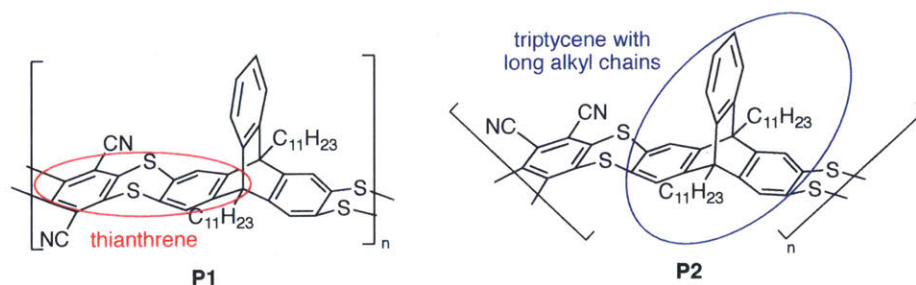


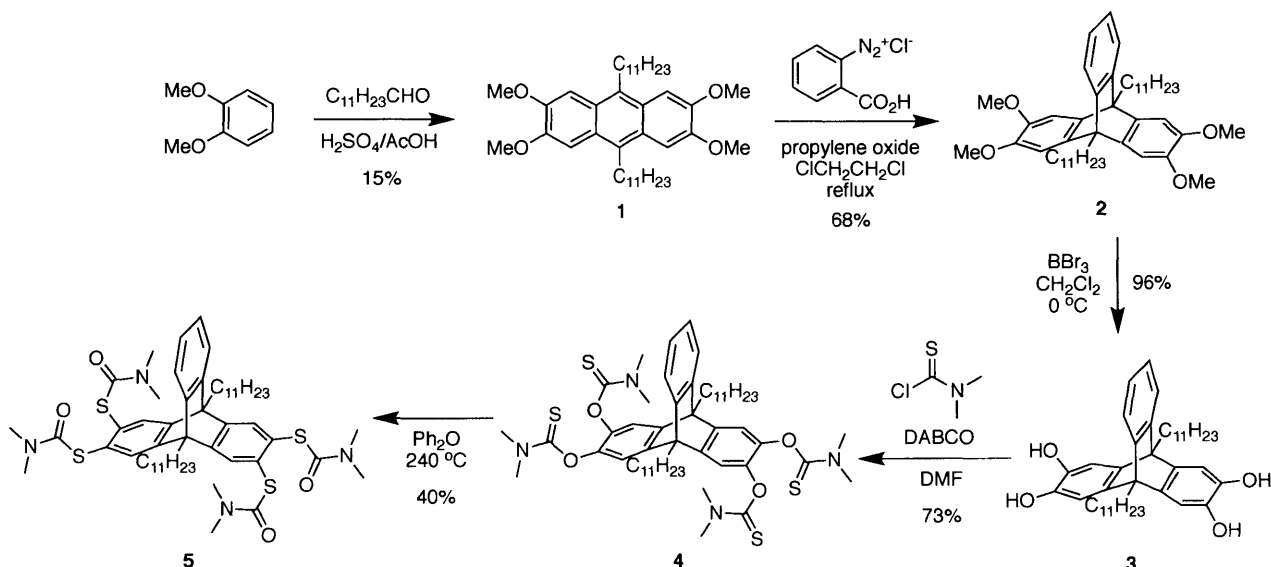
Figure 3.1. Structures of thianthrene ladder polymers **P1** and **P2**.

3.2 Results and Discussion

3.2.1 Synthesis

We commenced our study with the synthesis of our nucleophilic monomer (Scheme 3.1). Veratrole was condensed with lauric aldehyde to obtain anthracene **1**,¹⁸ which undergoes a benzyne addition to give triptycene **2**. Deprotection of the methoxy groups with BBr_3 afforded tetraol **3**. Tetraol **3** was then reacted with *N,N*-dimethylthiocarbamoyl chloride to yield *O*-

thiocarbamate **4**.¹⁹ Finally, four-fold Newman-Kwart rearrangement of *O*-thiocarbamate **4** gave *S*-thiocarbamate **5** in 40% yield.



Scheme 3.1. Synthesis of nucleophilic monomers **3** and **5**.

Ladder polymers **P1** and **P2** were synthesized by *in situ* deprotection of *S*-thiocarbamates **5** in the presence of catalytic Cs_2CO_3 and stoichiometric CaCO_3 base at 240 °C, followed by nucleophilic attacks of the resulting thiolates on 2,3,5,6-tetrafluoroterephthalonitrile **6** and 3,4,5,6-tetrafluorophthalonitrile **7** respectively (Fig. 3.2a).²⁰ Polymer **P1** was obtained in 74% conversion from monomers ($M_n = 10.1$ kDa, $\text{DP} = 12$, $\text{Đ} = 2.2$), while **P2** was obtained in 86% conversion ($M_n = 6.0$ kDa, $\text{DP} = 7$, $\text{Đ} = 1.6$). No signal was observed in the ^{19}F NMR spectra of **P1** and **P2**. The relatively high conversion and moderate molecular weight of **P2** are noteworthy as its synthesis is only possible by harnessing the dynamic, self-correcting nature of the $\text{S}_{\text{N}}\text{Ar}$ reaction.

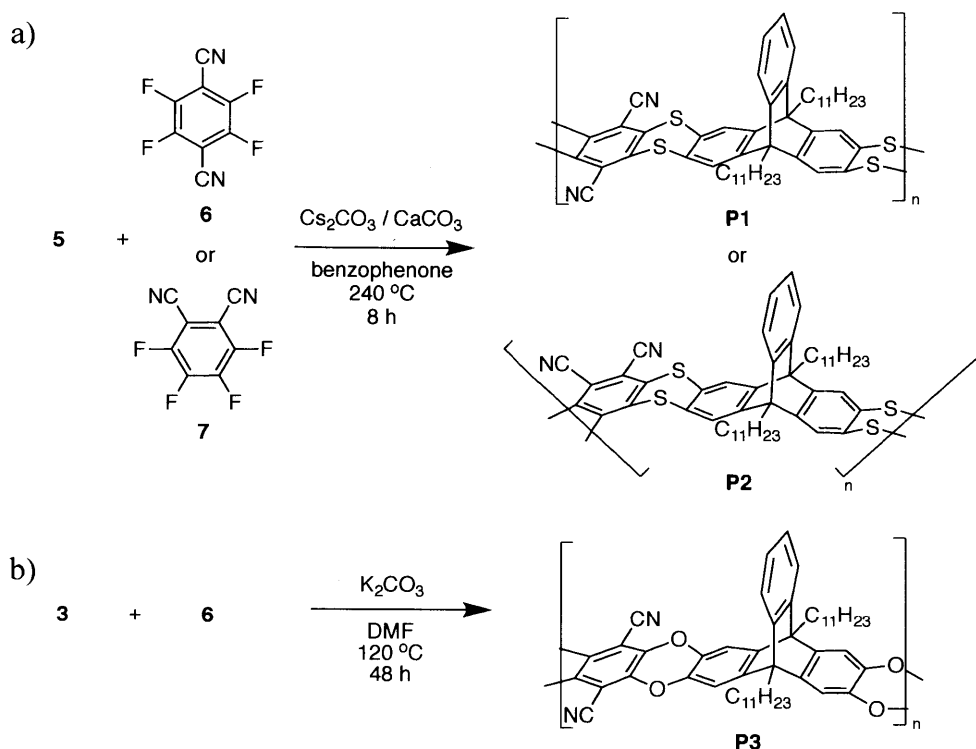


Figure 3.2. Synthesis of polymers a) **P1**, **P2**, and b) **P3** by $\text{S}_{\text{N}}\text{Ar}$ reactions.

To explore the effect of thianthrene on polymer properties, ladder polymer **P3** was also synthesized from tetraol **3** and **6** in the presence of K_2CO_3 in DMF at $120\text{ }^\circ\text{C}$ in 82% conversion from monomers (11.4 kDa, $\text{DP} = 15$, $\text{Đ} = 2.4$, Fig. 3.2b). No signal was observed in the ^{19}F NMR spectrum of **P3**. While thianthrene has a bent structure and is redox-active, dibenzo-1,4-dioxin is a planar molecule that does not possess redox properties.²¹ Hence, it is anticipated that **P3** would have significantly different properties to **P1** and **P2**.

3.2.2 Electrochemical Properties

To investigate the redox properties of the ladder polymers, **P1**, **P2** and **P3** were each drop casted onto a Pt button working electrode, and a cyclic voltammetry were performed on each of them. As expected, **P1** shows an oxidation peak at $E_{1/2} = 1.32\text{ V}$ vs. Ag/AgNO_3 (Fig. 3.3a), while

P3 shows no redox activity in the potential range tested (Fig. 3.3b). The redox peak of **P1** is comparatively higher than that of thianthrene ($E_{1/2} = 0.93$ V vs. Ag/AgNO₃, Supplementary Fig. 3.1) owing to the strong electron-withdrawing effects of the nitrile groups. Interestingly, **P2** exhibits an anomalous cyclic voltammetry with an irreversible, exponential spike in current (Supplementary Fig. 3.2). We hypothesize that the out-of-plane conformation of **P2** arising from the regiochemistry of nucleophilic attacks on 3,4,5,6-tetrafluorophthalonitrile **7** could result in appreciable molecular strain that hinders reversible flattening of thianthrene upon oxidation.

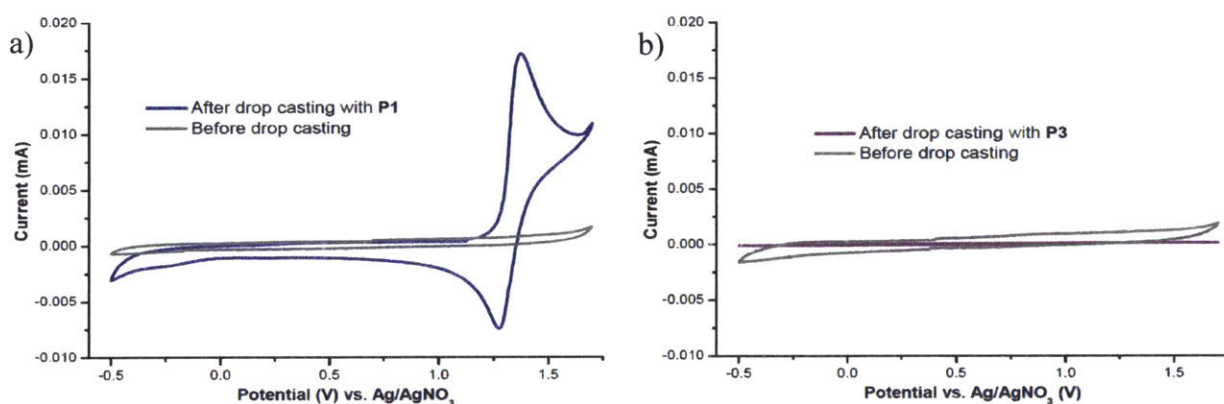


Figure 3.3. Cyclic voltammetry of a) **P1** and b) **P2** drop casted on a Pt button working electrode. The grey plots show cyclic voltammetry using the same electrode before the polymers were drop casted.

3.2.3 Photophysical Properties and Thermal Stability

Photophysical measurements of thianthrene-containing **P1** and **P2** reveal large Stokes shifts of 152 nm and 170 nm respectively between the absorption and emission spectra (Fig. 3.4a–b). In contrast, dibenzo-1,4-dioxin analog **P3** shows a much smaller Stokes shift of 45 nm (Fig. 3.4c). A similar large Stokes shift of 162 nm has also been observed in thianthrene-containing ladder macrocycle,¹⁴ suggesting that the thianthrene moiety is responsible for the large Stokes

shift. In addition, excitation spectra of **P1** and **P2** monitored at 550 nm coincided well with their respective absorption spectra, confirming that the adsorption and emission spectra observed are from the same species.

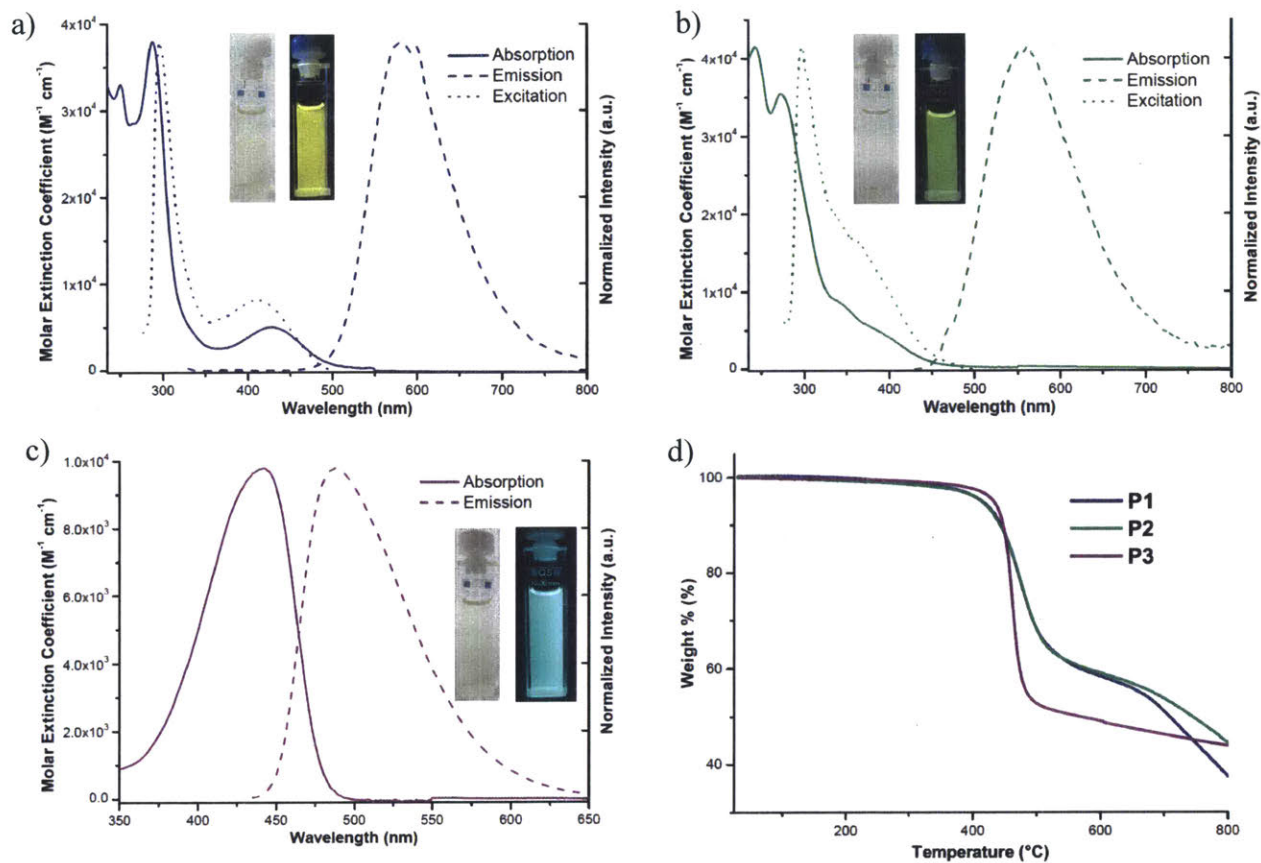


Figure 3.4. Photophysical properties of a) **P1**, b) **P2** and c) **P3**, and d) thermal stability of **P1**, **P2** and **P3**. The emission spectra of **P1**, **P2** and **P3** were excited at 300 nm, 410 nm and 420 nm respectively. The excitation spectra of **P1** and **P2** were both monitored at 550 nm.

Owing to the thermal stability of the ladder structure, **P1**, **P2** and **P3** are thermally stable up to 400 $^{\circ}C$ as demonstrated by thermogravimetric analysis (Fig. 3.4d). In particular,

dibenzodioxin-containing **P3** has a slightly higher decomposition onset temperature than thianthrene-containing **P1** and **P2**, presumably due to stronger C–O bond compared to C–S bond.

3.3 Conclusions

Two novel thianthrene ladder polymers have been synthesized in good conversions from monomers by exploiting the dynamic, self-correcting nature of the S_NAr reactions between *ortho*-aryldithiols and *ortho*-aryldifluorides. These polymers with triptycene and appending alkyl chains along their backbones possess good solubility in common organic solvents, and can be readily drop casted to form films. In contrast to dibenzodioxin, thianthrene confers the corresponding ladder polymers with interesting electrochemical and optoelectronic properties. The accompanying geometric change of thianthrene with reversible oxidation and reduction could potentially be exploited for molecular actuation, and efforts toward studying such actuation are underway.

3.4 Experimental Details

3.4.1 General

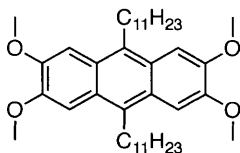
Anhydrous DMF was purchased from Aldrich as Sure-Seal Bottles and used as received. CH_2Cl_2 and THF were purified by passage through two alumina columns of an Inert solvent purification system. All other chemicals were of reagent grade and used as received. All air and water sensitive synthetic manipulations were performed in flame-dried glassware under an argon atmosphere using standard Schlenk techniques.

NMR spectra were recorded on a 400 MHz or 500 MHz spectrometer. Chemical shifts δ are reported in ppm downfield from tetramethylsilane using the residual solvent signals (CDCl_3 : δ_{H} 7.26 ppm, δ_{C} 77.16 ppm / $\text{THF-}d_8$: δ_{H} 3.58 ppm, δ_{C} 67.21 ppm) as an internal reference. For ^1H NMR, coupling constants J are given in Hz and the resonance multiplicity is described as s (singlet), d (doublet), t (triplet), p (pentet), dd (doublet of doublets), m (multiplet), and br (broad).

High-resolution mass spectrometry (HRMS) was performed using an Ion Cyclotron Resonance Mass Spectrometer with either Electrospray Ionization (ESI) or Direct Analysis in Real Time (DART) as the ionization technique. UV-vis spectroscopy was recorded on a UV-vis spectrophotometer, and corrected for background signal with a solvent-filled cuvette. Fluorescence spectra were measured using right-angle detection. Samples were excited with a 450 W xenon short arc lamp, and fluorescence was detected with a detector. The concentrations of **P1**, **P2** and **P3** used for UV-vis measurements are 2.1×10^{-5} M, 2.1×10^{-5} M and 4.5×10^{-5} M respectively. All photophysical measurements were performed with spectral grade CH_2Cl_2 .

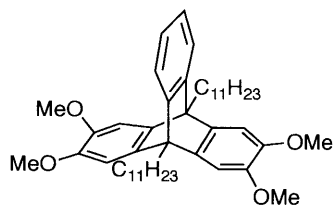
Electrochemical measurements were carried at a scan rate of 100 mV s^{-1} in 0.1 M tetrabutylammonium hexafluorophosphate (TBAPF_6) electrolyte in anhydrous MeCN, using a three-electrode cell configuration consisting of a quasi-internal Ag wire reference electrode submerged in 0.01 M AgNO_3 /0.1 M TBAPF_6 anhydrous MeCN solution, a Pt button (1.6 mm in diameter) working electrode, and a Pt coil counter electrode. All potentials were referenced to the Ag/AgNO_3 redox couple. THF Gel Permeation Chromatography (GPC) was performed (0.5 mg/mL) on an Agilent 1260 Infinity system, calibrated with polystyrene standards. Thermogravimetric analysis (TGA) was carried out with TA Instruments Q50 at $10 \text{ }^\circ\text{C min}^{-1}$ under N_2 atmosphere.

3.4.2 Synthetic Procedures



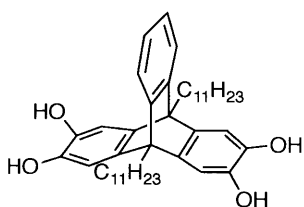
2,3,6,7-Tetramethoxy-9,10-diundecylanthracene (1)

To a cooled solution of veratrole (32 mL, 250 mmol) at 0 °C in acetic acid (300 mL) was slowly added ice-cold solution of lauric aldehyde (56 mL, 250 mmol) in MeCN (13 mL). The reaction mixture was stirred for 1 h. Concentrated H₂SO₄ (300 mL) was added dropwise over 1 h at 0 °C, causing the solution to turn pink and then dark red. The reaction was then stirred overnight, slowly warming to room temperature. The reaction mixture was then poured into ice-water and the crude product precipitated out as brown solid. The crude product was washed with water, MeOH and finally acetone (×2) with sonication to obtain 1 as a yellow powder (11.1 g, 15%). ¹H NMR (500 MHz, CDCl₃) δ 7.40 (s, 4H), 4.07 (s, 12H), 3.41 (m, 4H), 1.82 (p, *J* = 7.5 Hz, 4H), 1.59 (p, *J* = 7.2 Hz, 4H), 1.46 (p, *J* = 7.3, 4H), 1.36–1.28 (m, 24H), 0.89 (t, *J* = 6.8 Hz, 6H). ¹³C NMR (126 MHz, CDCl₃) δ 148.9, 129.6, 125.4, 102.6, 55.7, 32.0, 30.4, 30.3, 29.9, 29.81, 29.78, 29.7, 29.5, 28.8, 22.8, 14.3. HRMS (ESI) *m/z* calculated for C₄₀H₆₃O₄ [M+H]⁺: 607.4726; found: 607.4719.



(9s,10s)-2,3,6,7-Tetramethoxy-9,10-diundecyl-9,10-dihydro-9,10-[1,2]benzenoanthracene (2)

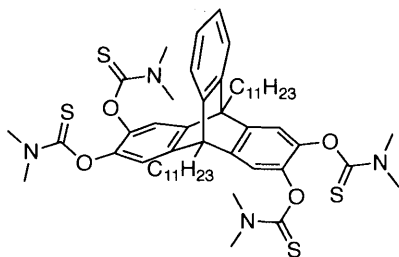
To a solution of **1** (11 g, 18.1 mmol) in 1,2-dichloroethane (200 mL) and propylene oxide (16 mL) was added 2-carboxybenzenediazonium chloride (6.7 g, 36.2 mmol). The reaction was stirred under reflux for 4 h. The reaction mixture was then filtered. The filtrate was concentrated and recrystallized from ethanol to obtain **2** as white solid (8.35 g, 68%). **¹H NMR** (500 MHz, CDCl₃) δ 7.43 (br, 2H), 7.06 (m, 6H), 3.92 (s, 12H), 2.95 (t, *J* = 7.3 Hz, 4H), 2.27 (p, *J* = 7.6 Hz, 4H), 1.92 (p, *J* = 7.5 Hz, 4H), 1.64 (p, *J* = 7.1 Hz, 4H), 1.52 (p, *J* = 6.5 Hz, 4H), 1.46 (m, 4H), 1.39 (m, 16H), 0.98 (t, *J* = 6.7 Hz, 6H). **¹³C NMR** (126 MHz, CDCl₃) δ 148.7, 145.3, 141.1, 124.2, 121.5, 107.6, 56.3, 52.7, 32.1, 32.0, 30.0, 29.81, 29.76, 29.7, 29.4, 28.7, 25.8, 22.7, 14.2. **HRMS** (DART) *m/z* calculated for C₄₆H₆₇O₄ [M+H]⁺: 683.5039; found: 683.5031.



(9s,10s)-9,10-Diundecyl-9,10-dihydro-9,10-[1,2]benzenoanthracene-2,3,6,7-tetraol (3)

To a stirred solution of **2** (6 g, 8.78 mmol) in CH₂Cl₂ (120 mL) at 0 °C was added BBr₃ (3.5 mL, 36.9 mmol) quickly, causing the orange solution to turn intense purple. After stirring for 4 h, the reaction mixture was quenched with cold water, concentrated to remove CH₂Cl₂, and filtered. The

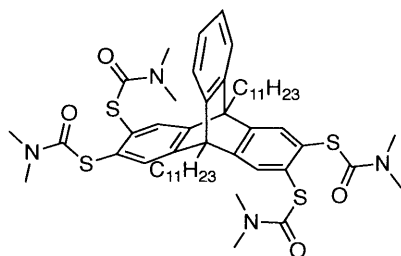
residue was washed with deionized water, and dried to obtain a light purple solid. The light purple solid was dissolved in THF (120 mL), and was added a solution of sodium dithionite (7.7 g, 44 mmol) in deionized water (30 mL). After stirring at room temperature for 30 mins, the reaction mixture was concentrated to remove THF, and filtered to obtain crude product **3** as a brown-orange solid (5.28 g, 96%) and used without purification. $^1\text{H NMR}$ (500 MHz, THF- d_8) δ 7.42 (br, 4H), 7.22 (br, 2H), 6.84 (s, 2H), 6.77 (s, 4H), 2.70 (m, 4H), 2.13 (m, 4H), 1.78 (p, $J = 7.6$ Hz, 4H), 1.56 (p, $J = 7.0$ Hz, 4H), 1.47 (m, 4H), 1.44–1.33 (s, 20H), 0.91 (t, $J = 6.8$ Hz, 6H). $^{13}\text{C NMR}$ (126 MHz, THF- d_8) δ 149.9, 140.9, 140.1, 123.4, 121.0, 110.5, 51.7, 32.1, 31.9, 30.0, 29.9, 29.8, 29.6, 29.5, 29.1, 25.5, 22.8, 13.8. **HRMS** (DART) m/z calculated for $\text{C}_{42}\text{H}_{59}\text{O}_4$ $[\text{M}+\text{H}]^+$: 627.4413; found: 627.4386.



***O,O',O'',O'''*-((9*s*,10*s*)-9,10-Diundecyl-9,10-dihydro-9,10-[1,2]benzenoanthracene-2,3,6,7-tetrayl) tetrakis(dimethylcarbamothioate) (**4**)**

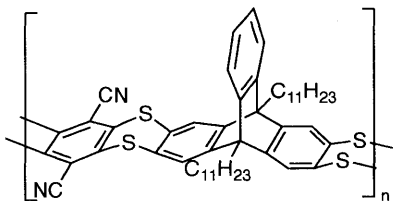
To a stirred solution of **3** (5.78 g, 9.22 mmol) in DMF (85 mL) under argon was added 1,4-diazabicyclo[2.2.2]octane (8.28 g, 73.8 mmol) and *N,N*-dimethylthiocarbamoyl chloride (9.12 g, 73.8 mmol). After stirring at room temperature overnight, the reaction mixture was poured into deionized water and filtered. The residue was purified by recrystallization using $\text{CH}_2\text{Cl}_2/\text{EtOH}$ to obtain **4** as an off-white solid (6.53 g, 73%). $^1\text{H NMR}$ (500 MHz, CDCl_3) δ 7.33 (br, 2H), 7.16 (s, 4H), 6.99 (dd, $J = 5.7, 3.0$ Hz, 2H), 3.38 (s, 12H), 3.22 (s, 12H), 2.80 (m, 4H), 2.13 (p, $J = 8.2$ Hz,

4H), 1.70 (p, $J = 7.5$ Hz, 4H), 1.51 (m, 4H), 1.43–1.30 (m, 24H), 0.90 (t, $J = 6.8$ Hz, 6H). ^{13}C NMR (126 MHz, CDCl_3) δ 186.7, 147.3, 146.0, 141.4, 124.6, 122.4, 118.6, 52.7, 43.3, 38.8, 32.0, 31.8, 29.8, 29.77, 29.73, 29.7, 29.5, 28.5, 25.0, 22.8, 14.2. HRMS (ESI) m/z calculated for $\text{C}_{54}\text{H}_{78}\text{N}_4\text{O}_4\text{S}_4\text{Na}$ $[\text{M}+\text{Na}]^+$: 997.4798; found: 997.4807.



***S,S',S'',S'''*-((9*s*,10*s*)-9,10-Diundecyl-9,10-dihydro-9,10-[1,2]benzenoanthracene-2,3,6,7-tetrayl) tetrakis(dimethylcarbamothioate) (5)**

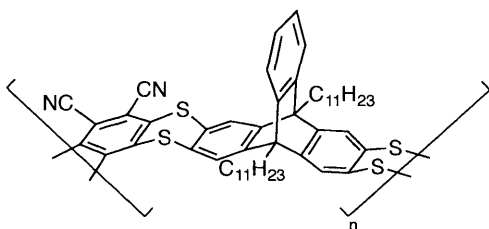
To a stirred Ph_2O solution (35 mL) at 240 °C under argon was added **4** (3 g, 3.08 mmol). After stirring for 1 h, the reaction mixture was cooled. The reaction mixture was purified by flash column chromatography, eluting with first hexane, then 1:1 ethyl acetate/hexane, and finally ethyl acetate to obtain **5** as a brown foam (1.86 g, 62%). R_f (1:1 ethyl acetate/hexane) = 0.1. ^1H NMR (500 MHz, CDCl_3) δ 7.64 (s, 4H), 7.35 (s, 2H), 6.99 (m, 2H), 3.05 (br., 12H), 2.98 (br., 12H), 2.86 (t, $J = 7.7$ Hz, 4H), 2.14 (t, $J = 7.9$ Hz, 4H), 1.75 (p, $J = 7.5$ Hz, 4H), 1.54 (p, $J = 7.1$ Hz, 4H), 1.43 (p, $J = 6.3$ Hz, 4H), 1.39–1.29 (m, 20H), 0.92 (t, $J = 6.7$ Hz, 6H). ^{13}C NMR (126 MHz, CDCl_3) δ 166.1, 149.0, 146.4, 131.0, 130.4, 124.6, 122.7, 77.4, 52.8, 36.9, 31.9, 31.7, 29.7, 29.64, 29.55, 29.4, 28.0, 24.8, 22.7, 14.1. HRMS (ESI) m/z calculated for $\text{C}_{54}\text{H}_{78}\text{N}_4\text{O}_4\text{S}_4\text{Na}$ $[\text{M}+\text{Na}]^+$: 997.4798; found: 997.4815.



Ladder Polymer (P1)

To a microwave tube was added *S*-thiocarbamates **5** (48.8 mg, 0.05 mmol), 2,3,5,6-tetrafluoroterephthalonitrile (10.0 mg, 0.05 mmol), CaCO₃ (30.0 mg, 0.30 mmol), Cs₂CO₃ (5.0 mg, 0.015 mmol), and benzophenone (0.6 g). The microwave tube was capped in a glovebox under nitrogen atmosphere. The mixture was reacted under microwave conditions at 240 °C for 8 h. The reaction mixture was cooled and precipitated into a dilute solution of HCl in MeOH. The precipitate was washed with MeOH, hot acetone and hot ethyl acetate, and finally dried in vacuo to obtain **P1** as a brown powder (30 mg, 74% conversion). ¹H NMR (400 MHz, THF-*d*₃) δ 7.59 (br, 4H), 7.40 (br, 2H), 6.99 (br, 2H), 2.88 (br, 4H), 2.07 (br, 4H), 1.86 (br, 4H), 1.56 (br, 4H), 1.45–1.34 (m, 24H), 0.90 (br, 6H). GPC (THF): M_n = 10.1 kDa, DP = 12, Đ = 2.2.

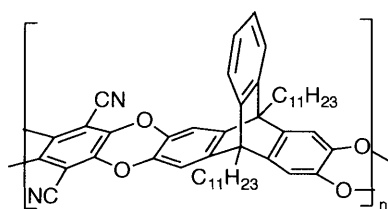
Ladder Polymer (P2)



To a microwave tube was added *S*-thiocarbamates **5** (48.8 mg, 0.05 mmol), 3,4,5,6-tetrafluorophthalonitrile (10.0 mg, 0.05 mmol), CaCO₃ (30.0 mg, 0.30 mmol), Cs₂CO₃ (5.0 mg, 0.015 mmol), and benzophenone (0.6 g). The microwave tube was capped in a glovebox under

nitrogen atmosphere. The mixture was reacted under microwave conditions at 240 °C for 8 h. The reaction mixture was cooled and precipitated into a dilute solution of HCl in MeOH. The precipitate was washed with MeOH, hot acetone and hot ethyl acetate, and dried in vacuo to obtain **P2** as a brown powder (35 mg, 86% conversion). **¹H NMR** (400 MHz, THF-*d*₈) δ 7.60 (br, 4H), 7.43 (br, 2H), 7.04 (br, 2H), 2.91 (br, 4H), 2.12 (br, 4H), 1.89 (br, 4H), 1.40–1.35 (m, 24H), 0.90 (br, 6H). **GPC** (THF): $M_n = 6.0$ kDa, DP = 7, Đ = 1.6.

Ladder Polymer (**P3**)



To a Schlenk flask containing tetraol **3** (62.7 mg, 0.1 mmol), 2,3,5,6-tetrafluoroterephthalonitrile (20.0 mg, 0.1 mmol) and K₂CO₃ (82.9 mg, 0.06 mmol) under argon, was added anhydrous DMF (3mL). The reaction was stirred at 80 °C for 3 h and then at 120 °C for 45 h. The mixture was cooled and precipitated into a dilute solution of HCl in MeOH. The precipitate was washed with MeOH, hot acetone and hot ethyl acetate, and dried to obtain **P3** as a bright yellow powder (61.9 mg, 82% conversion). **¹H NMR** (500 MHz, THF-*d*₈) δ 7.37 (br, 2H), 7.08 (br, 2H), 7.01 (br, 4H), 2.83 (br, 4H), 2.09 (br, 4H), 1.83 (br, 4H), 1.58 (br, 4H), 1.48–1.32 (m, 24H), 0.92 (m, 6H). **GPC** (THF): $M_n = 11.4$ kDa, DP = 15, Đ = 2.4.

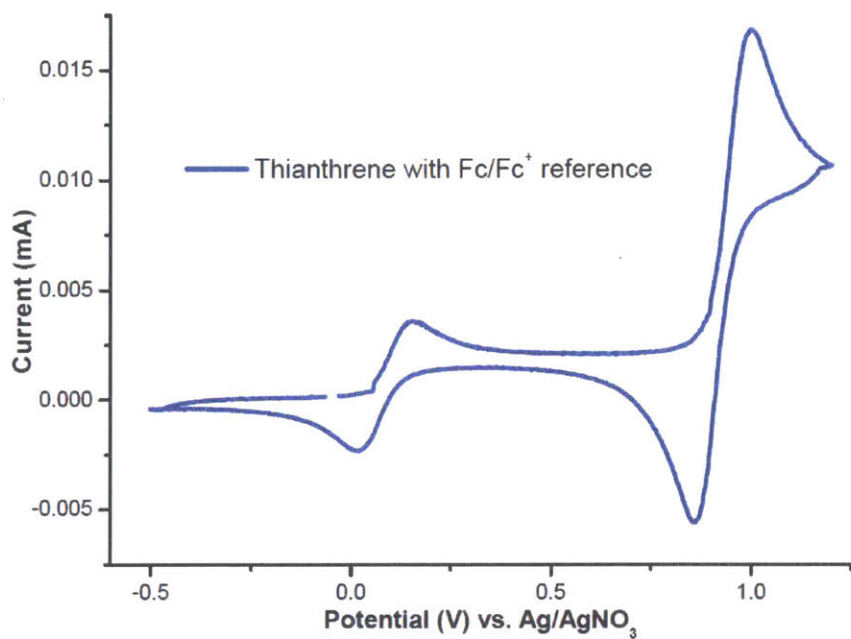
3.5 References

- 1 Jones, R. G.; Kahovec, J.; Stepto, R.; Wilks, E. S.; Hess, M.; Kitayama, T.; Metanomski, W. V. *Compendium of Polymer Terminology and Nomenclature - IUPAC Recommendations 2008*; The Royal Society of Chemistry, 2009.
- 2 Overberger, C. G.; Moore, J. A. *Ladder polymers in Advances in Polymer Science*; Springer: Berlin, Heidelberg, 1970.
- 3 McKeown, N. B.; Budd, P. M. *Chem. Soc. Rev.* **2006**, *35* (8), 675.
- 4 McKeown, N. B.; Budd, P. M. *Macromolecules* **2010**, *43* (12), 5163.
- 5 Chen, J.; Yang, K.; Zhou, X.; Guo, X. *Chem. Asian J.* **2018**, *13* (18), 2587.
- 6 Yu, L.; Chen, M.; Dalton, L. R. *Chem. Mater.* **1990**, *2* (6), 649.
- 7 Rose, I.; Bezzu, C. G.; Carta, M.; Comesaña-Gándara, B.; Lasseguette, E.; Ferrari, M. C.; Bernardo, P.; Clarizia, G.; Fuoco, A.; Jansen, J. C.; Hart, Kyle E.; Liyana-Arachchi, T. P.; Colina, C. M.; McKeown, N. B. *Nat. Mater.* **2017**, *16*, 932.
- 8 Carta, M.; Malpass-Evans, R.; Croad, M.; Rogan, Y.; Jansen, J. C.; Bernardo, P.; Bazzarelli, F.; McKeown, N. B. *Science* **2013**, *339* (6117), 303.
- 9 Lee, J.; Kalin, A. J.; Yuan, T.; Al-Hashimi, M.; Fang, L. *Chem. Sci.* **2017**, *8* (4), 2503.
- 10 Scherf, U. *J. Mater. Chem.* **1999**, *9* (9), 1853.

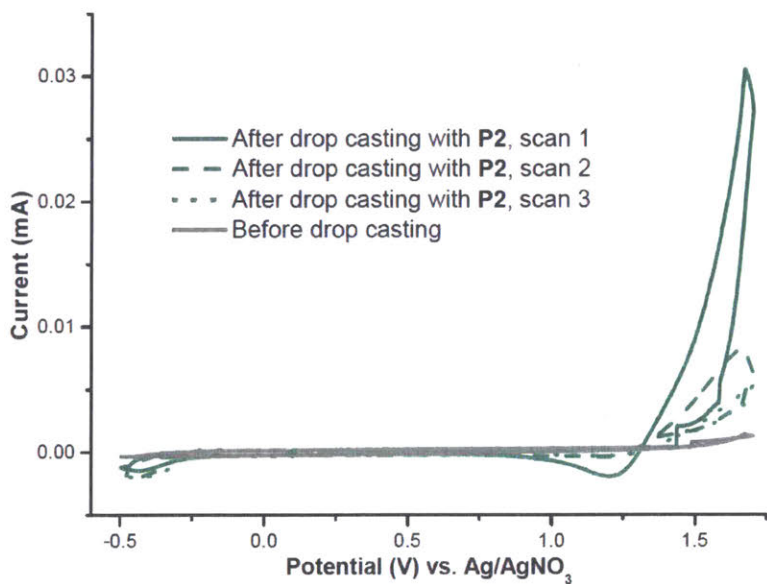
- 11 Parkhurst, R. R.; Swager, T. M. *Antiaromaticity in Nonbenzenoid Oligoarenes and Ladder Polymers in Polyarenes II*; Springer International Publishing: Cham, 2014.
- 12 Teo, Y. C.; Lai, H. W. H.; Xia, Y. *Chem. Eur. J.* **2017**, *23* (57), 14101.
- 13 Scherf, U.; Müllen, K. *The synthesis of ladder polymers in Synthesis and Photosynthesis*; Springer: Berlin, Heidelberg, 1995.
- 14 Ong, W. J.; Swager, T. M. *Nat. Chem.* **2018**, *10* (10), 1023.
- 15 Shine, H. J.; Piette, L. *J. Am. Chem. Soc.* **1962**, *84* (24), 4798.
- 16 Rapta, P.; Kress, L.; Hapiot, P.; Dunsch, L. *Phys. Chem. Chem. Phys.* **2002**, *4* (17), 4181.
- 17 Bock, H.; Rauschenbach, A.; Näther, C.; Kleine, M.; Havlas, Z. *Chem. Ber.* **1994**, *127* (10), 2043.
- 18 Zong, Q.-S.; Chen, C.-F. *Org. Lett.* **2006**, *8* (2), 211.
- 19 Mahendran, A.; Vuong, A.; Aebischer, D.; Gong, Y.; Bittman, R.; Arthur, G.; Kawamura, A.; Greer, A. *J. Org. Chem.* **2010**, *75* (16), 5549.
- 20 Ding, Y.; Hlil, A. R.; Hay, A. S.; Tsuchida, E.; Miyatake, K. *Macromolecules* **1999**, *32* (2), 315.
- 21 Mastryukov, V. S.; Chen, K.-H.; Simonsen, S. H.; Allinger, N. L.; Boggs, J. E. *J. Mol. Struct.* **1997**, *413–414* (0), 1.

3.6 Appendix for Chapter 3

Cyclic Voltammetry (CV) of Compounds

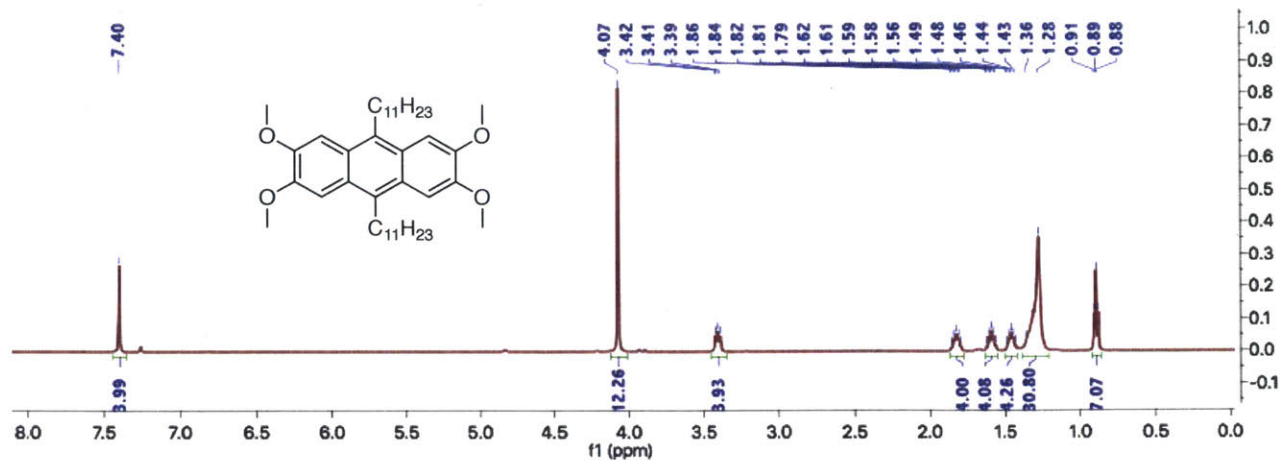


Supplementary Figure 3.1. CV of thianthrene with Fc/Fc⁺ as external reference.

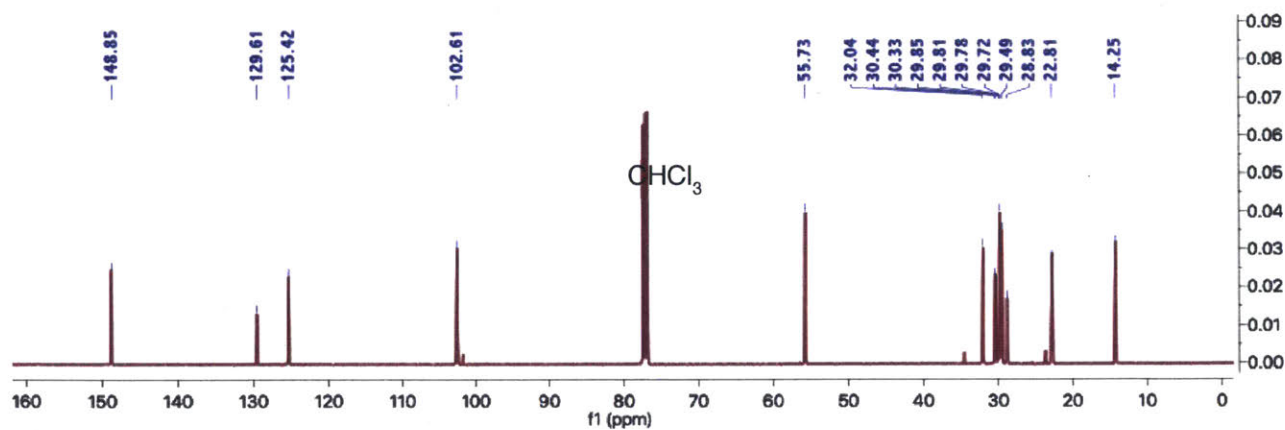


Supplementary Figure 3.2. CV of P2.

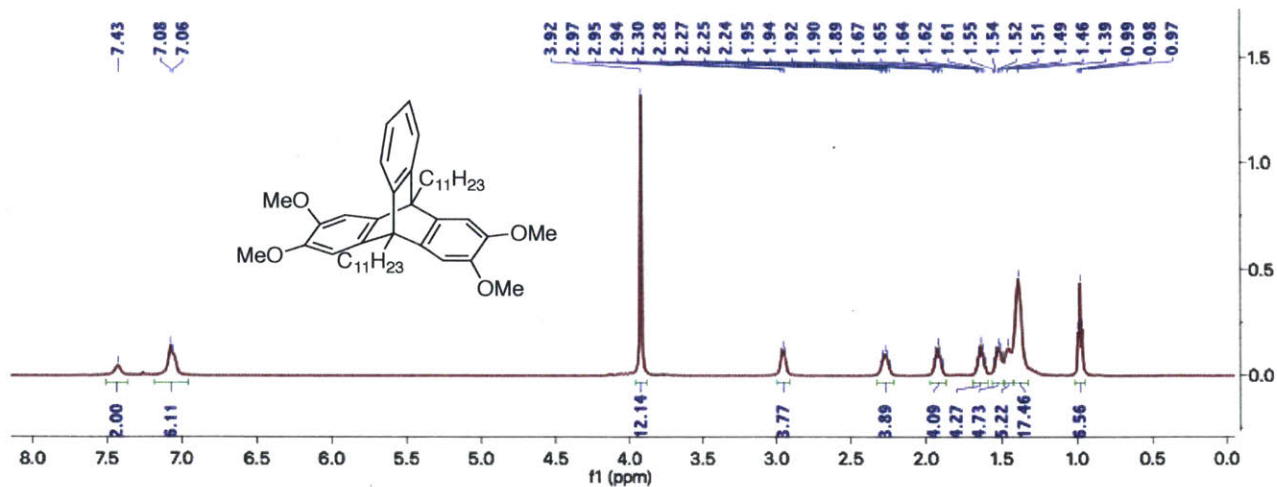
NMR Spectra



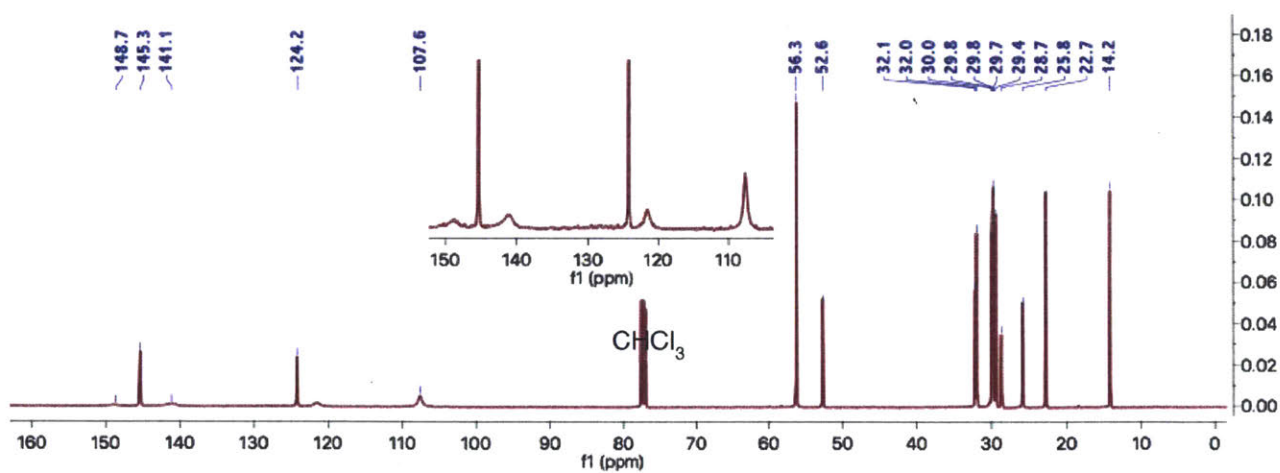
¹H NMR spectrum (500 MHz, CDCl₃) of 1.



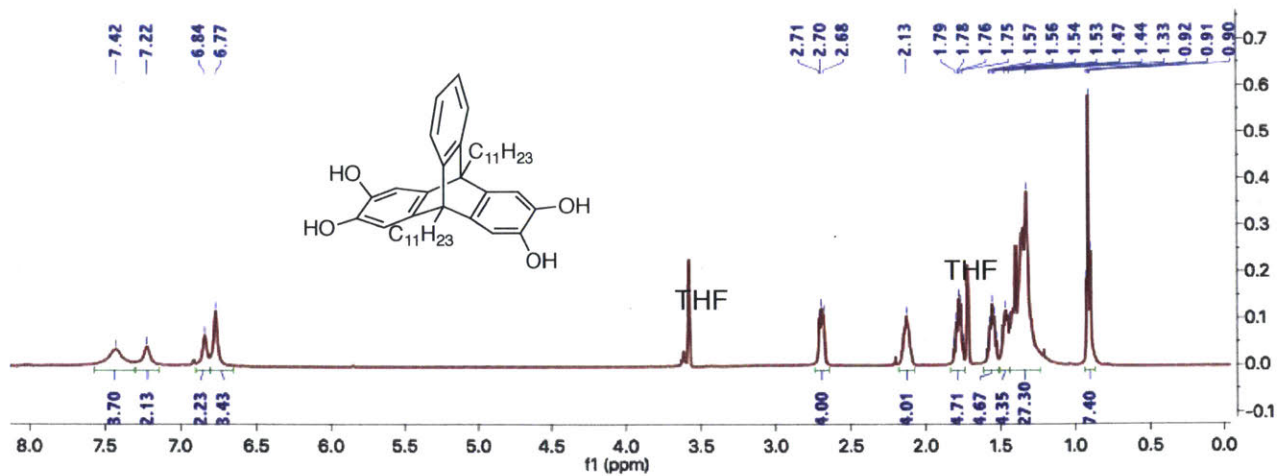
¹³C NMR spectrum (126 MHz, CDCl₃) of 1.



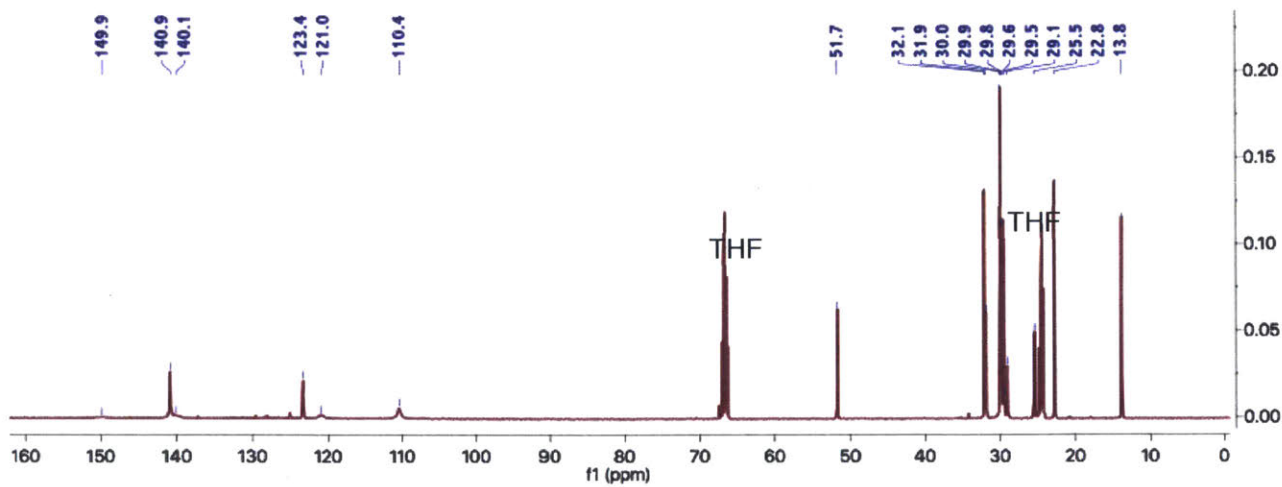
^1H NMR spectrum (500 MHz, CDCl_3) of **2**.



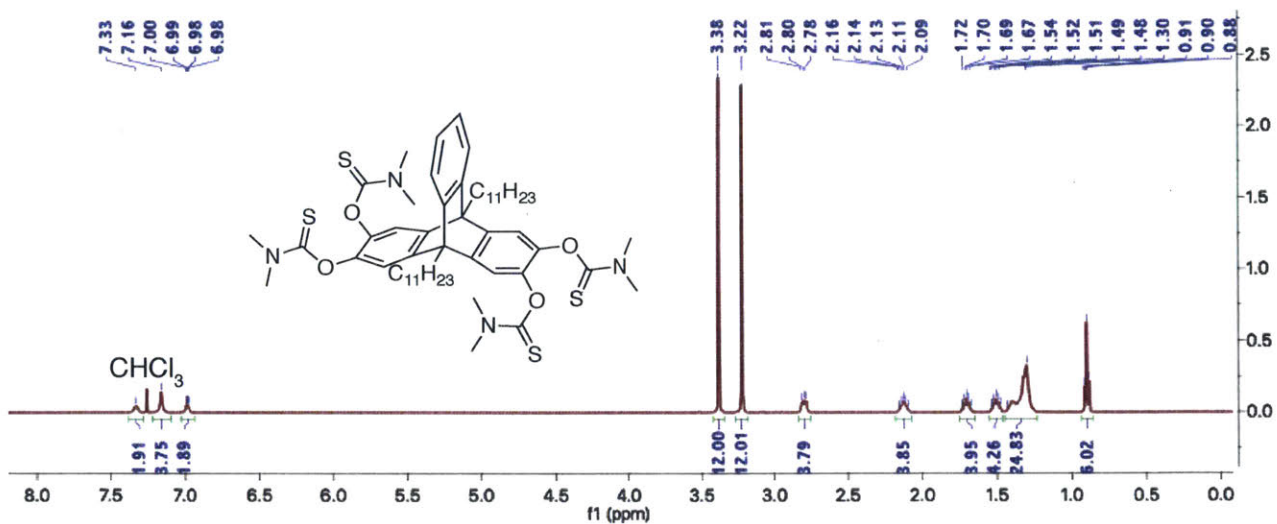
^{13}C NMR spectrum (126 MHz, CDCl_3) of **2**.



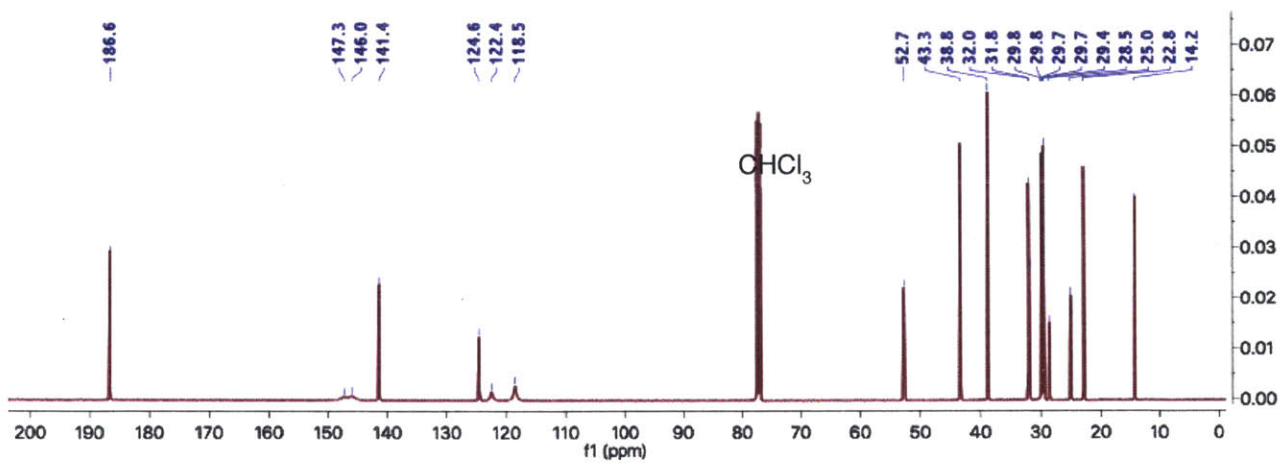
¹H NMR spectrum (500 MHz, THF-*d*₈) of 3.



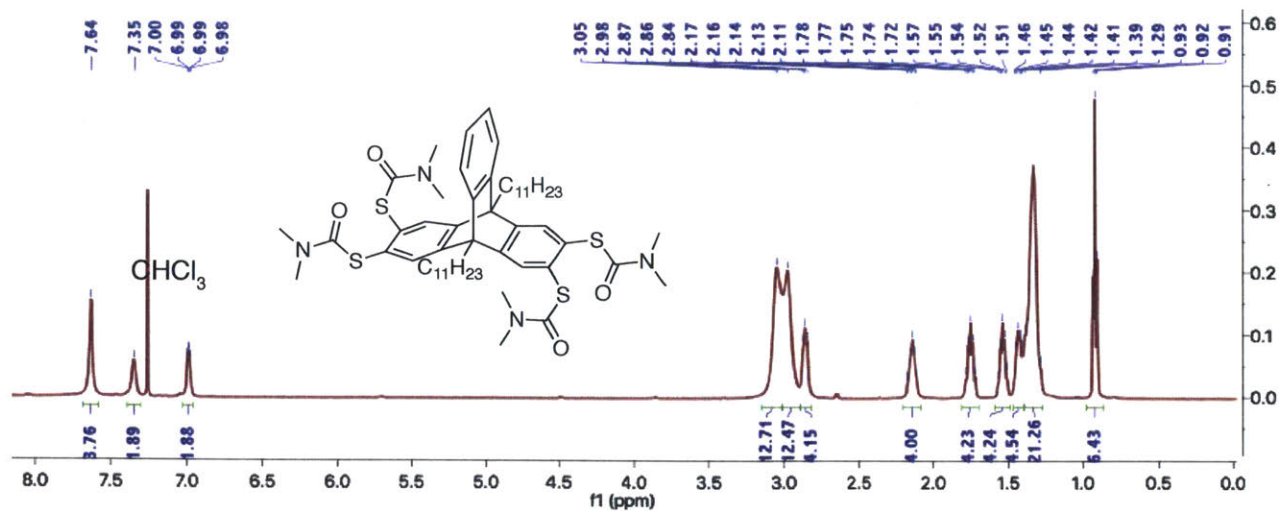
¹³C NMR spectrum (126 MHz, THF-*d*₈) of 3.



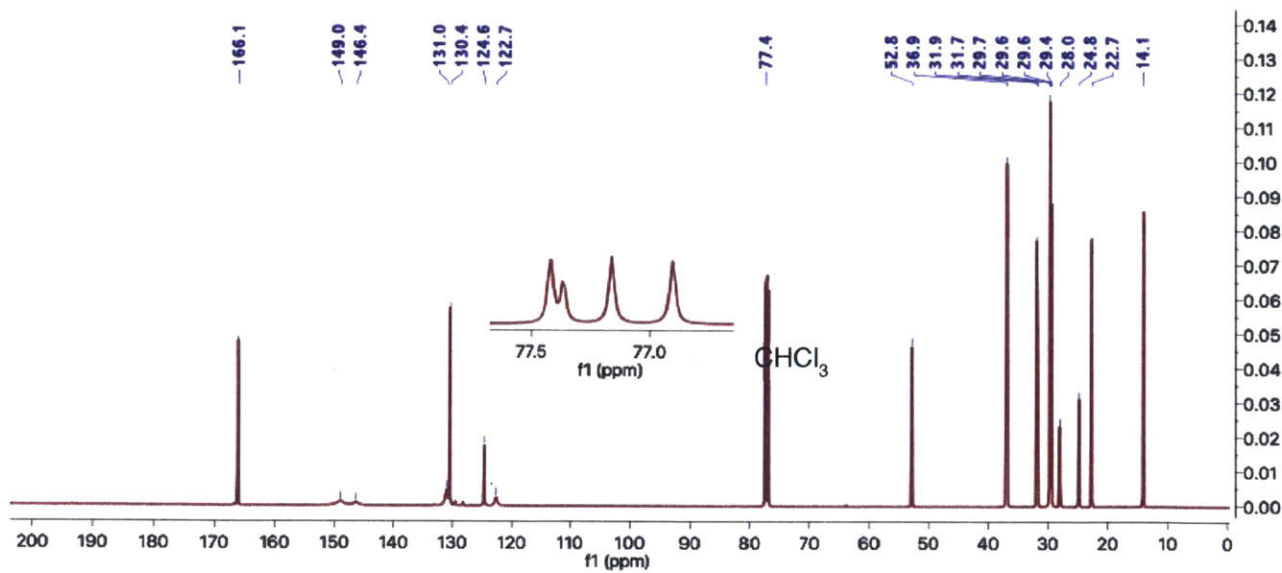
1H NMR spectrum (500 MHz, $CDCl_3$) of 4.



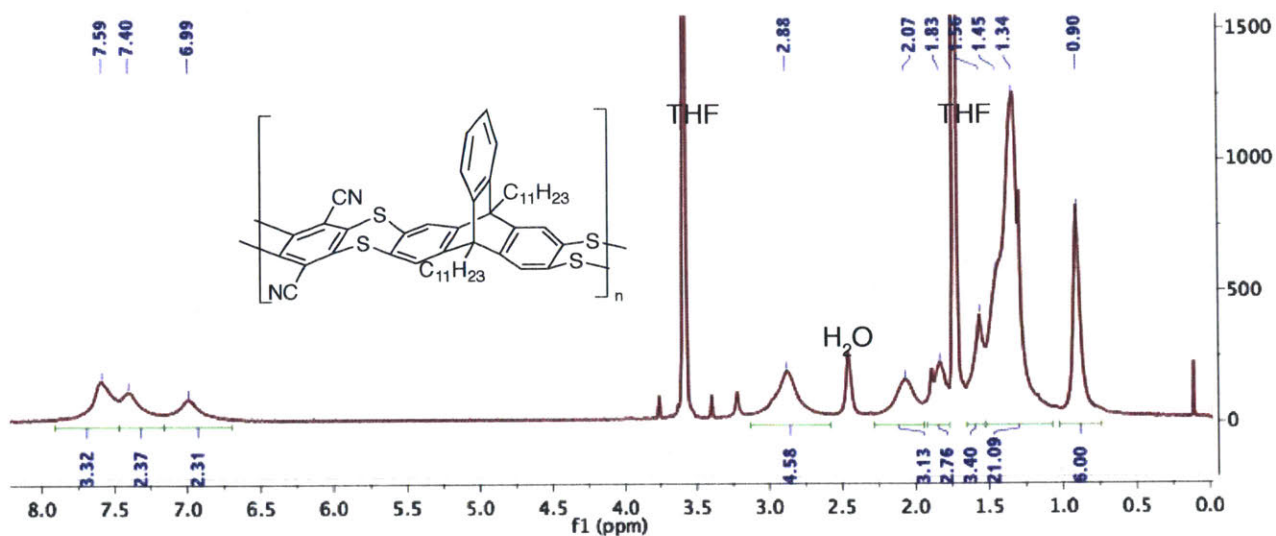
^{13}C NMR spectrum (126 MHz, $CDCl_3$) of 4.



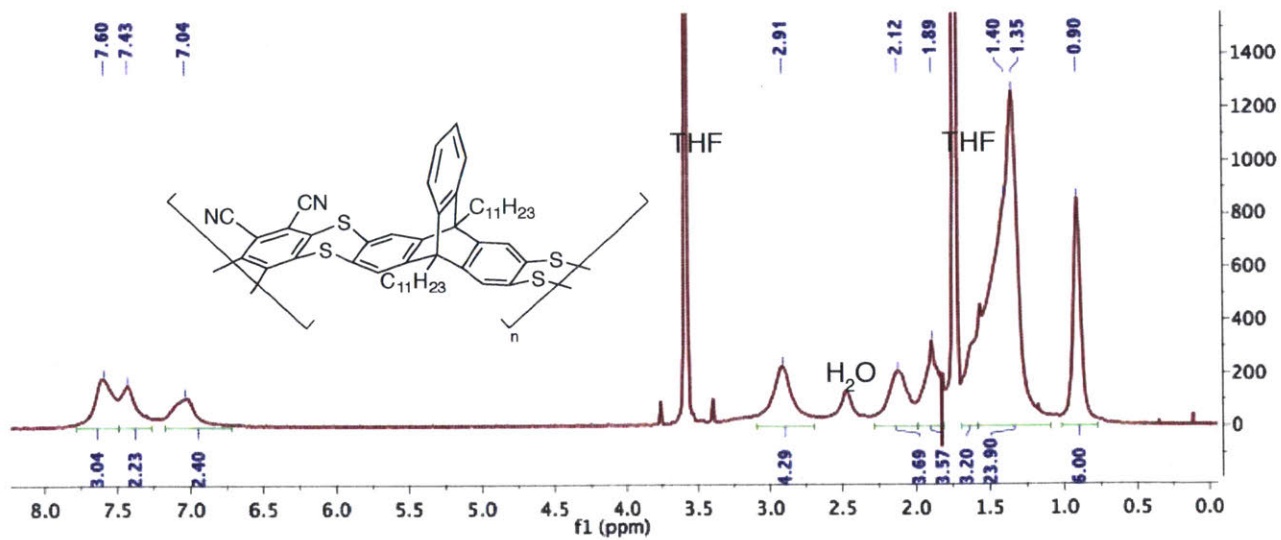
¹H NMR spectrum (500 MHz, CDCl₃) of **5**.



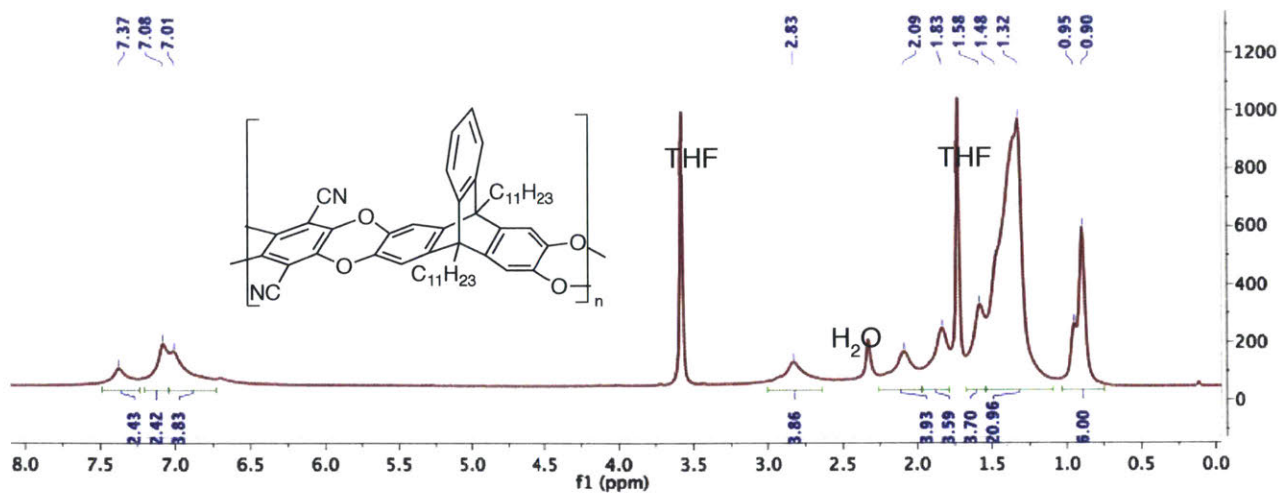
¹³C NMR spectrum (126 MHz, CDCl₃) of **5**.



^1H NMR spectrum (400 MHz, $\text{THF-}d_8$) of **P1**.



^1H NMR spectrum (400 MHz, $\text{THF-}d_8$) of **P2**.



¹H NMR spectrum (500 MHz, THF-*d*₈) of **P3**.

Chapter 4

Redox Switchable Thianthrene Cavitands

Abstract

A redox activated vase-to-kite conformational change is reported for a new resorcinarene-based cavitand appended with four quinoxaline-fused thianthrene units. In its neutral state, the thianthrene-containing cavitand was shown by ¹H NMR to adopt a closed vase conformation. Upon oxidation the electrostatic repulsion among the thianthrene radical cations promotes a kite conformation in the thianthrene-containing cavitand. The addition of acid produced a shoulder feature below 300 nm in cavitand's UV-Vis spectrum that we have assigned to the vase-to-kite conformation change. UV-Vis spectroelectrochemical studies of the cavitand revealed a development of a similar shoulder peak consistent with the oxidation-induced vase-to-kite conformation change. To support that the shoulder peak is diagnostic for a vase-to-kite conformation change, a model molecule constituting a single quinoxaline wall of the cavitand was synthesized and studied. As expected UV-Vis spectroelectrochemical studies of the cavitand arm did not display a shoulder peak below 300 nm. The oxidation-induced vase-to-kite conformation is further confirmed by the distinctive upfield shift in ¹H chemical shift of the methine signal.

Parts of this chapter were adapted and reprinted with permission from Ong, W. J.; Bertani, F.; Dalcanale, E.; Swager, T. M. "Redox switchable thianthrene cavitands" *Synthesis* 2017, 49, 358.

4.1 Introduction

Since the first reported synthesis of quinoxaline-bridged resorcinarene cavitand by Cram and co-workers in 1982,¹ the diversity and complexity in both the structures and functionalities of cavitand derivatives have expanded dramatically. To date, cavitands have found utility as switches,² receptors,³ sensors,⁴ catalysts,⁵ molecular hosts,⁶ molecular grippers⁷ and solid-phase microextractors.⁸ Many of these applications hinge on the ability of quinoxaline-bridged cavitands to adopt, often in response to an external stimulus, two spatially well-defined conformations: closed “vase” and open “kite” forms.

Resorcinarene cavitands with four quinoxaline bridges are known to undergo vase-kite conformational switching induced by changes in temperature,⁹ pH,¹⁰ and metal ion concentration.¹¹ To harness the unique conformational switching properties of these cavitands in electronic devices, we have sought to effect the vase-kite conformation by redox reactions. In 2006, Diederich reported electrochemical molecular switching using a tetrathiafulvalene (TTF)-bridged resorcinarene cavitand.¹² The incorporation of electroactive TTF groups in quinoxaline-based cavitands is synthetically challenging and changes in the cyclic voltammetry and differential pulse voltammetry spectra were used as evidence for electrochemically-induced vase-to-kite conformation change. More recently, the same group developed quinone-based, redox-active resorcinarene cavitands that utilize intramolecular hydrogen bonding, which is only present in the reduced hydroquinone state, to stabilize the vase conformation.¹³ While such a system successfully demonstrated the viability of redox switchable cavitands, the deployment of quinone-based cavitands in electronic devices is limited by the need for an external proton source (e.g. a protic solvent). Moreover, electrochemical kinetics requiring coupled delivery of protons is often

sluggish. To circumvent these problems, Peris and co-workers recently reported a tetraferrocenyl-resorcinarene cavitand as a redox-switchable host for ammonium salts.¹⁴ However, this cavitand remains in vase conformation in both the neutral and +4 oxidation states.

Hence, there is still a need for redox-active resorcinarene cavitands that are readily synthesized and undergo rapid electrochemically-induced vase-kite conformation changes. Herein, we report the synthesis and conformational switching properties of a novel resorcinarene-based cavitand **1** featuring four thianthrene-fused thianthrene units (Fig. 4.1).

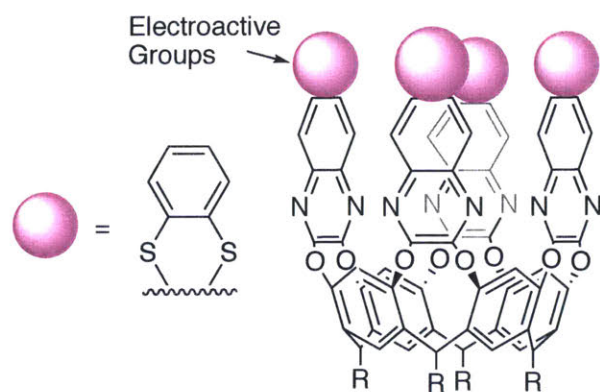


Figure 4.1. Structure of thianthrene-containing cavitand **1**.

Thianthrene has been studied extensively for its redox activity,¹⁵ and a peculiar aspect of its redox chemistry is the geometric changes that accompany oxidation (Fig. 4.2). In its neutral state, thianthrene is a bent molecule with a fold angle of 128° between the two planes of benzene rings. The folded structure appears to be favored in the neutral state to avoid repulsion between occupied $3p_z(\text{Sulfur})-\pi^*_{cc}$ orbitals.¹⁶ Upon oxidation, both the radical cation and the dication are planar with a fold angle of ~180° (Fig. 4.2).¹⁷ We hypothesized that neutral **1** will adopt the vase conformation and with oxidation electrostatic repulsion among the thianthrene radical cations will favor the kite conformation (Fig. 4.3). The combination of the thianthrene and cavitand

conformational changes has the prospect to endow these systems with new electroactive complexing properties.

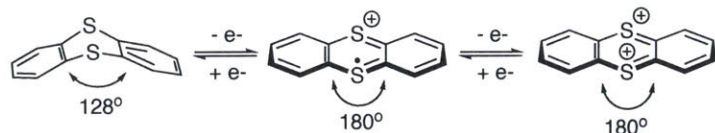


Figure 4.2. Different redox states of thianthrene and their corresponding fold angles.

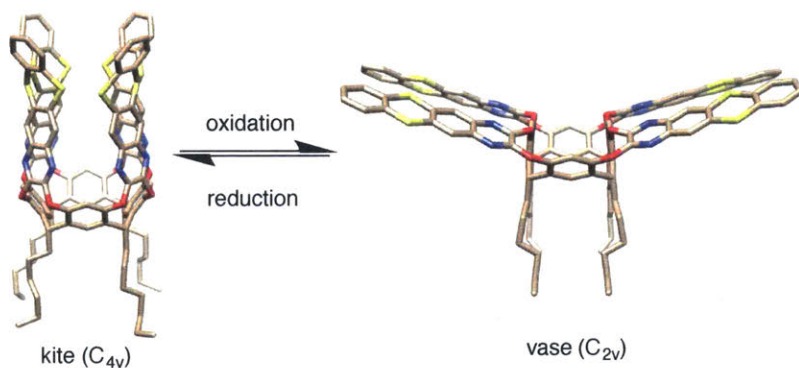
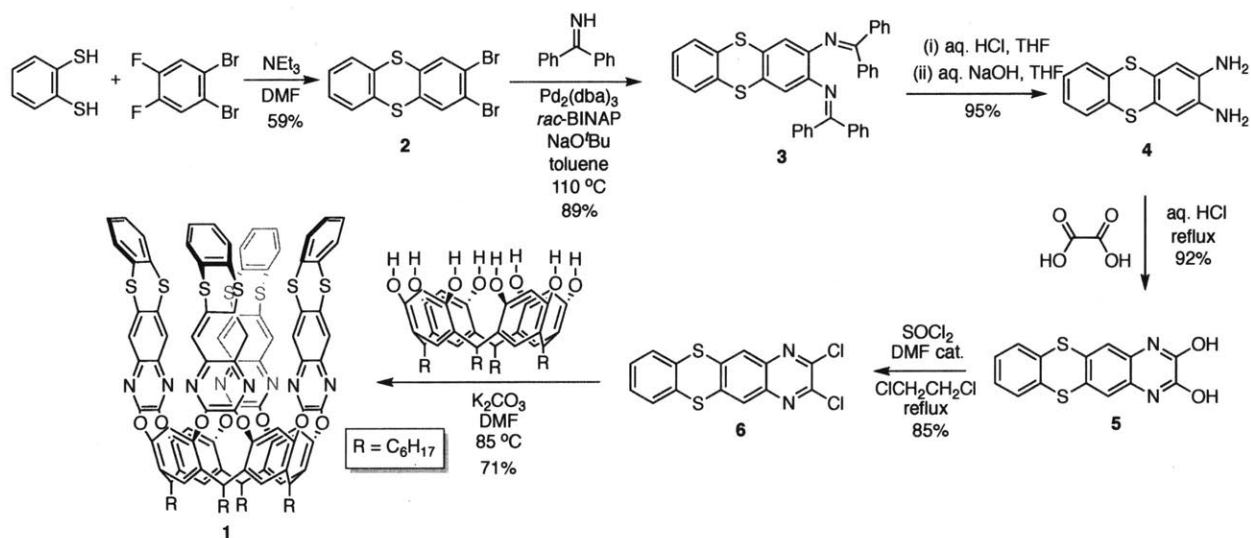


Figure 4.3. Vase-kite conformation change of thianthrene-containing cavitand **1** upon electrochemical stimuli.

4.2 Results and Discussion

To demonstrate electrochemical switching, thianthrene-containing cavitand **1** was synthesized (Scheme 4.1). Dibromo-thianthrene **2** was synthesized from an S_NAr reaction between benzene-1,2-dithiol and 1,2-dibromo-4,5-difluorobenzene as previously reported.¹⁸ Using a modified procedure,¹⁹ palladium-catalyzed Buchwald-Hartwig amination of **2** with benzophenone imine yielded diimine **3**, which upon acidic hydrolysis followed by basic work-up afforded diamine **4**. The condensation reaction of **4** with oxalic acid gave diol **5**, which was in turn subjected

to thionyl chloride to give dichloride **6**, a key intermediate to this synthesis. Finally, cavitand **1** was obtained by S_NAr reaction of **6** with resorcinarene ($R = C_6H_{13}$). This six-step synthesis is accomplished in an overall yield of 28%.



Scheme 4.1. Synthesis of thianthrene-containing cavitand **1**.

For electrochemical actuation cavitand **1** should be: (1) in the vase conformation while in a neutral state at room temperature, and (2) convert to the kite conformation upon oxidation. Vase-to-kite conformation changes can be monitored by the distinctive methine chemical shift from *ca.* 5.5 ppm (vase conformation) to *ca.* 3.8 ppm (kite conformation),²⁰ and by a change in the UV-Vis spectrum.¹⁰ Therefore, we sought to validate the abovementioned two criteria using both 1H NMR and UV-Vis spectroscopy.

The methine signal for cavitand **1** in neutral state at room temperature was 5.19 ppm and hence, based on literature data, **1** is in vase conformation. Quinoxaline-based cavitands are known to undergo vase-to-kite conformation change upon protonation and at low temperatures. Hence, we treated **1** with trifluoroacetic acid (TFA) and also did variable temperature studies. With

addition of TFA the thianthrene-containing cavitand **1** adopts the kite conformation, as evident from the 5.19 ppm methine signal (vase conformation) shifting to 3.90 ppm (kite conformation) (Fig. 4.4). Similarly, we observe a gradual upfield shift in the methine proton resonance with decreasing temperature (Supplementary Fig. 4.1).

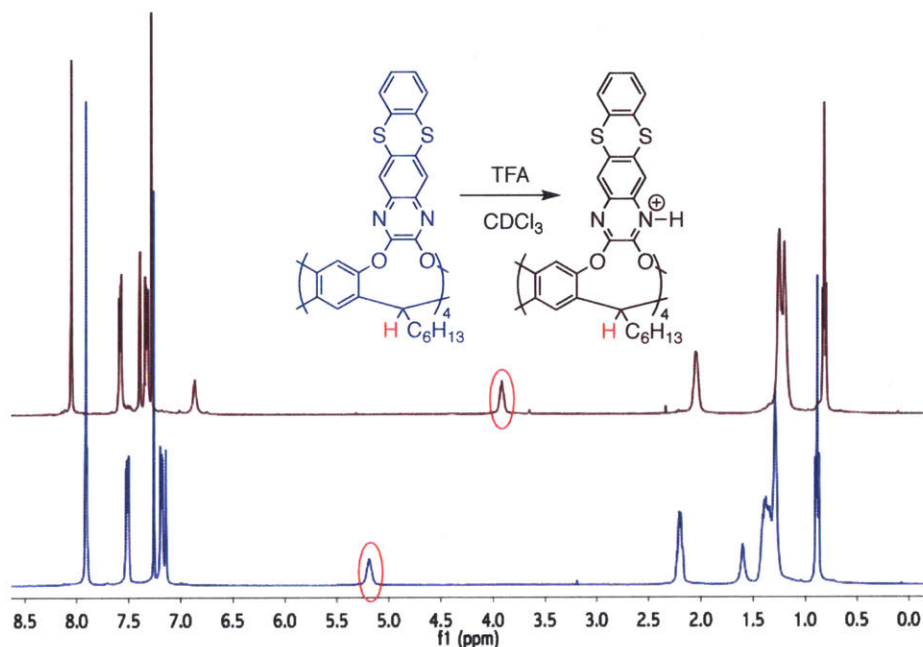


Figure 4.4. ¹H NMR spectra of **1** before (blue) and after (maroon) addition of TFA.

Treatment with TFA produced a shoulder peak below 300 nm in the UV-Vis spectra of **1** (Fig. 4.5), which led us to hypothesize that the vase-to-kite conformation change is responsible for the development of this shoulder peak. Compound **1** can also be oxidized electrochemically (Fig. 4.6) and UV-Vis spectroelectrochemical measurements conducted above the oxidation peak potential (Fig. 4.7) revealed the development of a similar shoulder peak below 300 nm. Again this is consistent with **1** undergoing a vase-to-kite conformation change upon oxidation. The peaks at 262 nm and 374 nm decrease in intensity, presumably as a result of the consumption of **1** by oxidation.

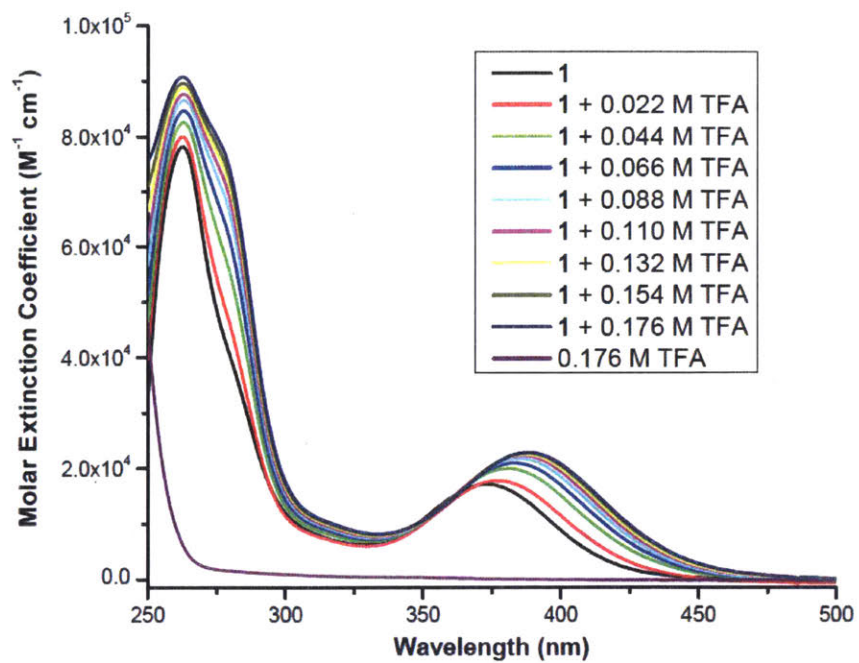


Figure 4.5. UV-Vis spectrum of **1** in CH₂Cl₂ at different TFA concentrations.

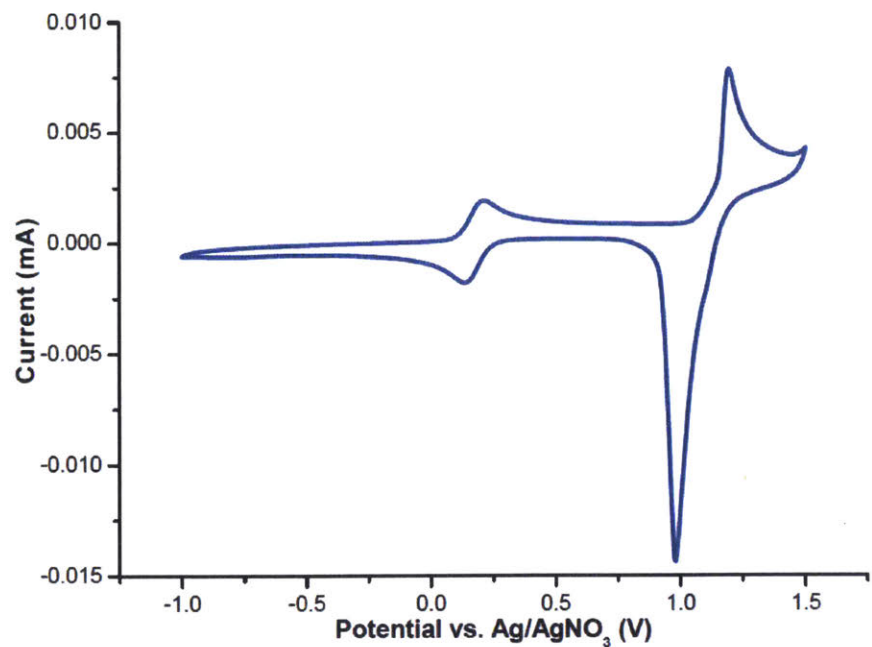


Figure 4.6. Cyclic voltammogram of **1** in CH_2Cl_2 at 100 mV s^{-1} scan rate with TBAPF_6 as supporting electrolyte and Fc/Fc^+ as external reference.

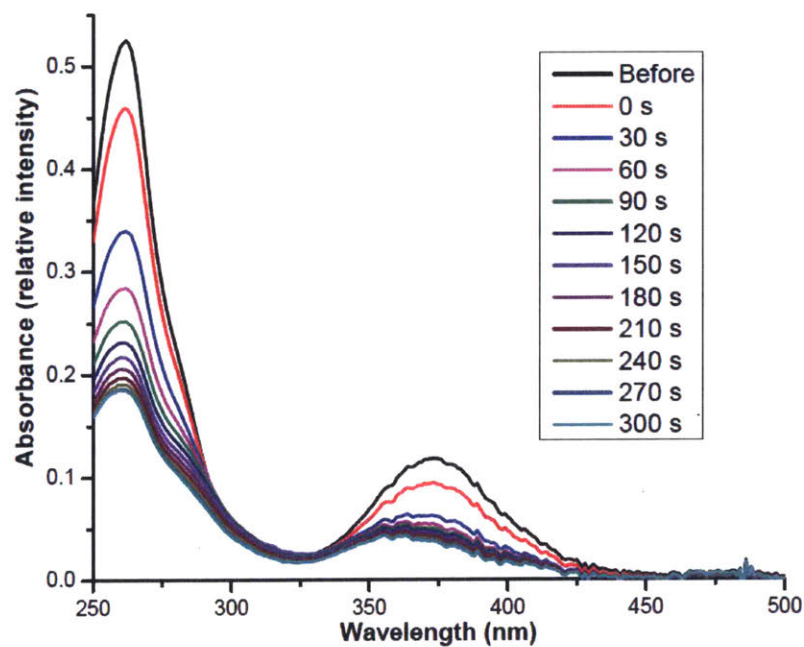
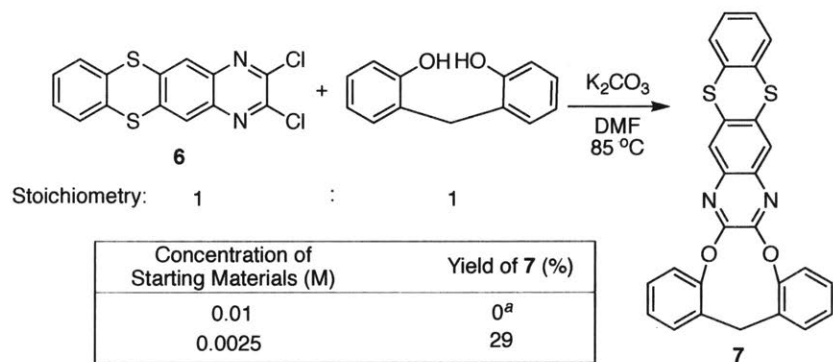


Figure 4.7. Spectroelectrochemistry of **1** in CH_2Cl_2 .

To provide further evidence that **1** undergoes a vase-to-kite conformation change upon oxidation, **7**, which constitutes a single quinoxaline wall of **1**, was synthesized (Scheme 4.2). A low concentration of starting materials was required to produce **7**, presumably at higher concentrations the S_NAr reaction produces oligomers.



Scheme 4.2. Synthesis of quinoxaline wall **7**. ^a A highly polar crude mixture (soluble in MeOH) was obtained.

In the absence of the resorcinarene framework, the single cavitand wall **7** should not have the vase-to-kite signatures of the shoulder peak in the UV-Vis spectra. Indeed, the UV-Vis spectra of **7** under different TFA concentrations and spectroelectrochemical studies did not display the shoulder peak below 300 nm (Supplementary Fig. 4.2 and 4.3). As a result, we are confident that this UV-Vis spectroscopic feature is specific to the cavitand and its vase-to-kite conformation change. We observe a new peak at 313 nm, corresponding to the newly formed radical cation of **7**, and a reduction in peak intensities at 264 nm and 363 nm, similar to **1**.

Although UV-Vis spectroscopy provided some evidence for vase-to-kite conformation change upon oxidation, the most definitive evidence is provided by NMR analysis of chemically oxidized cavitand **1**. Nitrosyl tetrafluoroborate (NOBF₄) has been previously reported to oxidize

thianthrene, generating the thianthrene radical cation tetrafluoroborate,²¹ and we treated cavitand **1** with NOBF₄ in deuterated chloroform. However, detecting definitive changes in the methine's chemical shift is potentially complicated by the fact that the oxidized material contains radical cations. Oxidation of the quinoxaline wall **7** gives a spectrum wherein the methylene chemical shift was largely unaffected (Fig. 4.8). The observed splitting is presumably due to the two methylene protons having slightly different chemical environments after oxidation. Subjecting cavitand **1** to the same oxidation conditions provided a definitive change in methine chemical shift from 5.19 ppm (vase conformation) to 3.71 ppm (kite conformation) (Fig. 4.9). EPR spectra of both oxidized **1** and **7** showed a single signal with $g_{iso} = 2.0075$ and 2.0076 respectively, suggesting the formation of radical cations from the chemical oxidation (Supplementary Fig. 4.4 and 4.5). Given that we were able to measure the NMR spectra on this system suggests that the radical cations are sufficiently removed from the methine protons such that they are not dramatically broadened.

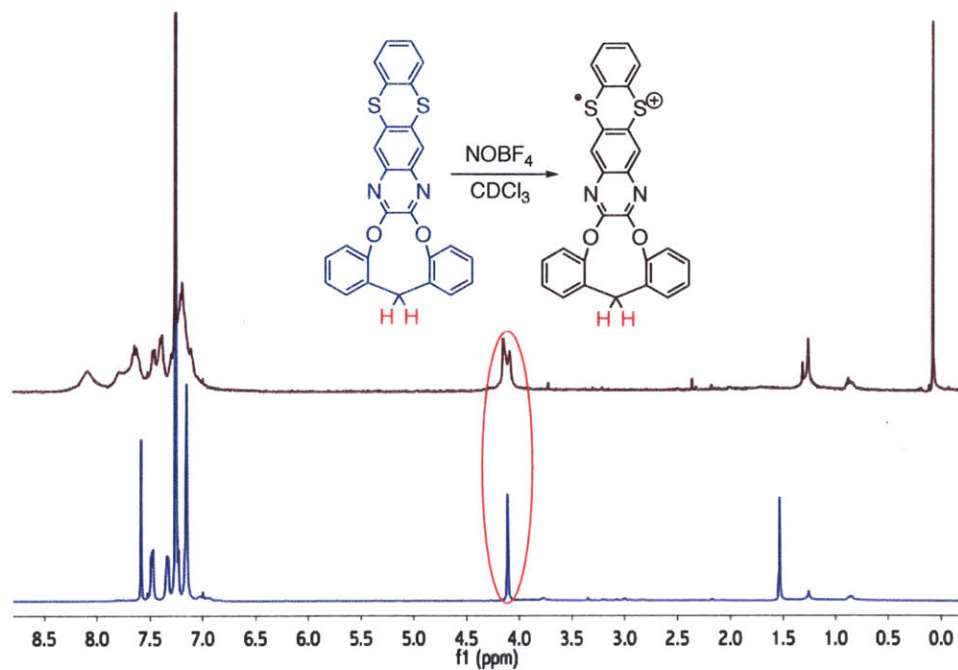


Figure 4.8. ^1H NMR spectra of **7** before (blue) and after (maroon) oxidation.

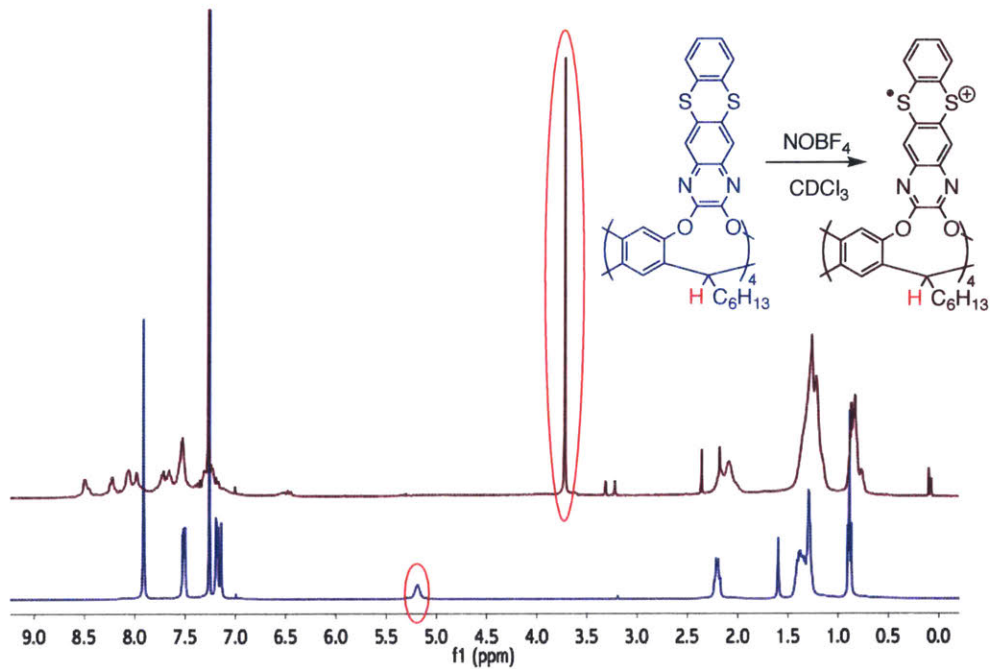


Figure 4.9. ^1H NMR spectra of **1** before (blue) and after (maroon) oxidation.

4.3 Conclusions

In summary, we have successfully demonstrated that cavitand **1** undergoes vase-to-kite conformation change upon oxidation. Thianthrene cavitands represent an attractive scaffold for the formation of new functional supramolecular structures with switchable conformations. Our ongoing studies will focus on generating related functional thianthrene-containing cavitands with applications in electronics and separations.

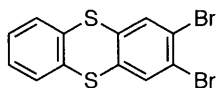
4.4 Experimental Details

4.4.1 General

NMR spectra were recorded on a 400 MHz spectrometer. Chemical shifts were reported in ppm and referenced to residual solvent peaks (CDCl_3 : δ 7.26 ppm for ^1H , δ 77.16 ppm for ^{13}C , DMSO: δ 2.50 ppm for ^1H , δ 39.52 ppm for ^{13}C). UV-Vis spectra were obtained using a diode array spectrometer. Electrochemical measurements were carried in a three-electrode cell configuration consisting of a quasi-internal Ag wire reference electrode submerged in 0.01 AgNO_3 / 0.1 M tetrabutylammonium hexafluorophosphate (TBAPF_6) in anhydrous CH_2Cl_2 with TBAPF_6 as supporting electrolyte, a Pt button (1.6 mm in diameter) electrode as the working electrode, and a Pt coil as the counter electrode. The ferrocene/ferrocenium (Fc/Fc^+) redox couple was used as an external reference. EPR spectra were obtained operating as the X-band with 100 kHz modulation at room temperature. All air and water sensitive synthetic manipulations were performed under an argon atmosphere using standard Schlenk techniques. Anhydrous DMF and 1,2-dichloroethane were purchased from Aldrich as Sure-Seal Bottles and used as received.

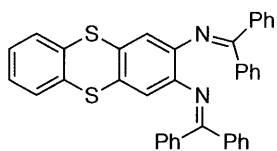
CH₂Cl₂ and toluene were purified by passage through two alumina columns of an Innovative Technologies purification system. All other chemicals were of reagent grade and used as received.

4.4.2 Synthetic Procedures



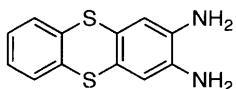
2,3-Dibromothianthrene (2)

To a 3-neck flask containing a solution of triethylamine (0.55 mL) in anhydrous DMF (5 mL), 1,2-benzenedithiol (0.75 mL, 6.53 mmol) in DMF (3 mL) and 1,2-difluoro-4,5-dibromobenzene (1.48 g, 5.44 mmol) in DMF (3 mL) were added *via* different syringes drop by drop at room temperature under argon. The reaction mixture was then stirred overnight at 80 °C. After cooling down to room temperature, the reaction mixture was then concentrated *in vacuo* and added to CH₂Cl₂ (50 mL) and the solution was washed with 1 M HCl solution and water. It was then dried with MgSO₄ and the solvent was removed *in vacuo*. The crude product was further purified by gel column chromatography eluting with 6:1 hexane/CH₂Cl₂ to yield **2** as a white powder (1.20 g, 59%). R_f (6:1 hexane/CH₂Cl₂) = 0.5. mp 159–161 °C. ¹H NMR (400 MHz, CDCl₃) δ: 7.71 (s, 2H), 7.47 (dd, 2H, *J* = 5.8, 3.3 Hz), 7.27 (dd, 2H, *J* = 5.8, 3.3 Hz). ¹³C NMR (101 MHz, CDCl₃) δ: 136.8, 134.7, 132.7, 129.1, 128.3, 123.8. HRMS (ESI) *m/z* calculated for C₁₂H₆Br₂S₂ [M]⁺: 373.8255; found: 373.8262.



***N,N'*-(Thianthrene-2,3-diyl)bis(1,1-diphenylmethanimine) (3)**

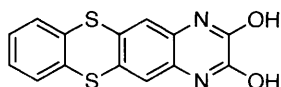
A solution of anhydrous toluene with Pd₂(dba)₃ (0.576 g, 0.629 mmol) and *rac*-BINAP (0.783 g, 1.26 mmol) was degassed by 3 freeze-pump-thaw cycles, filled with argon and stirred at 110 °C for 30 mins. After cooling to room temperature, **2** (2.94 g, 7.86 mmol), NaO^tBu (1.96 g, 20.4 mmol) and diphenylmethanimine (3.45 mL, 20.4 mmol) were added subsequently to the reaction. The reaction was then stirred overnight at 110 °C. The reaction mixture was cooled down and filtered through Celite, washing with CH₂Cl₂. The filtrate was concentrated *in vacuo* and the resulting crude product was purified by gel column chromatography eluting with hexane to 1:19 ethyl acetate/hexane to obtain **3** (4.02 g, 89%) as a bright yellow foam. R_f (1:19 ethyl acetate/hexane) = 0.2. mp 94–96 °C. ¹H NMR (400 MHz, CDCl₃) δ: 7.64 (d, 4H, *J* = 7.3 Hz), 7.40–7.37 (m, 4H), 7.34–7.29 (m, 6H), 7.24–7.22 (m, 4H), 7.18 (dd, 2H, *J* = 5.6, 3.4 Hz), 6.91 (d, 4H, *J* = 7.2 Hz), 6.64 (s, 2H). ¹³C NMR (101 MHz, CDCl₃) δ: 168.3, 141.6, 139.8, 136.5, 136.2, 130.7, 129.5, 129.3, 129.2, 129.1, 128.6, 128.14, 128.10, 127.4, 121.0. HRMS (ESI) *m/z* calculated for C₃₈H₂₇N₂S₂ [M+H]⁺: 575.1610; found: 575.1629.



Thianthrene-2,3-diamine (4)

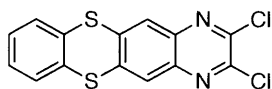
To a solution of **3** (3.97 g, 6.91 mmol) in THF (100 mL) was added 2 M HCl aqueous solution (10.5 mL). The reaction mixture was stirred at room temperature for 30 mins and then concentrated

in vacuo. To the crude product was added CH_2Cl_2 and the suspension was subjected to sonication for 30 mins, filtered and dried to obtain **4.2HCl**. To a solution of **4.2HCl** in THF (100 mL) was added 2 M NaOH aqueous solution (10 mL). The reaction mixture was stirred at room temperature for 30 mins before concentrating *in vacuo*. To the crude product was added water and the suspension was subjected to sonication for 30 mins, filtered and dried to obtain **4** as an off-white powder (1.61 g, 95%). mp 222–224 °C. $^1\text{H NMR}$ (400 MHz, DMSO) δ : 7.49 (dd, 2H, $J = 5.8, 3.3$ Hz), 7.26 (dd, 2H, $J = 5.8, 3.3$ Hz), 6.67 (s, 2H), 4.75 (s, 4H). $^{13}\text{C NMR}$ (101 MHz, DMSO) δ : 136.7, 135.7, 128.4, 127.4, 120.3, 113.8. **HRMS** (ESI) m/z calculated for $\text{C}_{12}\text{H}_{11}\text{N}_2\text{S}_2$ $[\text{M}+\text{H}]^+$: 247.0358; found: 247.0354.



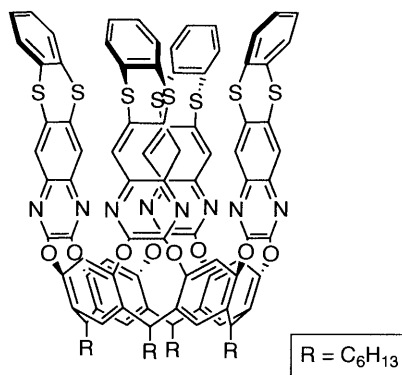
Benzo[5,6][1,4]dithiino[2,3-g]quinoxaline-2,3-diol (5**)**

To a solution of **4** (1.59 g, 6.45 mmol) in 4 M HCl aqueous solution (70 mL) was added oxalic acid in 4 M HCl aqueous solution (30 mL). The reaction mixture was stirred under reflux overnight. After cooling to room temperature, the reaction mixture was filtered and the residue was collected and dried to give **5** as a light brown powder (1.79 g, 92%). mp >300 °C. $^1\text{H NMR}$ (400 MHz, DMSO) δ : 12.00 (s, 2H), 7.59 (dd, 2H, $J = 5.8, 3.4$ Hz), 7.36 (dd, 2H, $J = 5.8, 3.4$ Hz), 7.27 (s, 2H). $^{13}\text{C NMR}$ (101 MHz, DMSO) δ : 154.9, 134.6, 128.9, 128.4, 128.3, 126.0, 114.7. **HRMS** (DART) m/z calculated for $\text{C}_{14}\text{H}_7\text{N}_2\text{O}_2\text{S}_2$ $[\text{M}-\text{H}]^-$: 298.9954; found: 298.9934.



2,3-Dichlorobenzo[5,6][1,4]dithiino[2,3-g]quinoxaline (6)

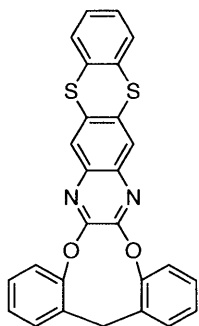
To a slurry of **5** (1.79 g, 5.86 mmol) and thionyl chloride (1.3 mL, 17.6 mmol) in anhydrous 1,2-dichloroethane (100 mL) was added 8 drops of anhydrous DMF. The reaction was stirred under reflux overnight. After cooling to room temperature, the reaction mixture was concentrated *in vacuo* and the crude product was purified by gel column chromatography eluting with 1:1 hexane/toluene to toluene to afford **6** as a bright yellow powder (1.69 g, 85%). R_f (1:1 hexane/toluene) = 0.5. mp 275–277 °C. $^1\text{H NMR}$ (400 MHz, CDCl_3) δ : 8.09 (s, 2H), 7.53 (dd, 2H, $J = 5.8, 3.4$ Hz), 7.32 (dd, 2H, $J = 5.8, 3.4$ Hz). $^{13}\text{C NMR}$ (101 MHz, CDCl_3) δ : 145.9, 140.5, 140.0, 133.8, 129.1, 128.6, 126.3. **HRMS** (ESI) m/z calculated for $\text{C}_{14}\text{H}_6\text{Cl}_2\text{N}_2\text{S}_2$ $[\text{M}]^+$: 335.9344; found: 353.9355.



Thianthrene-containing cavitand (1)

To a Schlenk flask containing resorcinarene ($\text{R} = \text{C}_6\text{H}_{13}$)¹⁰ (0.167 g, 0.202 mmol) and K_2CO_3 (0.419 g, 3.03 mmol) under argon was added anhydrous DMF (20 mL). After stirring the reaction at room temperature for 20 mins, **6** (0.300 g, 0.890 mmol) was added and the reaction was stirred

overnight at 85 °C. After cooling to room temperature, the reaction mixture was poured into 1 M HCl solution. The residue was collected, dissolved in CH₂Cl₂, and filtered to remove an orange residue. The filtrate was collected and concentrated to give the crude product. The crude product was purified by recrystallization (DCM/EtOH) to afford **1** as a yellow powder (0.272 g, 71%). mp >300 °C. ¹H NMR (400 MHz, CDCl₃) δ: 7.91 (s, 8H), 7.91 (s, 4H), 7.51 (dd, 8H, *J* = 5.8, 3.4 Hz), 7.18 (dd, 8H, *J* = 5.8, 3.4 Hz), 7.14 (s, 4H), 5.19 (s, 4H), 2.20 (dd, 8H, *J* = 14.2, 7.5 Hz), 1.41–1.28 (m, 32H), 0.89 (t, 12H, *J* = 6.8 Hz). ¹³C NMR (101 MHz, CDCl₃) δ: 152.6, 151.9, 139.0, 138.2, 135.1, 134.6, 129.0, 128.1, 126.1, 123.6, 117.9, 35.1, 32.4, 31.9, 29.4, 27.8, 22.8, 14.2. HRMS (MALDI) *m/z* calculated for C₁₀₈H₈₉N₈O₈S₈ [M+H]⁺: 1882.46; found: 1882.61.



5H-Benzo[5,6][1,4]dithiino[2,3g]dibenzo[5,6:8,9][1,4]dioxonino[2,3-b]quinoxaline (7)

To a Schlenk flask containing bis(2-hydroxyphenyl)methane (59.3 mg, 0.297 mmol) and K₂CO₃ (164 mg, 1.19 mmol) under argon was added anhydrous DMF (120 mL). The reaction mixture was stirred at room temperature for 20 mins before **6** (100 mg, 0.297 mmol) was added. The reaction was then heated to 85 °C and stirred overnight. After cooling to room temperature, the crude mixture was concentrated *in vacuo* and precipitated into a 1 M HCl aqueous solution. The suspension was filtered and the resulting crude solid was purified by recrystallization (CHCl₃/EtOH) to obtain **7** as a yellow powder (40mg, 29%). mp >300 °C. ¹H NMR (400 MHz,

CDCl₃) δ : 7.58 (s, 2H), 7.48 (dd, 8H, J = 5.8, 3.4 Hz), 7.35–7.33 (m, 2H), 7.25 (dd, 2H, J = 5.8, 3.4 Hz), 7.17–7.15 (m, 6H), 4.11 (s, 2H). ¹³C NMR (101 MHz, CDCl₃) δ : 150.9, 148.9, 136.9, 135.3, 134.9, 132.0, 131.2, 129.0, 128.0, 127.4, 125.8, 125.5, 121.6, 30.0. HRMS (DART) m/z calculated for C₂₇H₁₇N₂O₂S₂ [M+H]⁺: 465.0726; found: 465.0711.

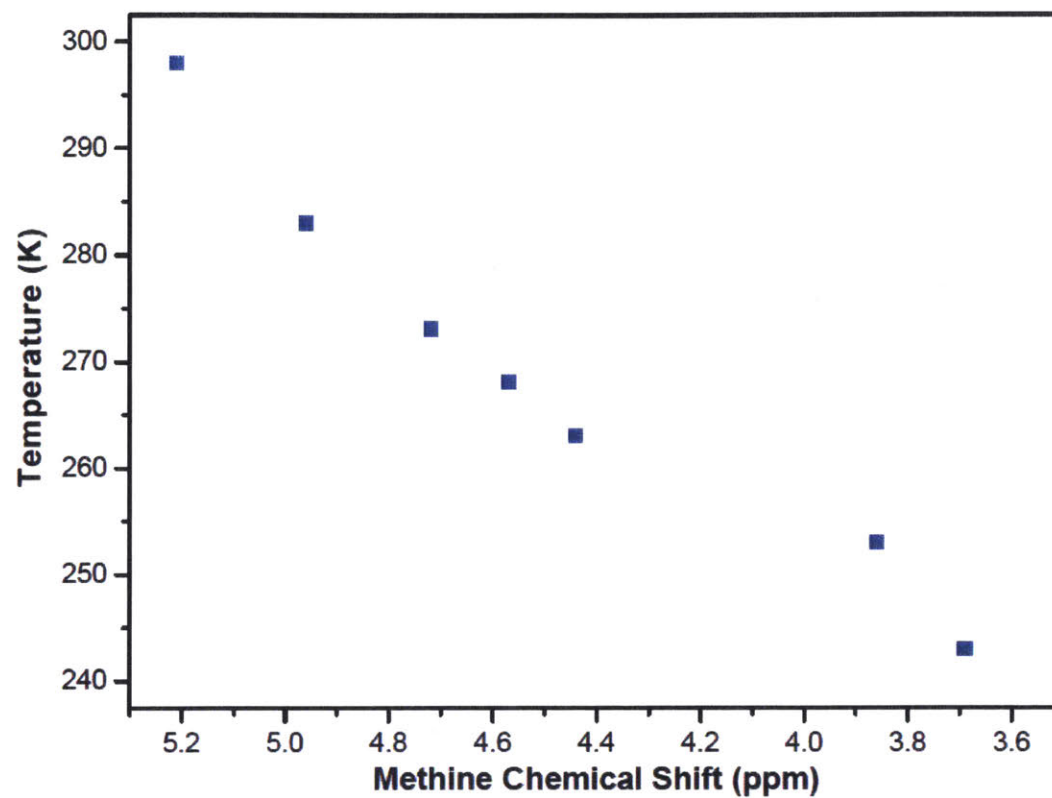
4.5 References

- 1 Moran, J. R.; Karch, S.; Cram, D. J. *J. Am. Chem. Soc.* **1982**, *104*, 5826.
- 2 Azov, V. A.; Beeby, A.; Cacciarini, M.; Cheetham, A. G.; Diederich, F.; Frei, M.; Gimzewski, J. K.; Gramlich, V.; Hecht, B.; Jaun, B.; Latsychevskaya, T.; Lieb, A.; Lill, Y.; Marotti, F.; Schlegel, A.; Schlittler, R. R.; Skinner, P. J.; Seiler, P.; Yamakoshi, Y. *Adv. Funct. Mater.* **2006**, *16*, 147.
- 3 (a) Bertani, F.; Riboni, N.; Bianchi, F.; Brancatelli, G.; Sterner, E. S.; Pinalli, R.; Geremia, S.; Swager, T. M.; Dalcanale, E. *Chem. Eur. J.* **2016**, *22*, 3312. (b) Pinalli, R.; Brancatelli, G.; Pedrini, A.; Menozzi, D.; Hernández, D.; Ballester, P.; Geremia, S.; Dalcanale, E. *J. Am. Chem. Soc.* **2016**, *138*, 8569.
- 4 (a) Zampolli, S.; Elmi, I.; Mancarella, F.; Betti, P.; Dalcanale, E.; Cardinali, G. C.; Severi, M. *Sens. Actuators, B* **2009**, *141*, 322. (b) Pinalli, R.; Dalcanale, E. *Acc. Chem. Res.* **2013**, *46*, 399.
- 5 (a) Purse, B. W.; Rebek, J. *Proc. Natl. Acad. Sci. U.S.A.* **2005**, *102*, 10777. (b) Hooley, R. J.; Rebek, J. Jr. *Chem. Biol.* **2009**, *16*, 255.

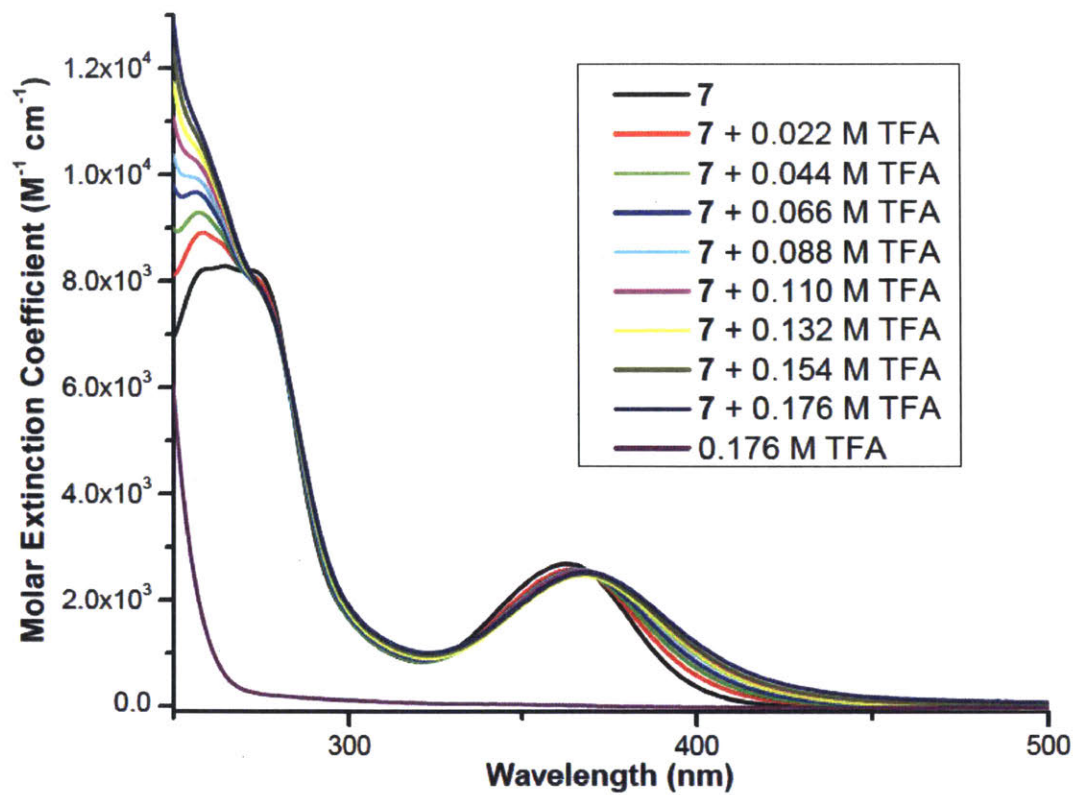
- 6 (a) Rebek, J. *Acc. Chem. Res.* **2009**, *42*, 1660. (b) Dumele, O.; Trapp, N.; Diederich, F. *Angew. Chem. Int. Ed.* **2015**, *54*, 3290.
- 7 Pochorovski, I.; Diederich, F. *Acc. Chem. Res.* **2014**, *47*, 2096.
- 8 (a) Bianchi, F.; Bedini, A.; Riboni, N.; Pinalli, R.; Gregori, A.; Sidisky, L.; Dalcanale, E.; Careri, M. *Anal. Chem.* **2014**, *86*, 10646. (b) Riboni, N.; Trzcinski, J. W.; Bianchi, F.; Massera, C.; Pinalli, R.; Sidisky, L.; Dalcanale, E.; Careri, M. *Anal. Chim. Acta* **2016**, *905*, 79.
- 9 Moran, J. R.; Ericson, J. L.; Dalcanale, E.; Bryant, J. A.; Knobler, C. B.; Cram, D. J. *J. Am. Chem. Soc.* **1991**, *113*, 5707.
- 10 Skinner, P. J.; Cheetham, A. G.; Beeby, A.; Gramlich, V.; Diederich, F. *Helv. Chim. Acta* **2001**, *84*, 2146.
- 11 Frei, M.; Marotti, F.; Diederich, F. *Chem. Commun.* **2004**, 1362.
- 12 Frei, M.; Diederich, F.; Tremont, R.; Rodriguez, T.; Echegoyen, L. *Helv. Chim. Acta* **2006**, *89*, 2040.
- 13 (a) Pochorovski, I.; Boudon, C.; Gisselbrecht, J.-P.; Ebert, M.-O.; Schweizer, W. B.; Diederich, F. *Angew. Chem. Int. Ed.* **2012**, *51*, 262. (b) Pochorovski, I.; Ebert, M.-O.; Gisselbrecht, J.-P.; Boudon, C.; Schweizer, W. B.; Diederich, F. *J. Am. Chem. Soc.* **2012**, *134*, 14702. (c) Pochorovski, I.; Milić, J.; Kolarski, D.; Gropp, C.; Schweizer, W. B.; Diederich, F. *J. Am. Chem. Soc.* **2014**, *136*, 3852.

- 14 Ruiz-Botella, S.; Vidossich, P.; Ujaque, G.; Vicent, C.; Peris, E. *Chem. Eur. J.* **2015**, *21*, 10558.
- 15 (a) Shine, H. J.; Piette, L. *J. Am. Chem. Soc.* **1962**, *84*, 4798. (b) Rapta, P.; Kress, L.; Hapiot, P.; Dunsch, L. *Phys. Chem. Chem. Phys.* **2002**, *4*, 4181.
- 16 Kim, S.; Kwon, Y.; Lee, J.-P.; Choi, S.-Y.; Choo, J. *J. Mol. Struct.* **2003**, *655*, 451.
- 17 Bock, H.; Rauschenbach, A.; Näther, C.; Kleine, M.; Havlas, Z. *Chem. Ber.* **1994**, *127*, 2043.
- 18 Yu, H.-h. PhD Dissertation; Massachusetts Institute of Technology: USA, 2003.
- 19 Rabbani, M. G.; Reich, T. E.; Kassab, R. M.; Jackson, K. T.; El-Kaderi, H. M. *Chem. Commun.* **2012**, *48*, 1141.
- 20 Azov, V. A.; Jaun, B.; Diederich, F. *Helv. Chim. Acta* **2004**, *87*, 449.
- 21 Boduszek, B.; Shine, H. J. *J. Org. Chem.* **1988**, *53*, 51.

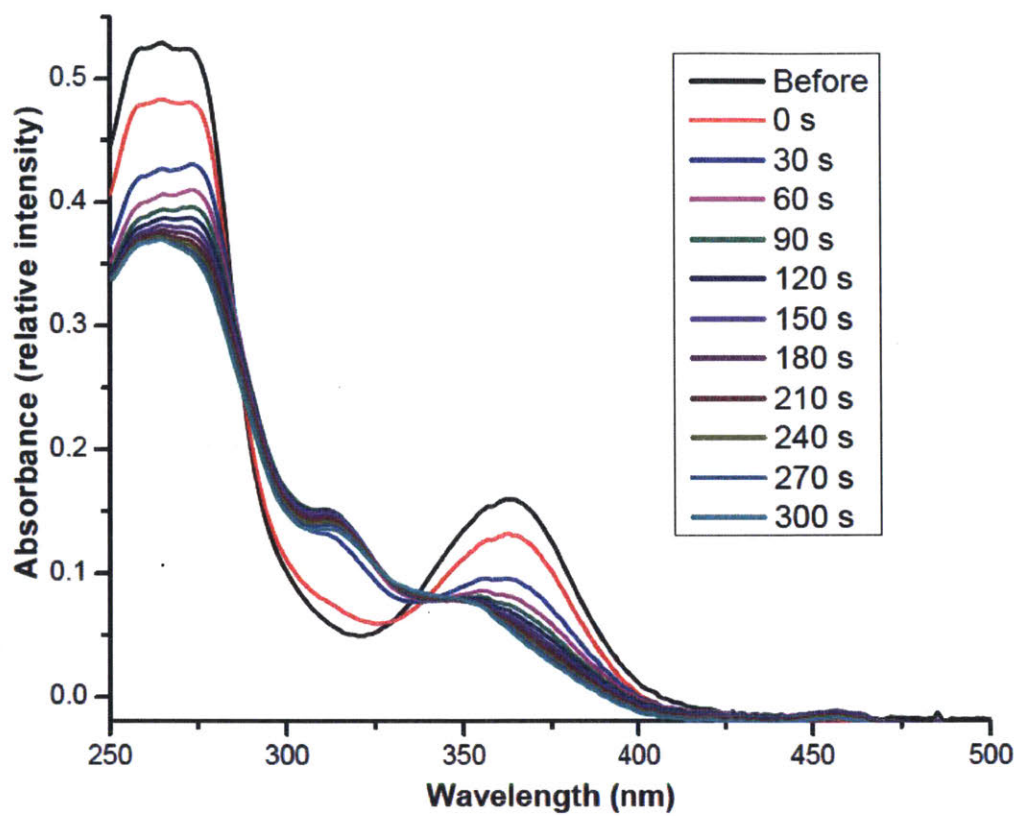
4.6 Appendix for Chapter 4



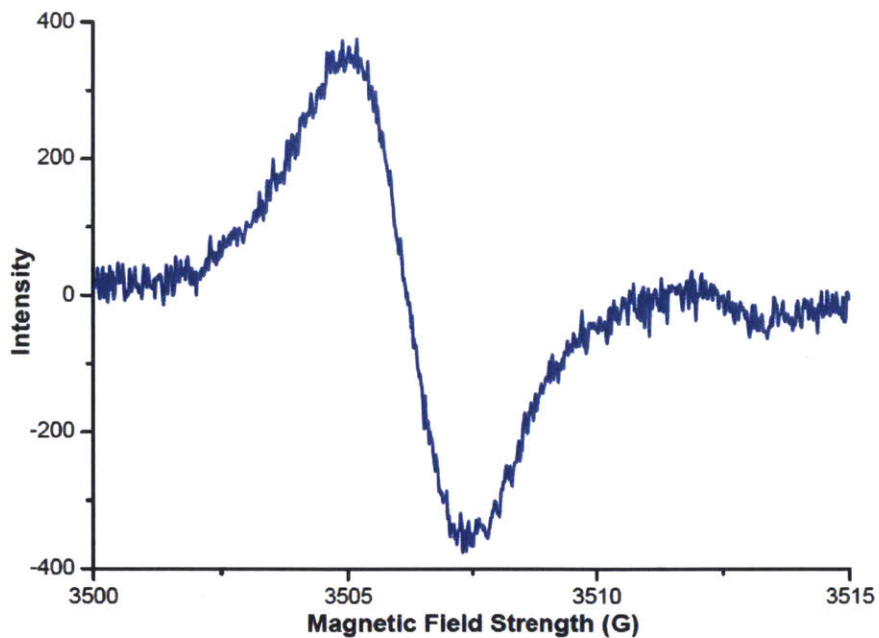
Supplementary Figure 4.1. Plot of temperature against methine chemical shift of **1** in CDCl_3 .



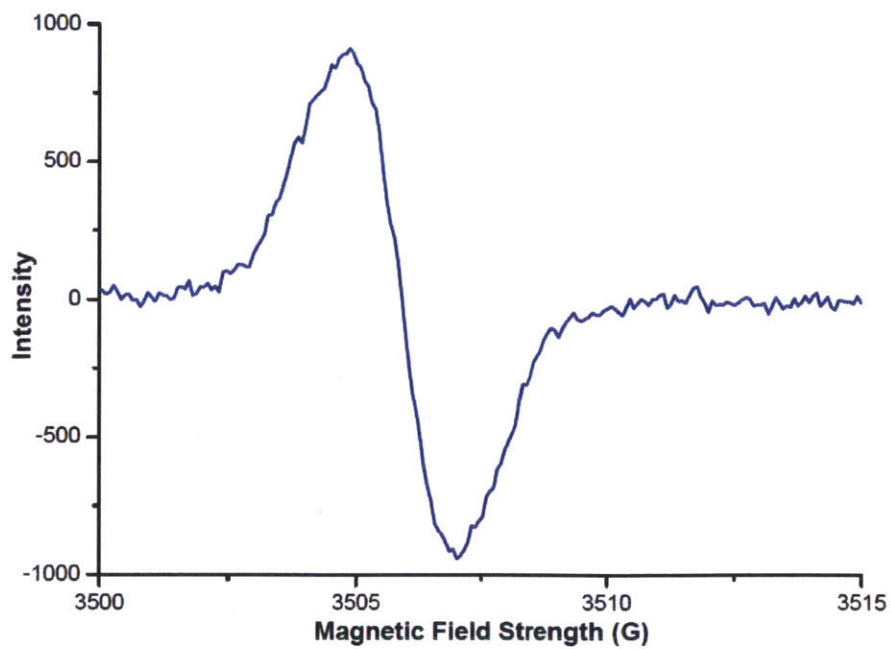
Supplementary Figure 4.2. UV-Vis spectrum of 7 in CH_2Cl_2 at different TFA concentrations.



Supplementary Figure 4.3. Spectroelectrochemistry of 7 in CH₂Cl₂.

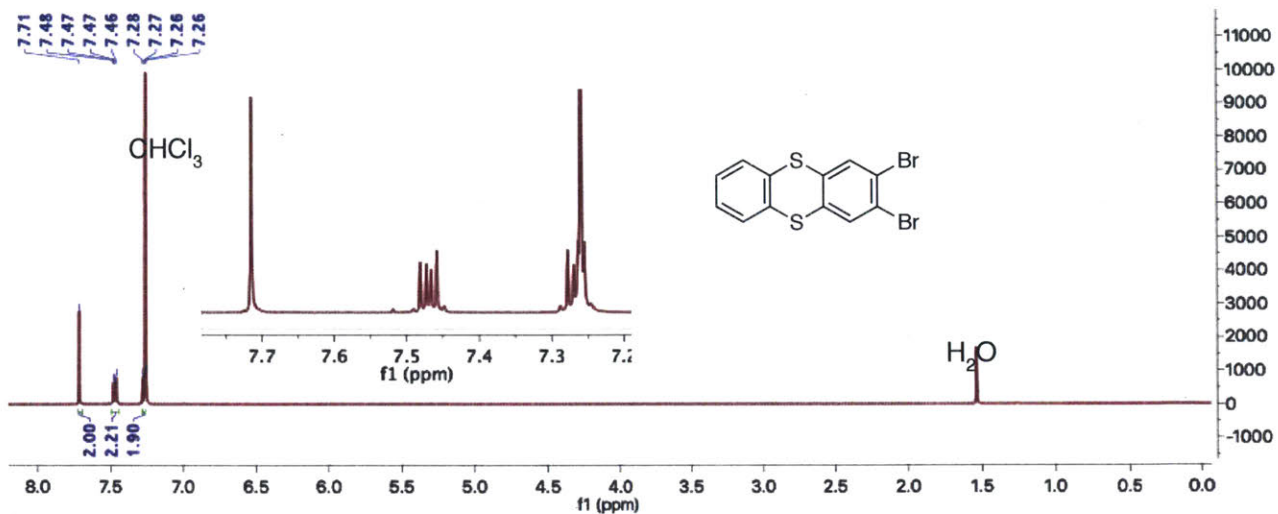


Supplementary Figure 4.4. EPR spectrum of Chemically Oxidized 1.

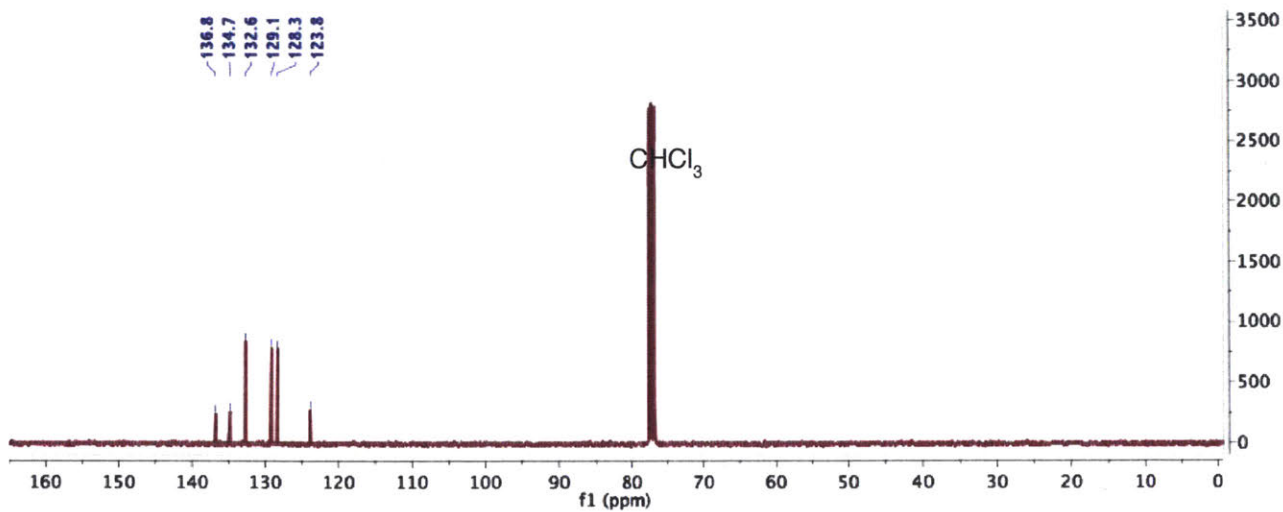


Supplementary Figure 4.5. EPR spectrum of Chemically Oxidized 7.

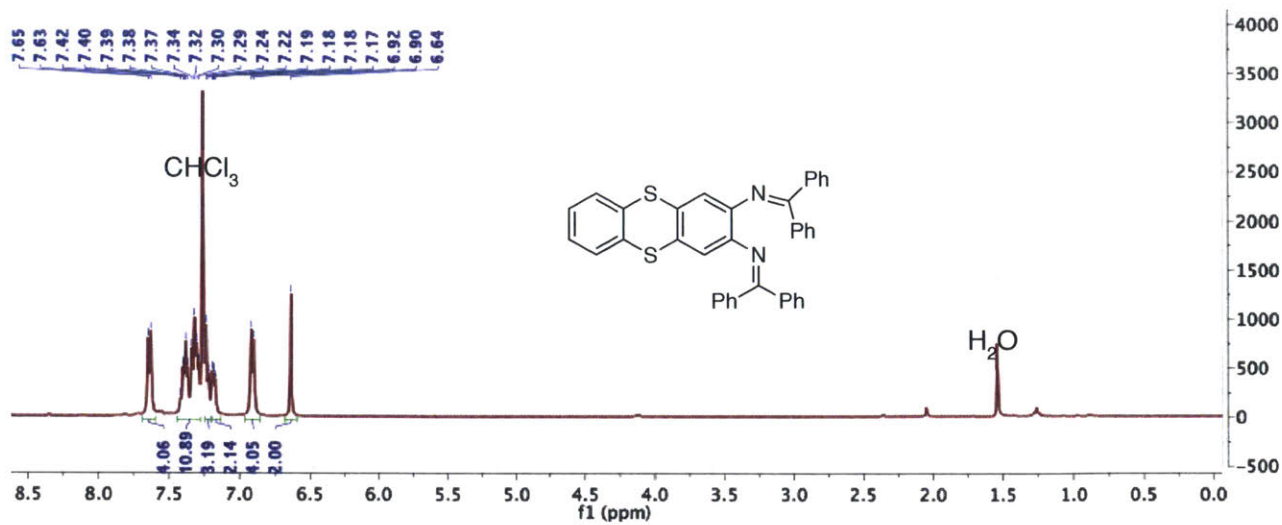
NMR Spectra



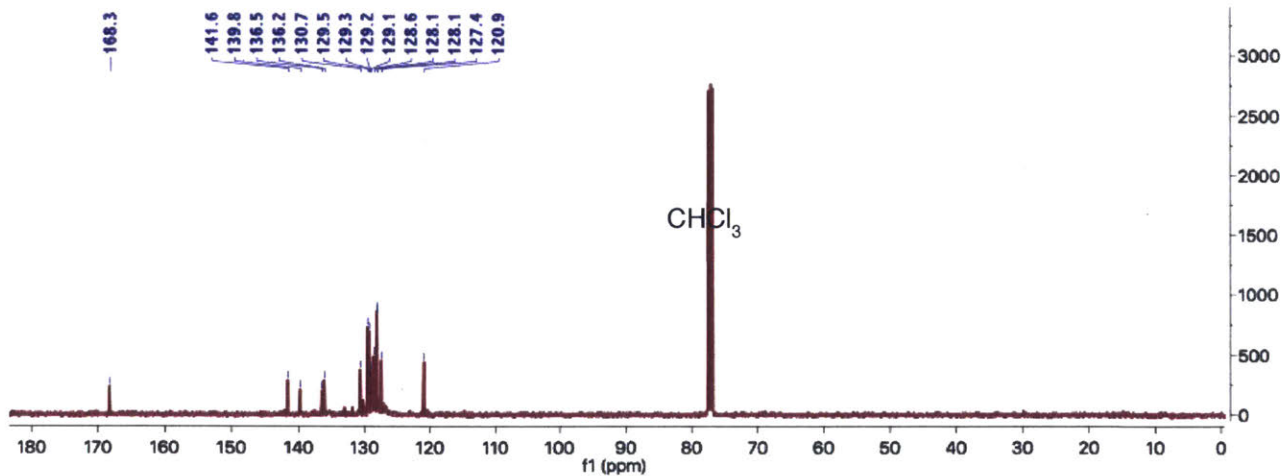
¹H NMR spectrum (400 MHz, CDCl₃) of **2**.



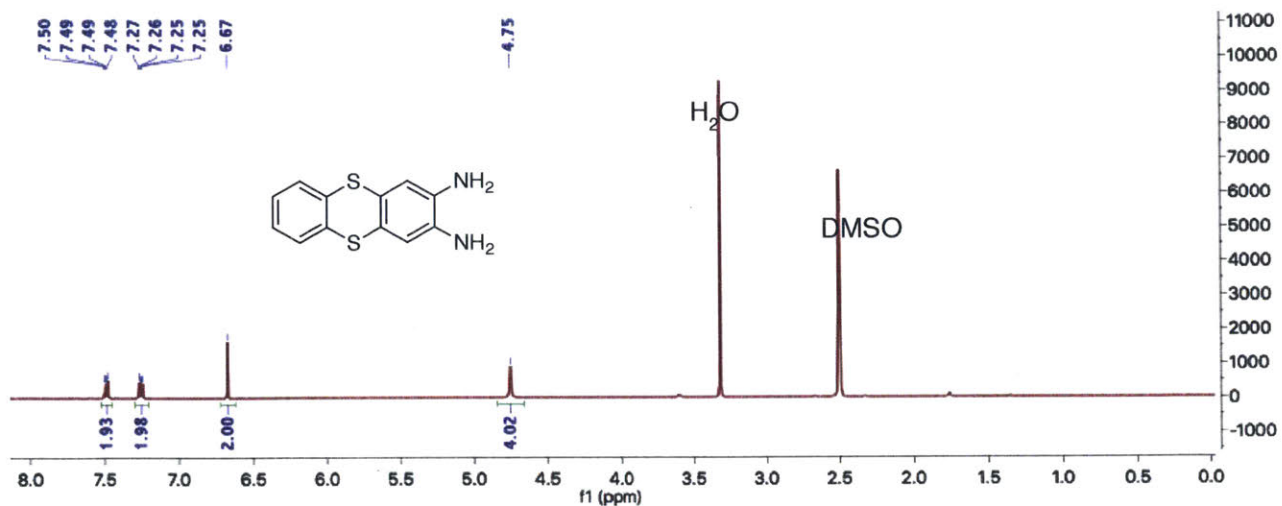
¹³C NMR spectrum (101 MHz, CDCl₃) of **2**.



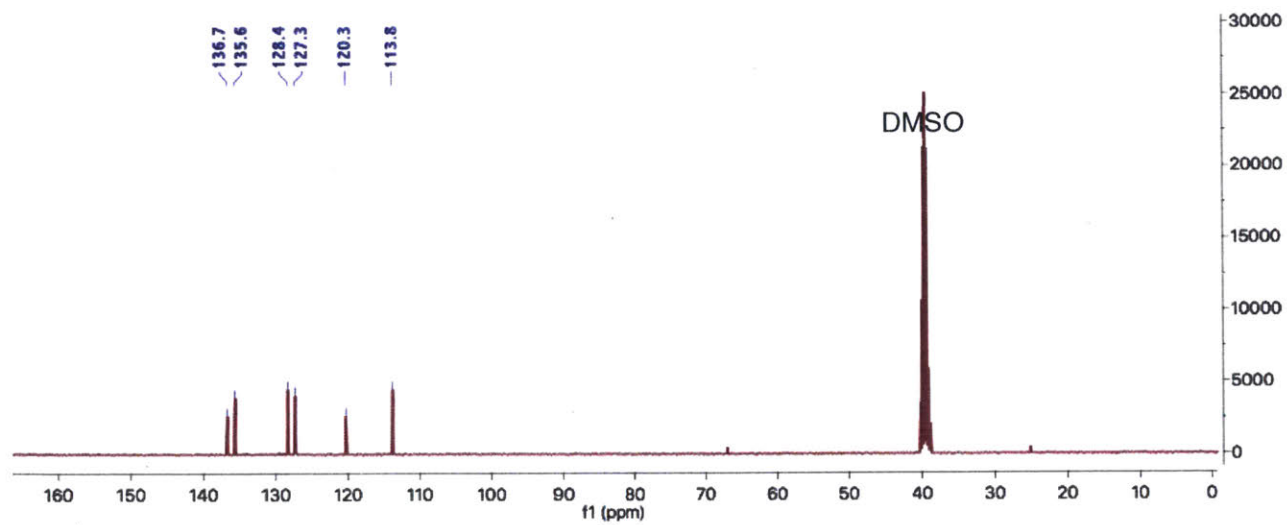
^1H NMR spectrum (400 MHz, CDCl_3) of **3**.



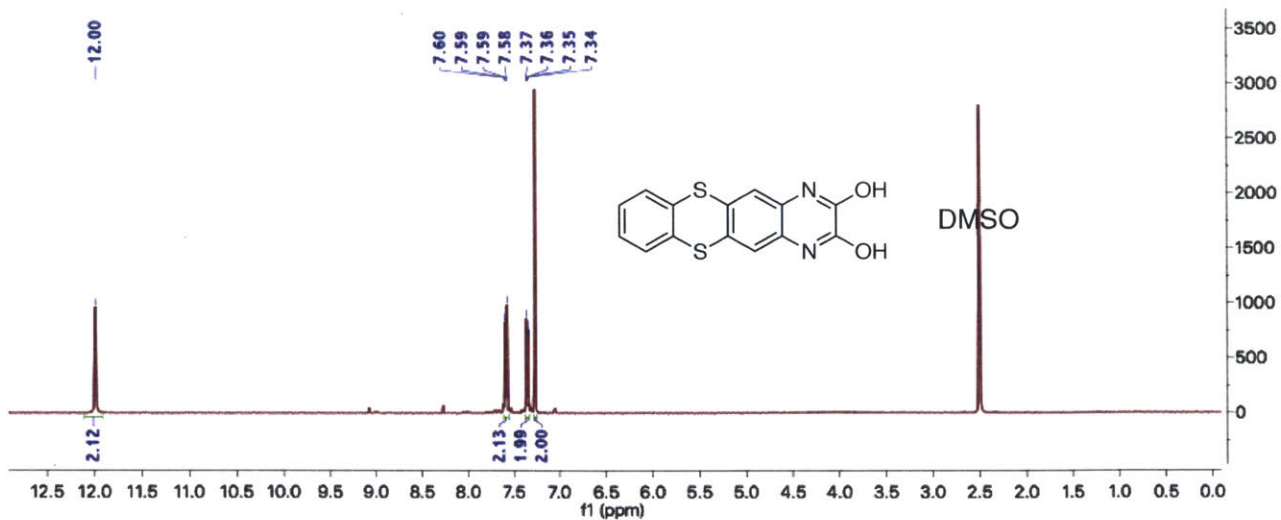
^{13}C NMR spectrum (101 MHz, CDCl_3) of **3**.



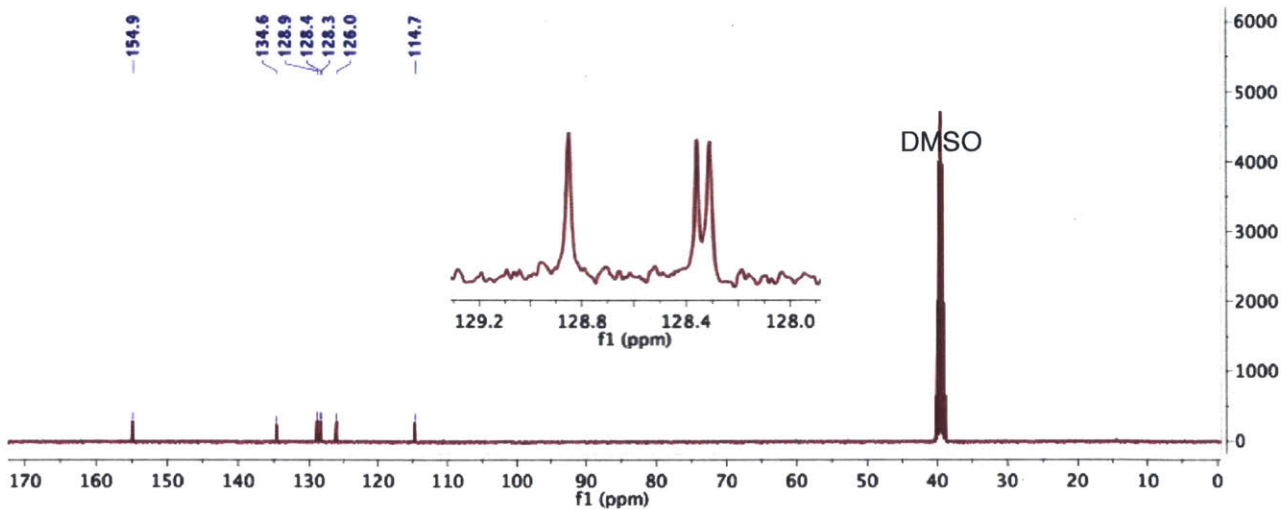
¹H NMR spectrum (400 MHz, DMSO-d₆) of 4.



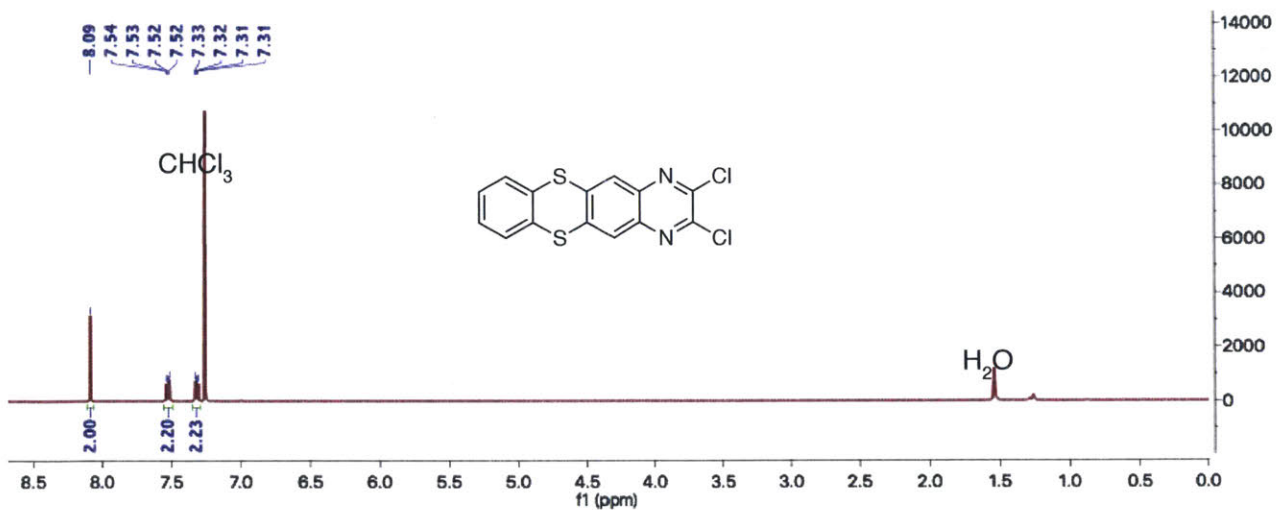
¹³C NMR spectrum (101 MHz, DMSO-d₆) of 4.



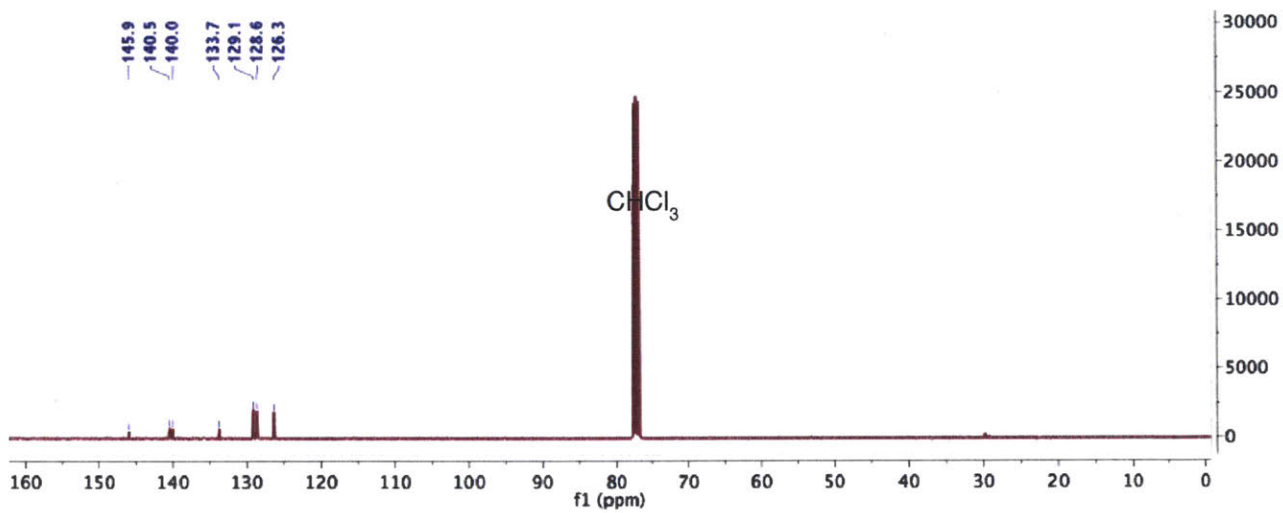
^1H NMR spectrum (400 MHz, DMSO- d_6) of **5**.



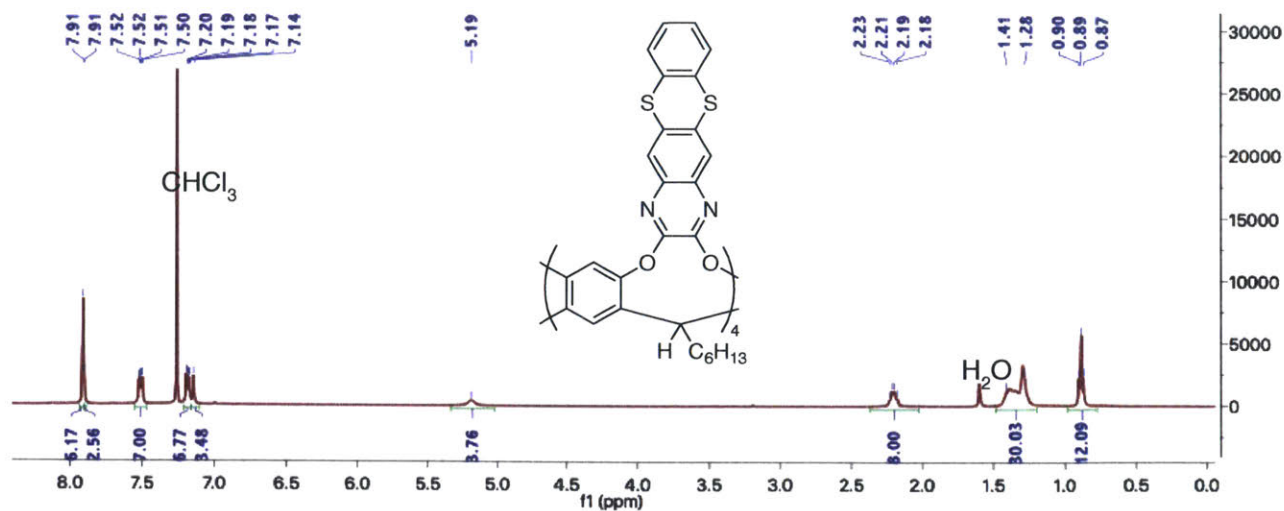
^{13}C NMR spectrum (101 MHz, DMSO- d_6) of **5**.



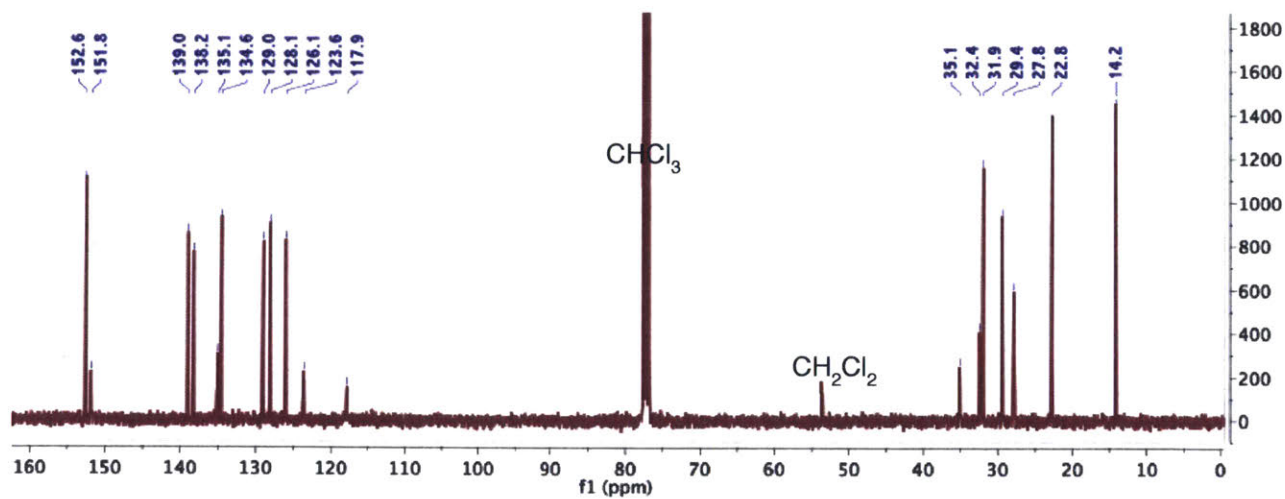
¹H NMR spectrum (400 MHz, CDCl₃) of 6.



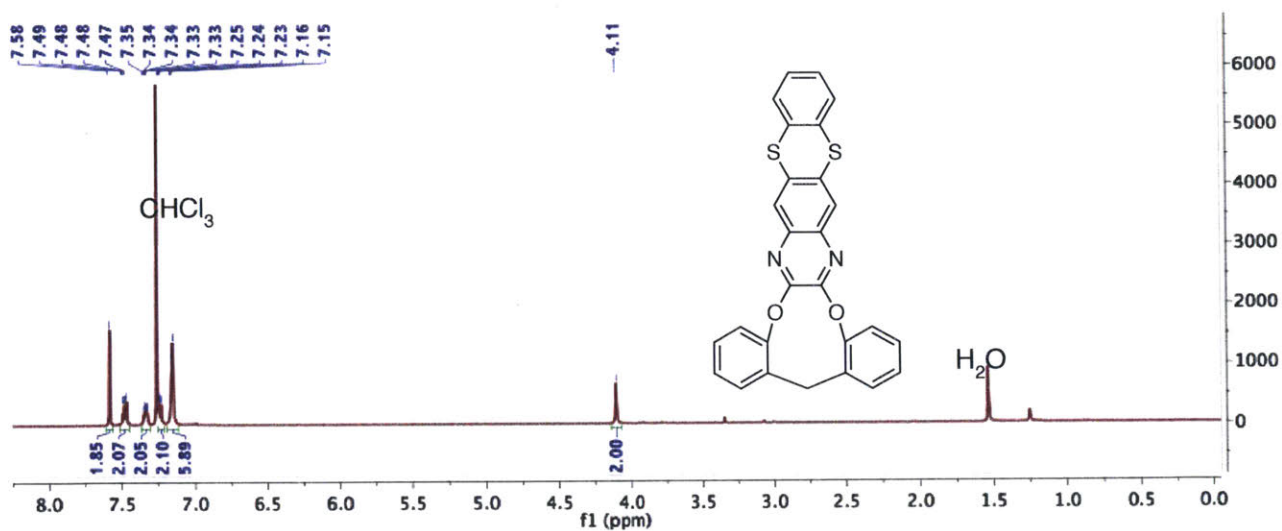
¹³C NMR spectrum (101 MHz, CDCl₃) of 6.



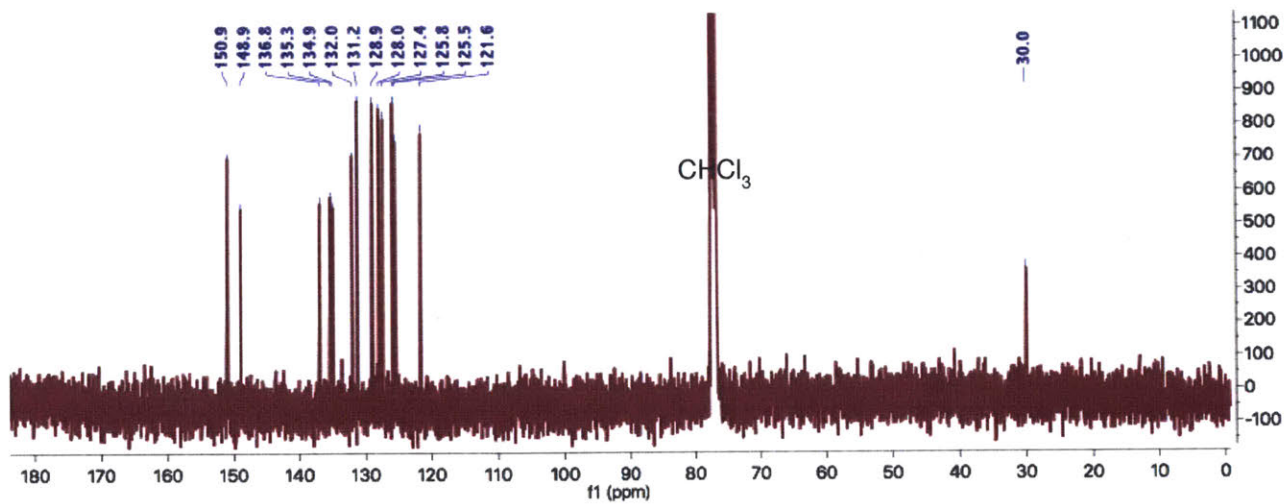
¹H NMR spectrum (400 MHz, CDCl₃) of **1**.



¹³C NMR spectrum (101 MHz, CDCl₃) of **1**.



¹H NMR spectrum (400 MHz, CDCl₃) of 6.



¹³C NMR spectrum (101 MHz, CDCl₃) of 6.

Chapter 5

Dual Anolyte-Catholyte Molecules

Abstract

The symmetric redox flow battery has recently emerged as an attractive solution to overcoming the perennial capacity decay problem encountered during cycling of a flow battery, by utilizing the same electrochemical species as both anolyte and catholyte. However, only a very limited number of molecules are known to inherently possess dual oxidative-reductive properties, thereby restricting the scope of possible flow battery systems. Herein, we propose a new approach for designing novel dual anolyte-catholyte molecules by deconstruction of relevant electroactive species. We report three new molecular scaffolds, which exhibit dual oxidative-reductive properties over a wide potential range (up to 3.27 V) and exceptional electrochemical stability over 100 cycles in cyclic voltammetry. Moreover, these molecular scaffolds can be made highly soluble by appending *tert*-butyl groups (>250 mg in 1 mL of CHCl₃), and are promising, high-energy density candidates for symmetric redox flow battery.

5.1 Introduction

With global energy demand set to rise exponentially with growing human population and energy consumption per capita, it is crucial to ensure a sustainable energy future for all without causing irreversible damage to the environment.¹ Renewable energy sources such as solar and wind are attractive options toward this goal, but their intermittency and unpredictability of supply hampers more rapid adoption. To circumvent this problem, renewable energy generation needs to be coupled with grid energy storage.² Redox flow batteries (RFBs) are an attractive candidate for large-scale energy storage applications, owing to their unique advantage of decoupled energy and power.³⁻⁴ RFBs store dissolved electroactive species, both anolyte and catholyte, in external reservoirs, which are circulated through the respective electrodes for energy conversion (Fig. 5.1).⁵

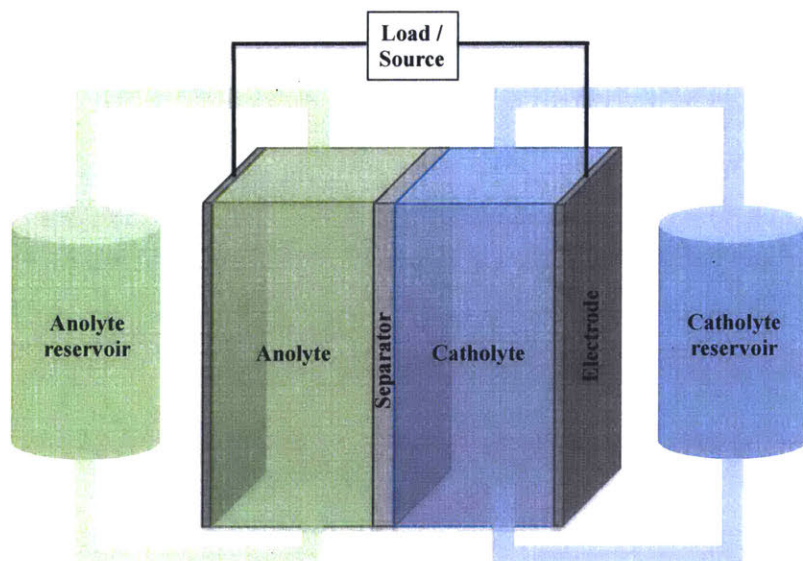


Figure 5.1. Schematic diagram of a RFB.

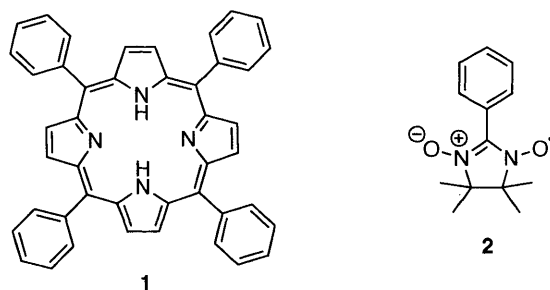
As compared to conventional aqueous RFBs, non-aqueous RFBs offer a broader electrochemical window (cf. water's operating potential window of 1.23 V) which could lead to

higher energy density, and a wider operating temperature. In particular, organic electroactive compounds have the advantages of greater structural and functional group diversity, as well as tunability in chemical structures, redox potentials and solubilities.⁶⁻⁷ Despite these advantages, non-aqueous RFBs still face major technical challenges, namely (1) low solubility of organic active materials, (2) limited electrolyte stability, and (3) capacity decay during cycling.

Symmetric redox flow batteries have recently emerged as a promising solution for avoiding capacity decay during cycling.⁸ By using the same redox species on both sides of the battery cell, any crossover of the redox species through the cell separator will have no impact on the overall cycling stability and performance. There are two general approaches toward designing dual anolyte-catholyte molecules: (1) using molecules that inherently possess dual oxidative and reductive properties, and (2) tethering an anolyte molecule and a catholyte molecule together.

The former approach is convenient because it uses commercially available molecules with known dual redox properties, but is narrow in scope due to the limited number of such molecules (Fig. 5.2a). Chen and coworkers recently reported a symmetric, non-aqueous RFB based on tetraphenylporphyrin **1** as the dual anolyte-catholyte molecule with a volumetric capacity of 8.72 Ah L⁻¹ and excellent cyclic stability.⁹ Duan et al. utilized highly soluble, ambipolar nitroxide radical **2** which can undergo reversible disproportionation reactions in a symmetric flow cell with a moderate cell potential of 1.73 V and good cyclability.¹⁰

a) Molecules possessing inherent dual oxidative and reductive chemistries



b) Tethered molecules possessing both anolyte and catholyte moieties

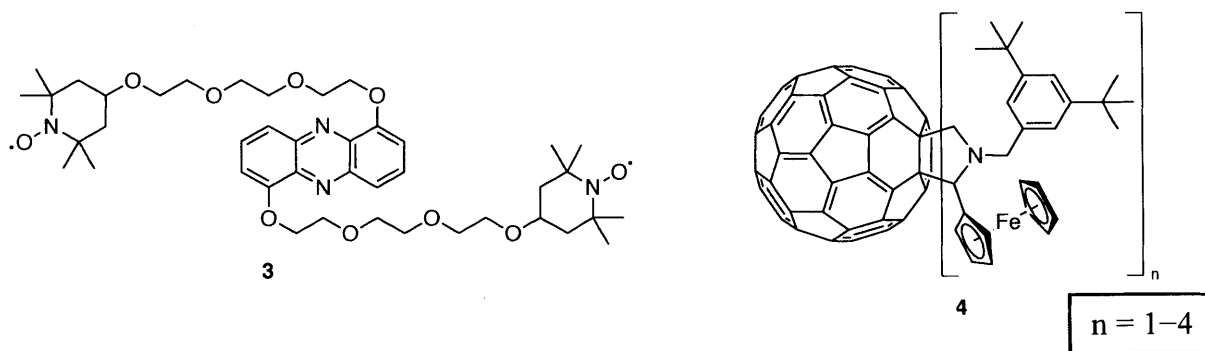


Figure 5.2. Two approaches for designing dual anolyte-catholyte molecules, namely by using a) molecules that inherently possess dual oxidative and reductive properties, and b) tethered molecules with both anolyte and catholyte moieties.

Another approach is to tether an anolyte molecule and a catholyte molecule together via a linker (Fig. 5.2b). Schubert and coworkers coupled a phenazine unit with two 2,2,6,6-tetramethylpiperidinyl-*N*-oxyl (TEMPO) units to obtain combined molecule **3**, which was applied to a symmetric aqueous RFB.¹¹ Friedl et al. reported a symmetric, non-aqueous RFB system using ferrocene-functionalized fullerene derivatives **4**, which demonstrated good energy density and cycling stability.¹² While this latter approach is more versatile than the previous approach given the large number of potential anolyte and catholyte components, it adds synthetic complexity involved in tethering the components and unnecessary molecular weight to the resultant molecules.

Hence, it is desirable to combine the synthetic simplicity of the first approach with the versatility of the second approach, and increase the pool of molecules that exhibit inherent dual oxidative-reductive properties, excellent electrochemical stability and high solubility. Herein, we propose a new approach for designing such molecules through the deconstruction of relevant electroactive species. We exemplify this approach using the second approach as a starting point, with thianthrene and anthraquinone as the prototypical anolyte and catholyte respectively (Fig. 5.3).

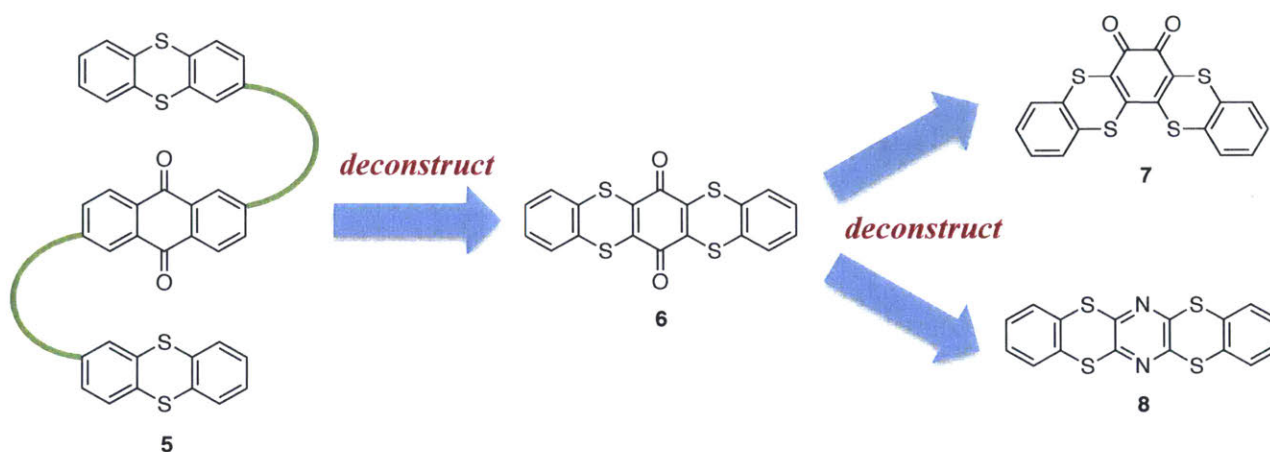


Figure 5.3. New approach toward designing novel dual anolyte-catholyte molecules by deconstruction of relevant electroactive species. The green lines represent linker molecules.

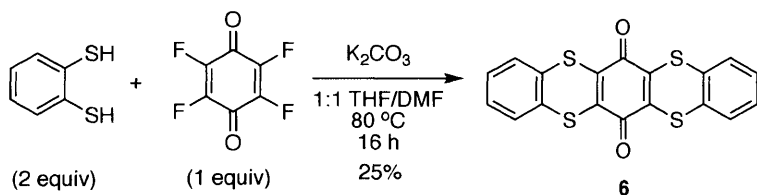
We first conceive tethered molecule **5** in a similar fashion to **3** and **4**, and remove all extraneous parts, such as aromatic rings that tend to reduce solubility and linkers, to afford deconstructed molecule **6**. The rationale for deconstruction is to simplify and obtain a minimalistic structure with low molecular weight that still resembles the redox properties of parent molecule **5**. Molecular weight is an important consideration because small molecules are more likely to attain high gravimetric energy density.

Further deconstruction of 1,4-quinone **6** by swapping its regiochemistry and electron-withdrawing functional group yields 1,2-quinone **7** and pyrazine **8** respectively, which are both novel structures. We anticipate pyrazine **8** to have a more negative reduction potential than quinone **6** and **7** and therefore an advantageous widening of the potential range, since pyrazine loses its aromaticity on reduction while quinone gains aromaticity on reduction.¹³⁻¹⁴ Furthermore, the negative charge resides predominately on less electronegative nitrogen in pyrazine as compared to oxygen in quinone upon reduction.

5.2 Results and Discussion

5.2.1 Synthesis and Electrochemical Studies of Model Molecule

We seek to first validate our approach by synthesizing deconstructed molecule **6** and studying its electrochemical properties. Despite its simple structure, there have only been two reports of compound **6** to date and only its solid-state and solution photophysical properties have been investigated.¹⁵⁻¹⁶ To our surprise, its electrochemical properties have been ignored until now. Two equivalents of benzene-1,2-dithiol were reacted with one equivalent of *p*-fluoranil to afford substituted product **6** (Scheme 5.1).



Scheme 5.1. Synthesis of model molecule **6**.

Cyclic voltammetry performed on **6** at a scan rate of 50 mV s^{-1} reveals two reversible one-electron oxidations of thianthrene-1,4-dione at $E_{1/2} = 0.99 \text{ V}$ and 1.18 V vs. Fc/Fc^+ and two reversible one-electron reductions of 1,4-quinone at $E_{1/2} = -0.65 \text{ V}$ and -1.39 V (Fig. 5.4a). With the exception of the first scan, the other 9 scans overlap on top of each other. Further cyclic voltammetry measurements were also conducted at higher scan rates. Again with the exception of the first scan, all remaining 19 and 49 scans overlap on top of each other at a scan rate of 200 mV s^{-1} (Fig. 5.4b) and 500 mV s^{-1} (Fig. 5.4c) respectively, suggesting excellent electrochemical stability.

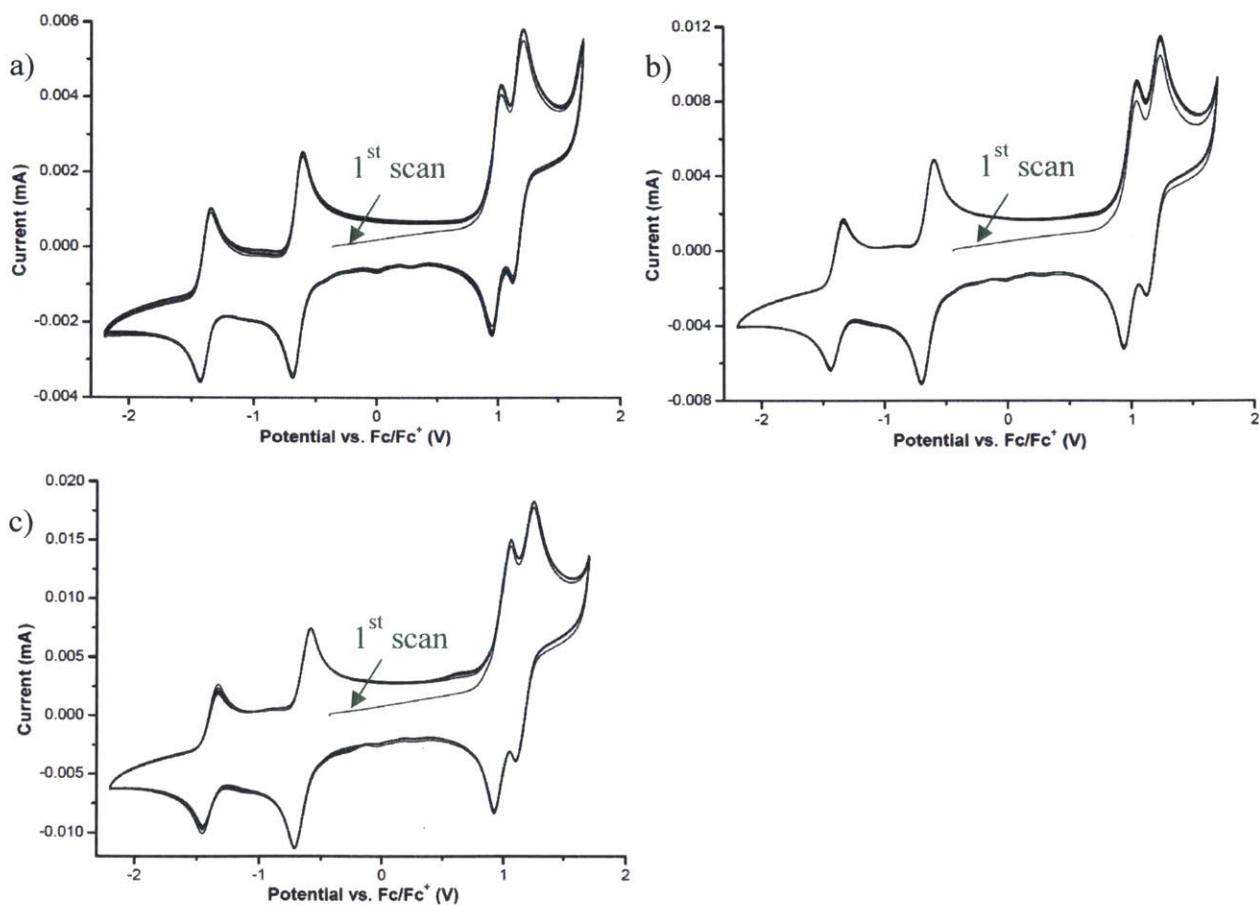
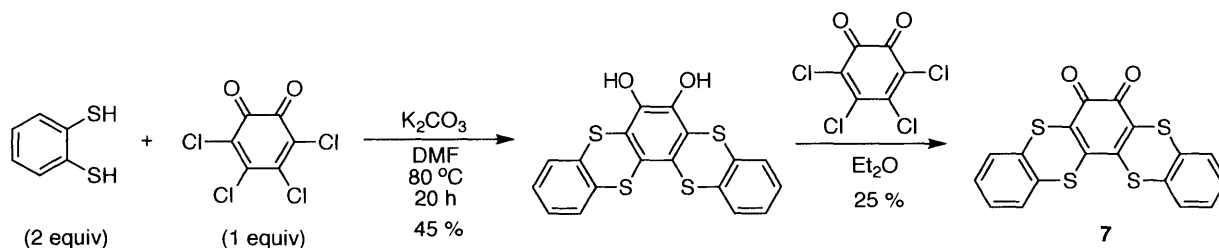


Figure 5.4. Cyclic voltammetry of model molecule **6** at a) 50 mV s^{-1} (10 scans), b) 200 mV s^{-1} (20 scans), and c) 500 mV s^{-1} (50 scans).

Despite having only a molecular weight of 384.50 g mol⁻¹ (cf. 614.75 g mol⁻¹ for tetraphenylporphyrin **1**), 1,4-quinone **6** possesses four distinct redox states ranging from +2 to -2, and exhibits a wide potential range of 2.57 V. These results suggest that deconstructed molecule **6** is a suitable candidate for symmetric RFB, and more importantly, supports our proposed approach of deconstructing relevant electroactive species to achieve novel dual oxidative-reductive molecules.

5.2.2 Further Synthesis and Electrochemical Studies

To further demonstrate the utility of our deconstruction approach, 1,2-quinone **7** was synthesized and tested for its redox activity. Two equivalents of benzene-1,2-dithiol were reacted with one equivalent of *o*-chloranil to give a reduced diol product, which was re-oxidized with an equivalent of *o*-chloranil to afford the desired product **7** (Scheme 5.2). In stark contrast to benzo-1,4-quinone, benzo-1,2-quinone has only received scant attention in the RFB literature despite their structural similarities.¹⁷



Scheme 5.2. Synthesis of 1,2-quinone **7**.

Cyclic voltammetry of **7** at 50 mV s⁻¹ scan rate showed as expected two reversible one-electron oxidations of thianthrene-1,2-dione at $E_{1/2} = 0.92$ V and 1.12 V vs. Fc/Fc⁺ and two reversible one-electron reductions of 1,2-quinone at $E_{1/2} = -0.61$ V and -1.35 V (Fig. 5.5a).

Compound **7** shows good electrochemical stability as demonstrated by the perfect overlap of scan 2-10. Scanning 100 cycles at a faster scan rate of 500 mV s^{-1} , the second reduction of **7** seems less reversible, possibly due to trace *o*-chloranil impurity left from the re-oxidation step (Fig. 5.5b). The potential range of 1,2-quinone **7** is 2.47 V , which is 0.1 V smaller than that of 1,4-quinone **6**.

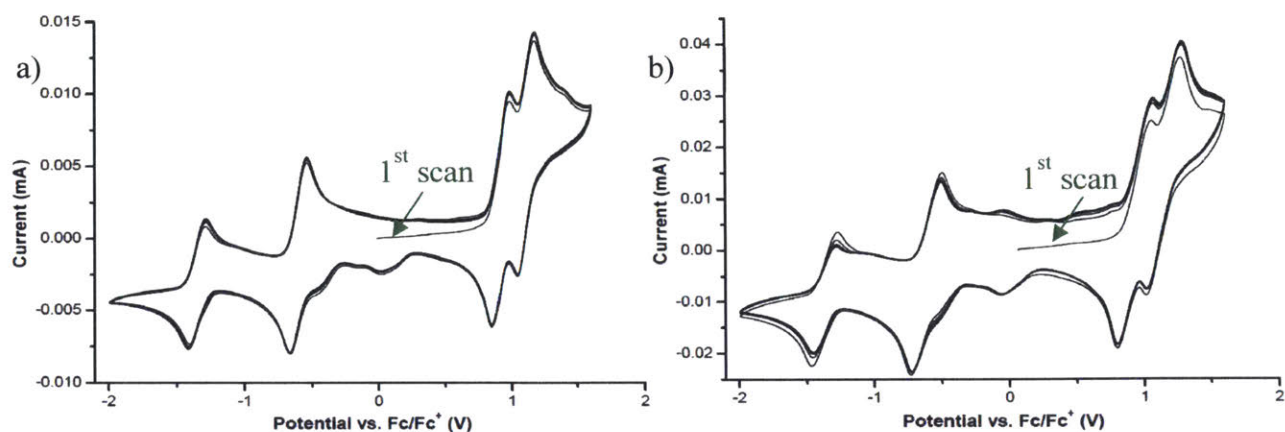
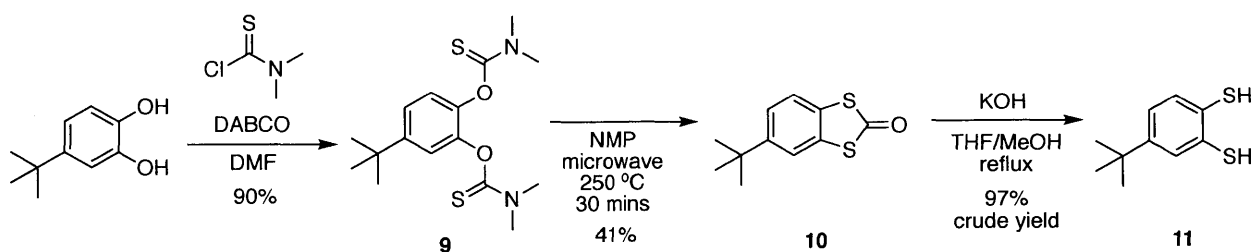


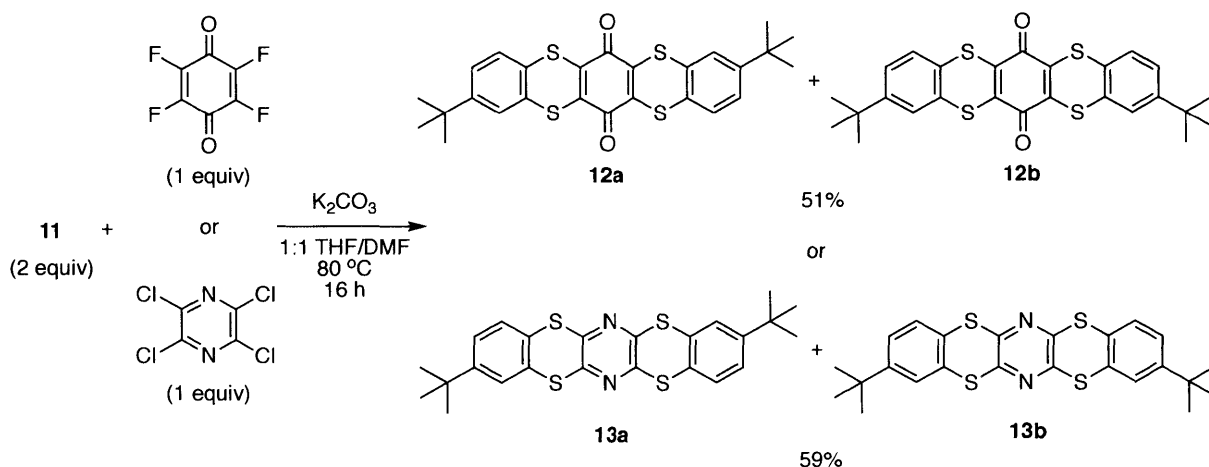
Figure 5.5. Cyclic voltammetry of **7** at a) 50 mV s^{-1} (10 scans), and b) 500 mV s^{-1} (100 scans).

In order to increase the solubility of the dual anolyte-catholyte species, we synthesize a dithiol nucleophile with a *tert*-butyl side chain, which proves to be an effective solubilizing group despite its small molecular weight. Thiocarbamate **9** was obtained by reacting 4-(*tert*-butyl)benzene-1,2-diol with *N,N*-dimethylthiocarbamoyl chloride (Scheme 5.3).¹⁸ Newman-Kwart rearrangement of **9** at $250 \text{ }^\circ\text{C}$ under microwave conditions gives dithiol-2-one **10**, which was deprotected using KOH to afford dithiol **11**.



Scheme 5.3. Synthesis of dithiol nucleophile **11**.

Dithiol **11** was used without purification and reacted with *p*-fluoranil and perchloropyrazine to yield highly soluble dual anolyte-catholyte molecules **12** and **13** in 51% and 59% respectively (Scheme 5.4). Two regioisomers are obtained as expected for both **12** and **13**. In addition to having superior solubility (>250 mg in 1 mL CHCl₃), it is anticipated that the regioisomers of **12** and **13** have negligible differences in their redox potentials, and the presence of regioisomers is beneficial in preventing crystallization from a concentrated solution which would be detrimental to flow battery performance.



Scheme 5.4. Synthesis of highly soluble dual anolyte-catholyte molecules **12** and **13**.

Cyclic voltammetry of **12** performed at a scan rate of 50 mV s⁻¹ reveals two reversible one-electron oxidations of thianthrene-1,4-dione at $E_{1/2} = 0.88$ V and 1.07 V vs. Fc/Fc⁺ and two reversible one-electron reductions of 1,4-quinone at $E_{1/2} = -0.72$ V and -1.46 V (Fig. 5.6a). The oxidative potentials of **12** are 0.11 V lower than that of **6** while the reductive potentials of **12** are 0.07 V more negative than that of **6**, presumably due to the electron-donating effects of the *tert*-butyl groups and the closer proximity of the sulfur atoms to the *tert*-butyl group than the quinone. Compound **12** exhibits a wide potential range of 2.53 V. Figure 5.6b shows that with the exception of the first scan, all remaining 99 scans of **12** at 500 mV s⁻¹ scan rate overlap perfectly with each other, supporting the electrochemical stability of molecular scaffold **6**.

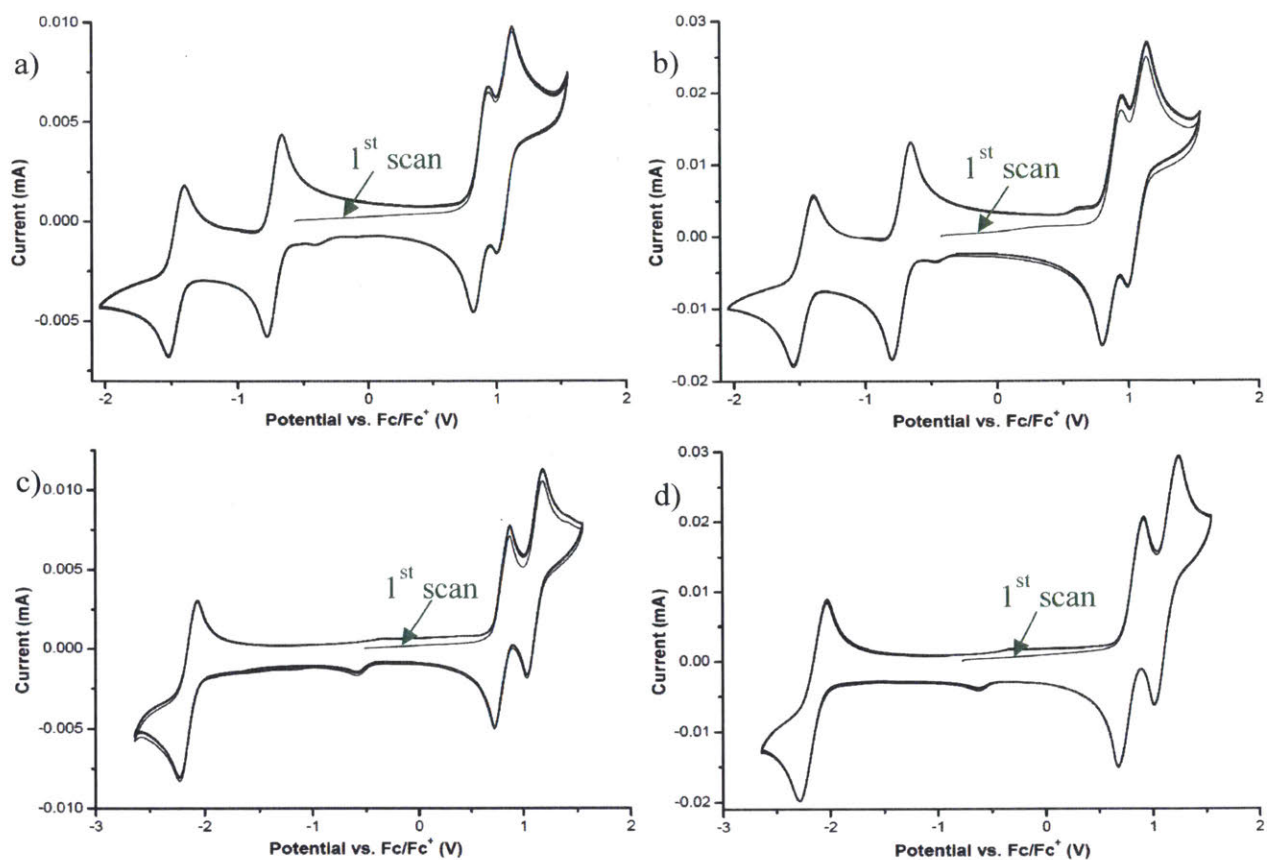


Figure 5.6. Cyclic voltammetry of **12** at a) 50 mV s⁻¹ (10 scans) and b) 500 mV s⁻¹ (100 scans), and **13** at c) 50 mV s⁻¹ (10 scans) and d) 500 mV s⁻¹ (100 scans).

Similarly, cyclic voltammetry of **13** performed at a scan rate of 50 mV s⁻¹ reveals two reversible one-electron oxidations of benzodithiinopyrazine at $E_{1/2} = 0.80$ V and 1.12 V vs. Fc/Fc⁺ and one reversible one-electron reductions of pyrazine at $E_{1/2} = -2.15$ V (Fig. 5.6c). The second reduction of pyrazine was not accessible within the 4:1 *o*-dichlorobenzene (*o*-DCB)/MeCN solvent window. In spite of the latter, an extraordinary potential range of 3.27 V is achieved with **13**, which is the widest potential range reported to date for a symmetric RFB. Pyrazine **13** also exhibits excellent electrochemical stability, as demonstrated by the perfect overlap of 100 scans at 500 mV s⁻¹ scan rate (Fig. 5.6d).

5.3 Conclusions

A new approach for designing novel dual anolyte-catholyte molecules by deconstruction of relevant electroactive species has been proposed and demonstrated. Three new molecular scaffolds **6–8** have been successfully synthesized, and shown to possess dual oxidative-reductive properties over a wide potential range and exceptional electrochemical stability over 100 cycles in cyclic voltammetry. Moreover, *tert*-butyl functionalized 1,4-quinone **12** and pyrazine **13** are highly soluble (>250 mg in 1 mL of CHCl₃), and are promising candidates for symmetric RFB. In particular, **13** has the largest potential range reported to date of 3.27 V for a symmetric RFB. Efforts are currently underway to test these new dual anolyte-catholyte molecules in a symmetric RFB.

5.4 Experimental Details

5.4.1 General

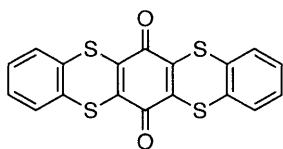
Anhydrous DMF was purchased from Aldrich as Sure-Seal Bottles and used as received. CH₂Cl₂ and THF were purified by passage through two alumina columns of an Inert solvent purification system. All other chemicals were of reagent grade and used as received. All air and water sensitive synthetic manipulations were performed in flame-dried glassware under an argon atmosphere using standard Schlenk techniques.

NMR spectra were recorded on a 400 MHz, 500 MHz or 600 MHz spectrometer. Chemical shifts δ are reported in ppm downfield from tetramethylsilane using the residual solvent signals (CDCl₃: δ_{H} 7.26 ppm, δ_{C} 77.16 ppm/TCE-*d*₂: δ_{H} 6.00) as an internal reference. For ¹H NMR,

coupling constants J are given in Hz and the resonance multiplicity is described as s (singlet), d (doublet), dd (doublet of doublets), and m (multiplet).

High-resolution mass spectrometry (HRMS) was performed using an Ion Cyclotron Resonance Mass Spectrometer with Direct Analysis in Real Time (DART) as the ionization technique. Electrochemical measurements were carried at various scan rates in 0.1 M tetrabutylammonium hexafluorophosphate (TBAPF₆) electrolyte in anhydrous 4:1 *o*-DCB/MeCN, using a three-electrode cell configuration consisting of a quasi-internal Ag wire reference electrode submerged in 0.01 M AgNO₃/0.1 M TBAPF₆ anhydrous MeCN solution, a Pt button (1.6 mm in diameter) working electrode, and a Pt coil counter electrode. All potentials were referenced to the Fc/Fc⁺ redox couple.

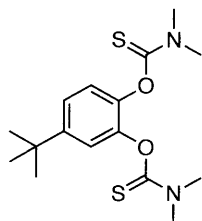
5.4.2 Synthetic Procedures



Benzo[5,6][1,4]dithiino[2,3-*b*]thianthrene-6,13-dione (**6**)

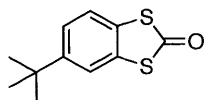
To a Schlenk flask with a stirrer bar containing K₂CO₃ (415 mg, 3.0 mmol) and 2,3,5,6-tetrafluorocyclohexa-2,5-diene-1,4-dione (90 mg, 0.5 mmol) under argon was added THF (1 mL), benzene-1,2-dithiol (115 μ L, 1.0 mmol) and DMF (1 mL). The reaction was stirred at 80 °C for 16 h. The mixture was precipitated into an aqueous 1M HCl solution, filtered and washed with MeOH, acetone, hexane and ethyl acetate. The residue was purified by gel column chromatography using 1:1 toluene/hexane to obtain **6** as a black powder (48.2 mg, 25%). R_f (1:1 toluene/hexane) = 0.45.

$^1\text{H NMR}$ (500 MHz, $\text{TCE-}d_2$) δ 7.28 (dd, $J = 5.7, 3.4$ Hz, 4H), 7.24 (dd, $J = 5.7, 3.4$ Hz, 4H). A $^{13}\text{C NMR}$ could not be obtained due to insufficient solubility. **HRMS** (DART) m/z calculated for $\text{C}_{18}\text{H}_{19}\text{O}_2\text{S}_4$ $[\text{M}+\text{H}]^+$: 384.9485; found: 384.9475.



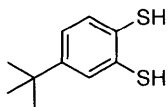
***O,O'*-(4-(*tert*-Butyl)-1,2-phenylene) bis(dimethylcarbamothioate) (9)**

To a stirred solution of 4-(*tert*-butyl)benzene-1,2-diol (10 g, 60 mmol) in DMF (90 mL) under argon was added DABCO (27 g, 240 mmol) and *N,N*-dimethylthiocarbamoyl chloride (29.7 g, 240 mmol). After stirring for 2 h at room temperature, the reaction mixture was poured into deionized water and then filtered. The residue was purified by recrystallization using DCM/EtOH to obtain **9** as a white solid (18.5 g, 90%). $^1\text{H NMR}$ (600 MHz, CDCl_3) δ 7.29 (dd, $J = 8.5, 2.3$ Hz, 1H), 7.15 (d, $J = 2.3$ Hz, 1H), 7.08 (d, $J = 8.5$ Hz, 1H), 3.412 (s, 3H), 3.407 (s, 3H), 3.27 (s, 3H), 3.26 (s, 3H), 1.33 (s, 9H). $^{13}\text{C NMR}$ (151 MHz, CDCl_3) δ 187.02, 187.01, 150.0, 144.9, 143.1, 123.5, 123.3, 121.5, 43.33, 43.31, 38.80, 38.79, 34.72, 31.36. **HRMS** (DART) m/z calculated for $\text{C}_{16}\text{H}_{25}\text{N}_2\text{O}_2\text{S}_2$ $[\text{M}+\text{H}]^+$: 341.1357; found: 341.1361.



5-(*tert*-Butyl)benzo[d][1,3]dithiol-2-one (**10**)

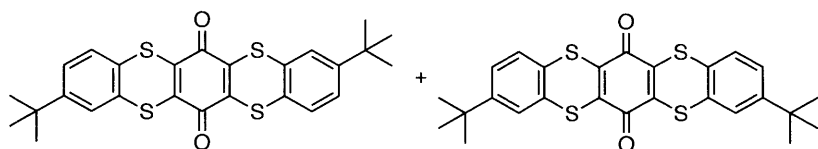
To a 20 mL microwave tube containing a stirrer and **9** (3 g, 8.81 mmol) was added anhydrous NMP (16 ml) and capped in a glovebox under nitrogen atmosphere. The reaction mixture was heated at 250 °C under microwave conditions for 30 mins. After cooling, ethyl acetate was added to the reaction mixture and the organic layer was extracted using brine ($\times 3$) and then deionized water to remove NMP. The organic layer was then dried using MgSO₄, concentrated, and purified by gel column chromatography eluting with 1:4 CH₂Cl₂/hexane to obtain **10** as a yellow oil (0.814 g, 41%). R_f (1:4 CH₂Cl₂/hexane) = 0.3. ¹H NMR (500 MHz, CDCl₃) δ 7.49 (d, J = 1.9 Hz, 1H), 7.40 (d, J = 8.6 Hz, 1H), 7.36 (dd, J = 8.6, 1.9 Hz, 1H), 1.33 (s, 9H). ¹³C NMR (126 MHz, CDCl₃) δ 190.8, 150.8, 132.6, 129.5, 124.8, 122.8, 120.0, 35.0, 31.3. HRMS (DART) m/z calculated for C₁₁H₁₃O₁S₂ [M+H]⁺: 225.0408; found: 225.0400.



4-(*tert*-Butyl)benzene-1,2-dithiol (**11**)

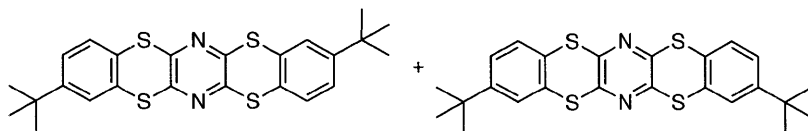
To a Schlenk flask with a stirrer containing **10** (0.654 g, 2.91 mmol) in degassed THF (20 mL) under argon was added a degassed solution of KOH (0.8 g, 14.6 mmol) in MeOH (5 mL), causing the solution to turn from colorless to pale yellow. The reaction was stirred overnight under reflux. The solvents were removed *in vacuo*, and an aqueous solution of 1 M HCl was added. The reaction mixture was extracted with CH₂Cl₂. The organic layer was washed with water ($\times 2$), dried with

MgSO₄, and concentrated to obtain **11** without purification as a yellow oil (0.557 g, 97% crude yield). ¹H NMR (500 MHz, CDCl₃) δ 7.38 (d, *J* = 2.2 Hz, 1H), 7.31 (d, *J* = 8.2 Hz, 1H), 7.10 (dd, *J* = 8.2, 2.2 Hz, 1H), 3.77 (s, 1H), 3.62 (s, 1H), 1.28 (s, 9H). ¹³C NMR (126 MHz, CDCl₃) δ 150.6, 131.4, 131.3, 128.1, 127.3, 124.3, 34.6, 31.3. HRMS (DART) *m/z* calculated for C₁₀H₁₅S₂ [M+H]⁺: 199.0615; found: 199.0602.



Regioisomers of di-*tert*-butylbenzo[5,6][1,4]dithiino[2,3-*b*]thianthrene-6,13-dione (**12**)

To a Schlenk flask with a stirrer bar containing K₂CO₃ (1.24 g, 9 mmol) and 2,3,5,6-tetrafluorocyclohexa-2,5-diene-1,4-dione (270 mg, 1.5 mmol) under argon was added a solution of **11** (0.6 g, 3.0 mmol) in THF (5 mL), followed by DMF (5 mL). The reaction was stirred at 80 °C for 16 h. The reaction mixture was concentrated, precipitated into an aqueous 1M HCl solution, and filtered. The residue was washed with water, dried and purified by gel column chromatography eluting with 1:4 CH₂Cl₂/hexane to obtain the product as a purple foam (382.2 mg, 51%). R_f (1:4 CH₂Cl₂/hexane) = 0.2. ¹H NMR (500 MHz, CDCl₃) δ 7.28 (d, *J* = 2.0 Hz, 2H), 7.24 (dd, *J* = 8.2, 2.0 Hz, 2H), 7.18 (d, *J* = 8.2 Hz, 2H), 1.27 (s, 18H). ¹³C NMR (126 MHz, CDCl₃) δ 172.5, 153.0, 142.43 and 142.38 (regioisomers), 141.94 and 141.89 (regioisomers), 130.3, 128.3, 127.1, 126.4, 125.9, 34.9, 31.1. HRMS (DART) *m/z* calculated for C₂₆H₂₅O₂S₄ [M+H]⁺: 497.0737; found: 497.0729.



Regioisomers of di-tert-butylbenzo[5,6][1,4]dithiino[2,3-*b*]benzo[5,6][1,4]dithiino[2,3-*e*]pyrazine (13)

To a Schlenk flask with a stirrer bar containing K_2CO_3 (622 mg, 4.5 mmol) and perchloropyrazine (163 mg, 0.75 mmol) under argon was added a solution of **11** (300 mg, 1.5 mmol) in THF (3 mL), followed by DMF (3 mL). The reaction was stirred at 80 °C for 16 h. The reaction mixture was concentrated, precipitated into an aqueous 1M HCl solution, and filtered. The residue was washed with water, dried, and purified by gel column chromatography eluting with 1:4 CH_2Cl_2 /hexane to obtain the product as a yellow foam (206 mg, 59%). R_f (1:4 CH_2Cl_2 /hexane) = 0.3. 1H NMR (500 MHz, $CDCl_3$) δ 7.44 (d, J = 2.1 Hz, 2H), 7.35 (d, J = 8.3 Hz, 2H), 7.28 (dd, J = 8.3, 2.1 Hz, 2H), 1.29 (s, 18H). ^{13}C NMR (151 MHz, $CDCl_3$) δ 152.0, 150.2 and 150.1 (regioisomers), 150.00 and 149.97 (regioisomers), 131.8, 128.53, 128.50, 125.9, 125.7, 34.7, 31.1. HRMS (DART) m/z calculated for $C_{24}H_{25}N_2S_4$ $[M+H]^+$: 469.0901; found: 469.0928.

5.5 References

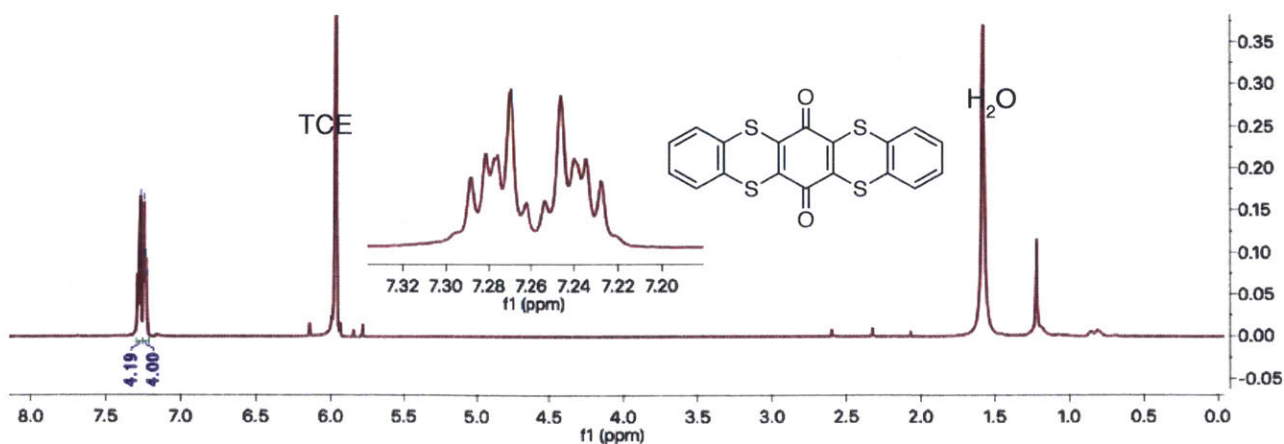
- 1 International Energy Agency. World Energy Outlook; International Energy Agency: Paris, France, 2017.
- 2 Yang, Z.; Zhang, J.; Kintner-Meyer, M. C. W.; Lu, X.; Choi, D.; Lemmon, J. P.; Liu, J. *Chem. Rev.* **2011**, *111* (5), 3577.

- 3 Winsberg, J.; Hagemann, T.; Janoschka, T.; Hager, M. D.; Schubert, U. S. *Angew. Chem. Int. Ed.* **2017**, *56* (3), 686.
- 4 Soloveichik, G. L. *Chem. Rev.* **2015**, *115* (20), 11533.
- 5 Noack, J.; Roznyatovskaya, N.; Herr, T.; Fischer, P. *Angew. Chem. Int. Ed.* **2015**, *54* (34), 9776.
- 6 Ding, Y.; Zhang, C.; Zhang, L.; Zhou, Y.; Yu, G. *Chem. Soc. Rev.* **2018**, *47* (1), 69.
- 7 Leung, P.; Shah, A. A.; Sanz, L.; Flox, C.; Morante, J. R.; Xu, Q.; Mohamed, M. R.; Ponce de León, C.; Walsh, F. C. *J. Power Sources* **2017**, *360*, 243.
- 8 Potash, R. A.; McKone, J. R.; Conte, S.; Abruña, H. D. *J. Electrochem. Soc.* **2016**, *163* (3), A338.
- 9 Ma, T.; Pan, Z.; Miao, L.; Chen, C.; Han, M.; Shang, Z.; Chen, J. *Angew. Chem. Int. Ed.* **2018**, *57* (12), 3158.
- 10 Duan, W.; Vemuri, R. S.; Milshtein, J. D.; Laramie, S.; Dmello, R. D.; Huang, J.; Zhang, L.; Hu, D.; Vijayakumar, M.; Wang, W.; Liu, J.; Darling, R. M.; Thompson, L.; Smith, K.; Moore, J. S.; Brushett, F. R.; Wei, X. *J. Mater. Chem. A* **2016**, *4* (15), 5448.
- 11 Winsberg, J.; Stolze, C.; Muench, S.; Liedl, F.; Hager, M. D.; Schubert, U. S. *ACS Energy Lett.* **2016**, *1* (5), 976.
- 12 Friedl, J.; Lebedeva, M. A.; Porfyraakis, K.; Stimming, U.; Chamberlain, T. W. *J. Am. Chem. Soc.* **2018**, *140* (1), 401.

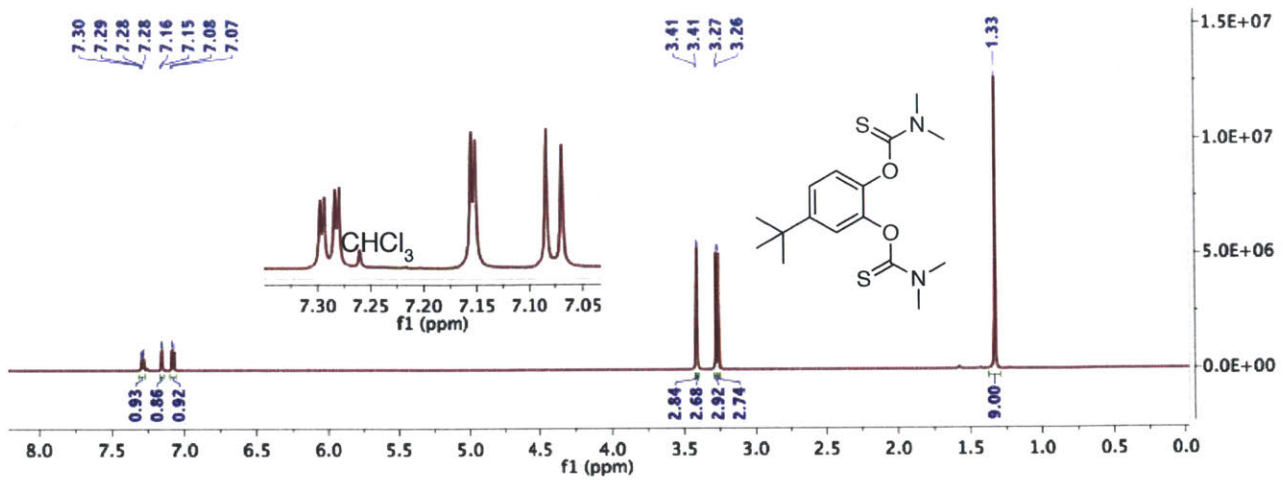
- 13 Kaim, W. *Angew. Chem. Int. Ed.* **1983**, 22 (3), 171.
- 14 Chambers, J. Q., *Electrochemistry of quinones in The Chemistry of the Quinonoid Compounds*; John Wiley & Sons, 1974.
- 15 Takagi, K.; Mizuno, A.; Iwamoto, A.; Furusyo, M.; Matsuoka, M. *Dyes Pigm.* **1998**, 36 (1), 35.
- 16 Matsumoto, S.; Miura, H.; Mizuguchi, J. *Dyes Pigm.* **2002**, 52 (1), 9.
- 17 Ding, Y.; Li, Y.; Yu, G. *Chem* **2016**, 1 (5), 790.
- 18 Mahendran, A.; Vuong, A.; Aebisher, D.; Gong, Y.; Bittman, R.; Arthur, G.; Kawamura, A.; Greer, A. *J. Org. Chem.* **2010**, 75 (16), 5549.

5.6 Appendix for Chapter 5

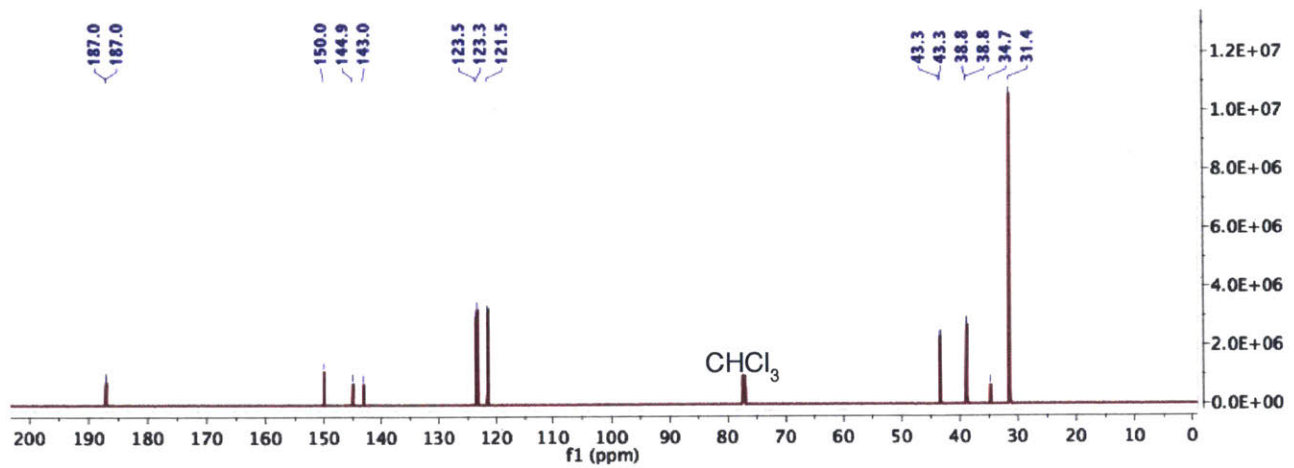
NMR Spectra



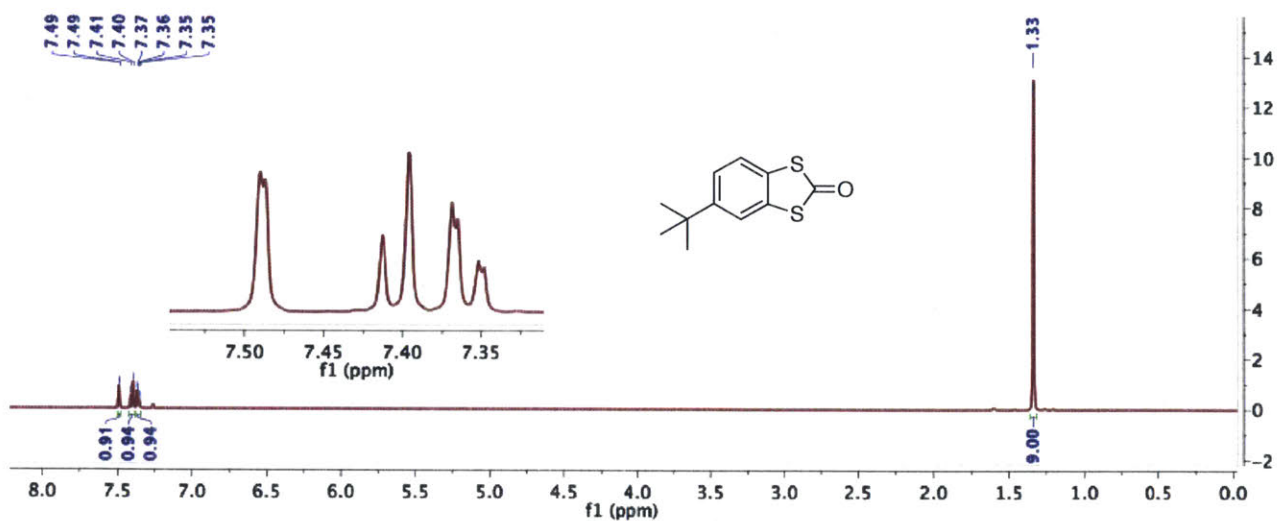
¹H NMR spectrum (500 MHz, TCE-*d*₂) of **6**.



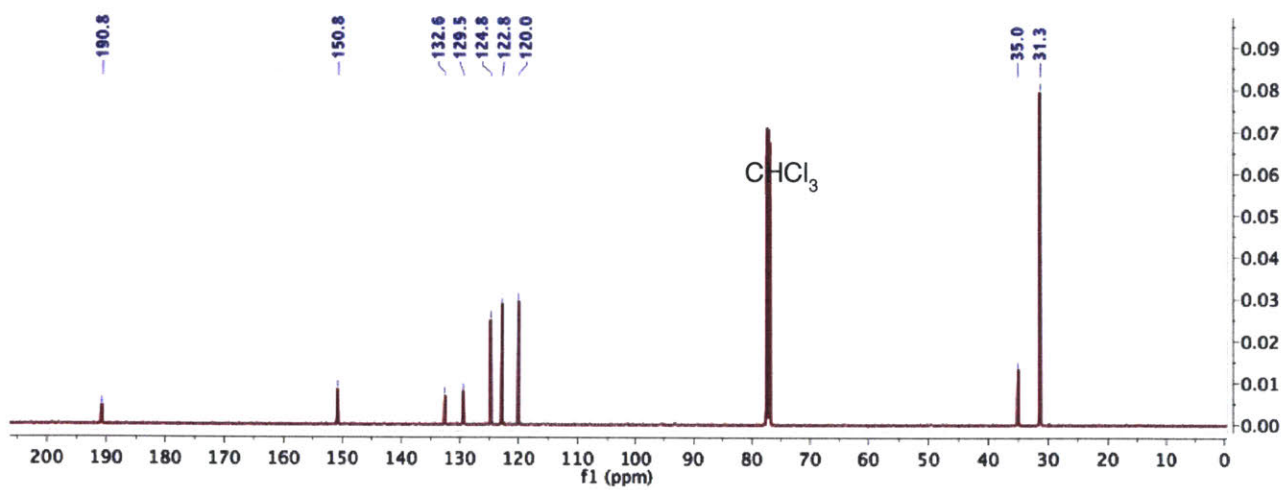
¹H NMR spectrum (600 MHz, CDCl₃) of **9**.



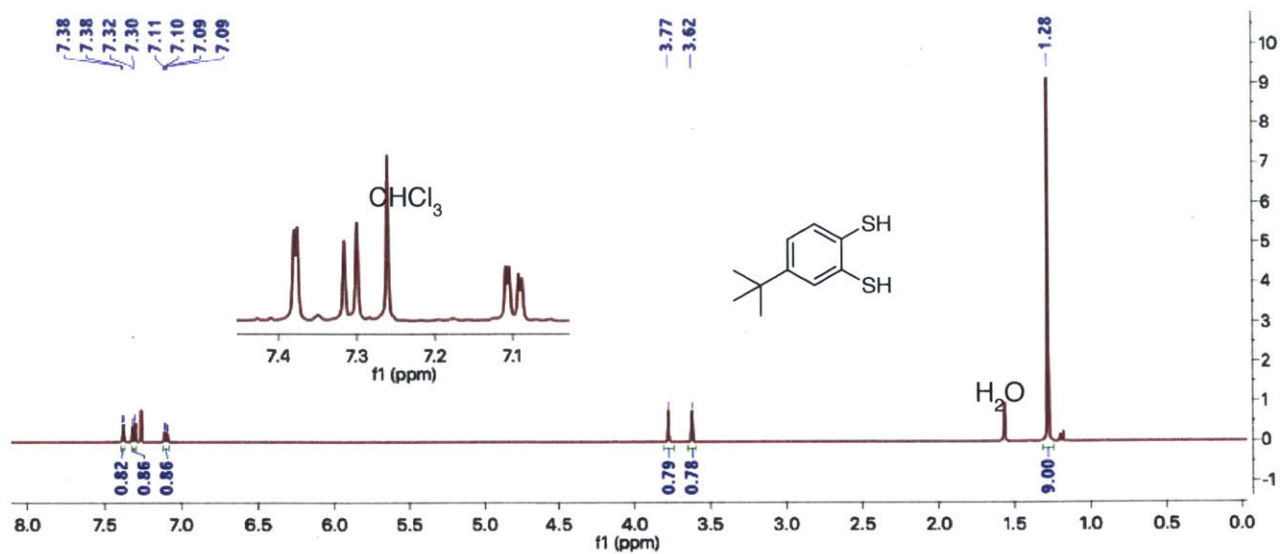
¹³C NMR spectrum (151 MHz, CDCl₃) of **9**.



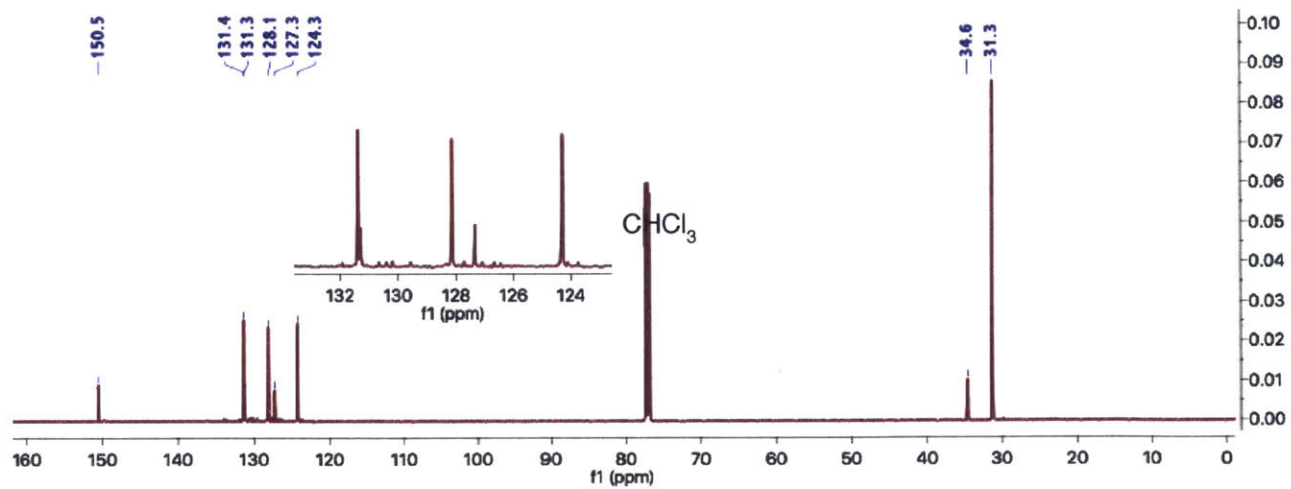
^1H NMR spectrum (500 MHz, CDCl_3) of **10**.



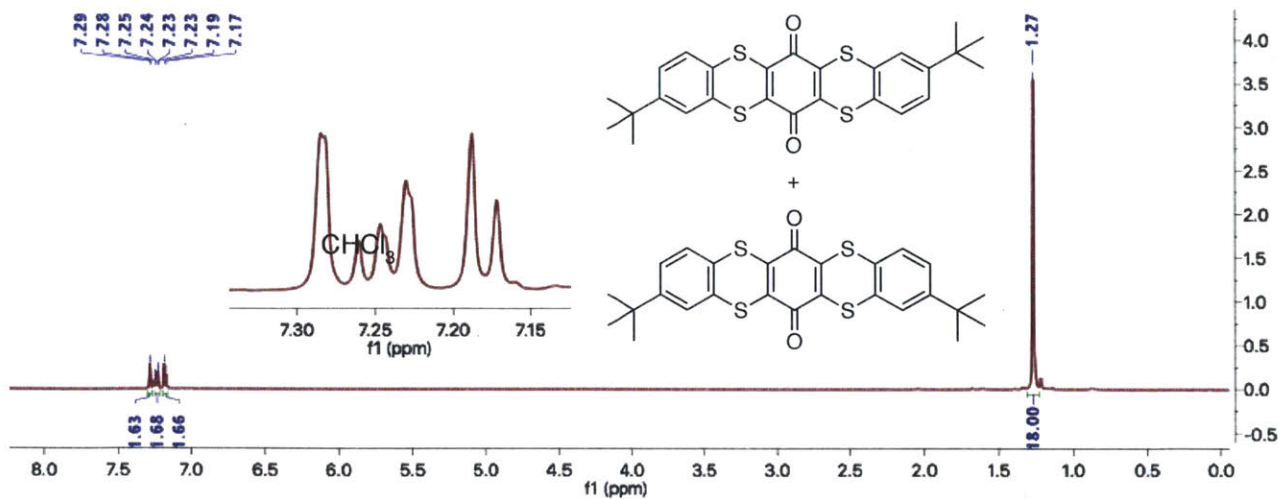
^{13}C NMR spectrum (126 MHz, CDCl_3) of **10**.



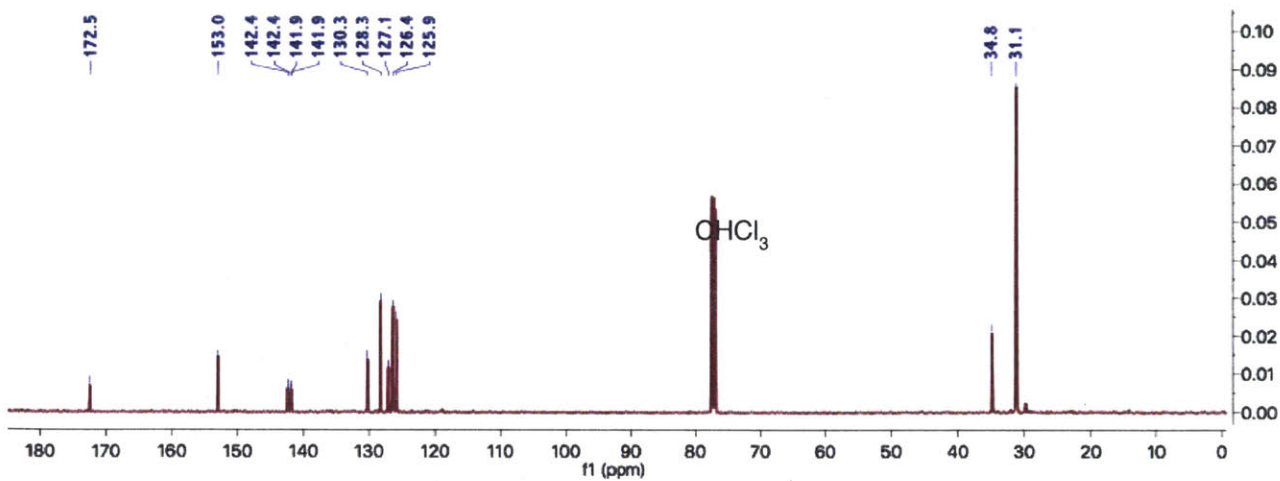
^1H NMR spectrum (500 MHz, CDCl_3) of **11**.



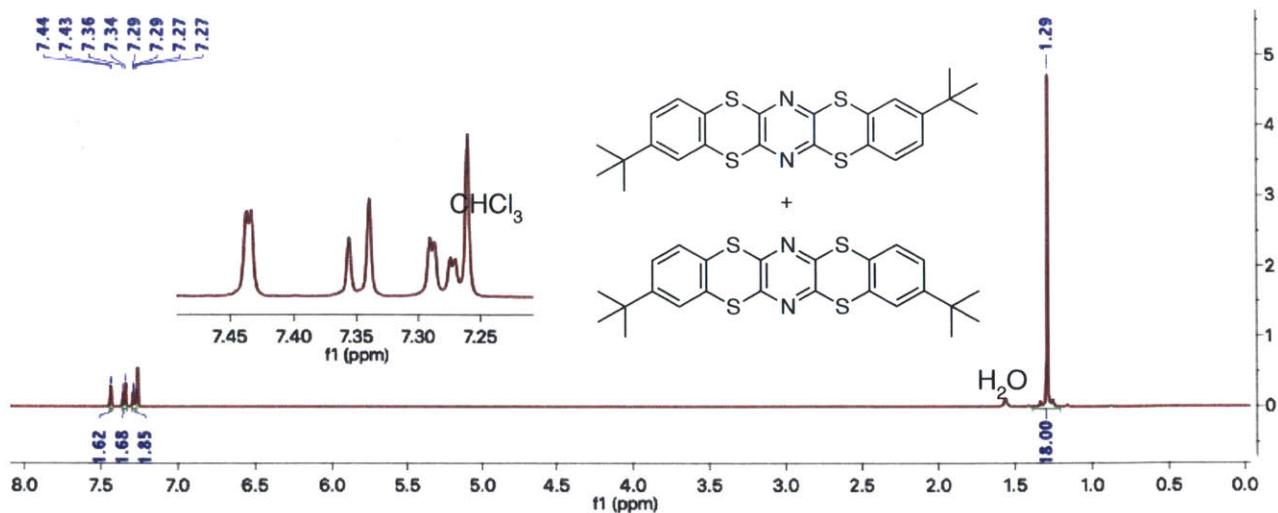
^{13}C NMR spectrum (126 MHz, CDCl_3) of **11**.



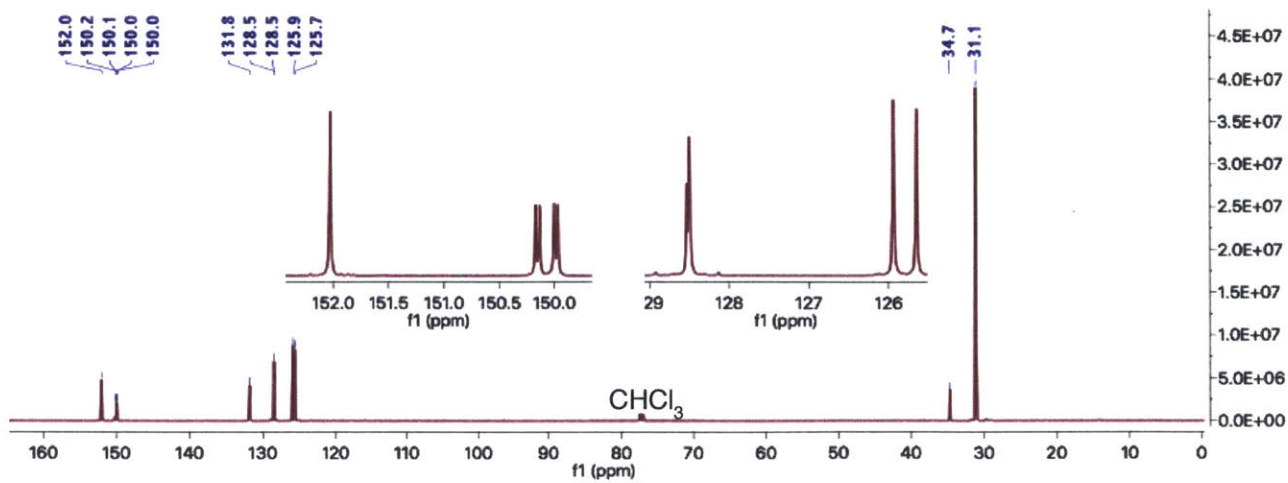
¹H NMR spectrum (500 MHz, CDCl₃) of 12.



¹³C NMR spectrum (126 MHz, CDCl₃) of 12.



^1H NMR spectrum (500 MHz, CDCl_3) of **13**.



^{13}C NMR spectrum (126 MHz, CDCl_3) of **13**.

Acknowledgements

Coming to MIT has been my dream since high school, and I have many people to thank for making this dream possible. My foremost gratitude goes to my research advisor, Prof. Timothy M. Swager. Tim is a top-notch scientist who is highly creative and entrepreneurial. He inspires me with his chemical intuition on novel materials design and astute business acumen, and guided me toward high-impact research. I am extremely grateful to him for giving me the freedom to conceive and pursue my research ideas, and to pursue my interests outside of the lab. In particular, Tim encouraged me to pursue entrepreneurial activities on campus, and commercialize my research in water treatment. I would also like to thank my thesis chair Prof. Jeremiah A. Johnson, and thesis committee members Prof. Stephen L. Buchwald and Prof. Jeffrey F. Van Humbeck for their guidance and helpful advice.

Working in the Swager group has been a wonderful experience. This would not be possible without the dedication of our current and former lab managers Brian Pretti and Dr. Joseph Walsh in maintaining the lab. I especially thank Brian for helping me fix the EChem glovebox multiple times, and helping me with equipment repairs and countless chemical orders. I also thank our current and former group administrative assistants Emily Wensberg, Kathy Sweeney and Rachael Fuller for taking care of the group's administrative work.

I would like to extend my profound gratitude to my many co-workers and collaborators. I am extremely grateful to Prof. Yanchuan Zhao, Prof. Cagatay Dengiz, Dr. Maggie He, Dr. Katsuaki Kawasumi and Prof. Tomoyuki Ikai for their patient mentorship in the lab and invaluable advice on my research projects. I also greatly appreciate working with Dr. Federico Bertani and Prof. Ellen Sletten on the cavitand and squitch project. I thank Dr. Jeff Lopez and Sam Etkind for collaborating with me on the flow battery project, and Dr. Yoonseob Kim for collaborating on the heavy metals removal project. I also thank Dr. Bora Yoon, Dr. Maggie He and Dr. Intak Jeon for the characterization of the porous polymer networks, Kosuke Yoshinaga for the quantum yield and MALDI measurements of the ladder polymers, and Dr. Myles Herbert and Dr. Nathan Romero for proofreading my S_NAr manuscript.

I am deeply honored with the friendship I established in the Swager group. I am extremely thankful for my bay mates Bora Yoon and Qifan Zhang. Bora has been a great elder sister to me in the group, supporting me through difficult times. I very much enjoy my many discussions with Qifan and appreciate her help throughout the stressful recruiting process. I also thank Maggie for her constant encouragement and support. I am grateful to have fellow Singaporeans Lionel Moh and Tran Truong in the group. I am also glad to have the enjoyable companionship of fellow batch mates Kathleen White and John Fennell in the group. I appreciate others for their friendship and support in my development as a scientist: Pan, Hiro, Soichi, Sarah, Suchol, Hongkun, Sibon, Lukas, Julia, Kazu, Yoshi, Seon-Jin, Che-Jen, Frank, Vera, Yifan, Alberto, Grace, Elisabeth, Joe, Alessandro, Constantin, Kelvin, Liz, Won-Tae, Jens, Kent, Jon, Mason, Ben, Martin, Monika,

Jessica, Madeleine, Lennon, Zach, Cassie, Henry, Georgios, Sophie, Graham, Haleema, Jie, Shun and Cen.

I would like to end the Acknowledgements with my heartfelt gratitude to the most important people in my life. I am indebted to my mum and dad for their unconditional love and support. They work hard to support me through school despite having little education themselves. I owe my success to them. I thank my three siblings for taking care of my parents over the 10 years while I am abroad pursuing my studies. It was not easy to balance research, professional pursuits and personal life simultaneously, and I am extremely thankful to Jiajing for her love, support and patience over the last 2 years. Jiajing is a loving and caring girlfriend, and has been instrumental in giving me the courage to pursue my dreams. She has been and will continue to be the source of my strength, and I believe, together, we will overcome all difficulties. I dedicate this thesis to Jiajing and my family.